1-1-2013

Asymmetric Hydrogenation of α, β-Unsaturated Carboxylic Acid Over Chiral-Modified Palladium Catalyst

Shuai Tan
University of South Carolina

ASYMMETRIC HYDROGENATION OF α, β-UNSATURATED CARBOXYLIC ACID OVER CHIRAL-MODIFIED PALLADIUM CATALYST

by

Shuai Tan

Bachelor of Science in Chemical Engineering
Tianjin University, Tianjin, China, 2008

Bachelor of Science in Chemistry
Nankai University, Tianjin, China, 2008

Submitted in Partial Fulfillment of the Requirements

For the Degree of Doctor of Philosophy in

Chemical Engineering

College of Engineering and Computing

University of South Carolina

2013

Accepted by:

Christopher T. Williams, Ph.D. (Chairman, Examining Committee)

Andreas Heyden, Ph.D. (Committee Member)

Jochen Lauterbach, Ph.D. (Committee Member)

Michael L. Myrick, Ph.D. (Committee Member)

John W. Weidner, Ph.D. (Committee Member)

Lacy Ford, Vice Provost and Dean of Graduate Studies

DEDICATION

I dedicate my dissertation work to my family. A special feeling of gratitude to my loving parents, Huiying Tan and Qiuhua Ma, who act themselves as the first tutors in my life; whose words of encouragement inspire me all the time; who have never left my side.

ACKNOWLEDGEMENTS

Thank to my committee members, who were more than generous with their expertise and precious time.

I would like to express my deepest gratitude to Dr. Chris Williams, my advisor, for his countless hours of reading, dedicated guidance, and thoughtful ideas throughout the entire process. I would never have been able to finish my work and dissertation without his help. He is not only my mentor in academic, but also a friend during past years. I'm very appreciated to Dr. John Monnier, who is always willing to help and provide best suggestions. I enjoy all of our discussion regarding the research, especially in kinetic, and catalysis. All your words have a great impact on my professional development. Special thanks also go to all academic brothers and sisters in my group.

Many friends in Columbia, especially the *ForeverStrong* team players, should be thankful for giving me unforgettable memories in USC.

Thanks to *Google, Wikipedia, Baidu, and Emuch.* Those websites and forums always provide first-hand technique support and information regarding my research.

Also, thanks to *Facebook, RenRen, Weibo, Wechat, and QQ,* best platform to share my depression, excitement with acquaintances.

Juventus, my favorite team since I was a kid, is always being a spiritual support.

To my future girlfriend/wife, regardless who you are, thanks. Yours absence is definitely a driven force to finish PhD study ASAP.

ABSTRACT

The production of optically pure chemicals through enantioselective catalytic reaction plays a key role in a variety of industrials (e.g., pharmaceutical, agrochemical). Chiral-modified supported transition metal catalysts have been addressed attentions since past decades due to an environmental concern. Among the known catalytic systems, cinchona-modified Pd catalyst has been found to be modifier-sensitive and substrate-sensitive in the asymmetric hydrogenation of α, β-unsaturated carboxylic acids. Nevertheless, the exact structure of the intermediate complex, which is responsible for the enantioselectivity, as well as the kinetic mechanism of such reaction system are still not clearly understood and require further study from a molecular level. Accordingly, in the present work, a model substrate, as well as a classic chiral modifier was chosen to examine in this catalytic reaction using both spectroscopic and kinetic approaches.

To be specific, the hydrogenation of a model aliphatic unsaturated carboxylic acid (2-methyl-2-pentenoic acid) over cinchonidine (chiral modifier) modified Pd/Al_2O_3 catalyst has been examined. The adsorption behaviors of the acid and the modifier, as well as the acid-modifier interaction complex over metal and oxide surface have been characterized by *in-situ* attenuated total reflection infrared (ATR-IR) spectroscopy. It has been found that the substrate acid primarily dissociatively adsorbs on the metal surface as a bridging bidentate carboxylate, together with some molecular species. The modifier and substrate form a 1:1 structure complex either in

solution or adsorbed on surface, regardless of solvent. Moreover, the actual hydrogenation process over Pd surface is *in-situ* observed by ATR-IR.

Both racemic and enantioselective hydrogenation has been carried out in a batch reactor. Various kinetic aspects (e.g., H_2 pressure, solvent effect, modifier effect) of the catalytic performance were examined. To summary, the reaction exhibits a strong solvent-dependent behavior, with polar solvent provides higher activity. H_2 pressure shows 1^{st} reaction order at low regime (< 8 atm), while become pressure-independent when greater than 20 atm. The substrate shows 1^{st} reaction order at low conversion region (< ca. 60%), but increase to higher order (ca. 1.5-2) afterward. The addition of the modifier leads to enantioselectivity while simultaneously causing a dramatic decrease of the overall reaction rate due to the high occupied percentage of modified site, and its rather low TOF. However, it does not affect the reaction order with respect to acid and H_2 pressure. The accumulation of the product appears to correlate with an increasing reaction order in acid substrate at high conversion, although this does not affect the final e.e. value. The current study has bridged the gap between macro-scale kinetic performance and micro-scale spectroscopic observation in this catalytic system, which could in turn lead to design more efficient.

TABLE OF CONTENTS

LIST OF FIGURES

LIST OF TABLES

LIST OF ABBREVIATIONS

AAS.....atomic absorption spectroscopy

ATR-IR.....attenuated total reflection infrared

CD.....cinchonidine

DI.....deionized

FID.....flame ionization detector

FT-IR.....Fourier transform infrared

GC.....gas chromatography

HRTEM.....high resolution transmission electron microscopy

ID.....inside diameter

IRE.....internal reflection element

MPaA.....*trans*-2-methylpentanoic acid

MPeA.....*trans*-2-methyl-2-pentenoic acid

UHP.....ultra high purity

1. Introduction

The chirality of organic substances was first observed by Jean-Baptiste Biot in 1815, and is a property of considerable importance for the fragrance, sugar, and pharmaceutical industries, as well as the ever developing fields of analytical and synthetic chemistry. In 1848, Louis Pasteur first deduced that this phenomenon had a molecular basis via optical polarization rotation measurements of naturally derived tartaric acid. Chiral properties play a key role in natural world. For example, enzymes and other natural binding sites recognize substrates with a particular chirality to generate a variety of biological functions [1]. Therefore, finding out an efficient way to produce enantiopure chemicals is currently one of the most challenging and interesting scientific and technological problems in chemistry and chemical engineering. Especially, significantly increasing research effort is being directed in pharmaceutical, fragrance, and agro-chemistry, with the aim of producing optically pure chemicals. Since pure enantiomer drugs always exhibit a superior performance rather than a racemic mixture [2], enantioselective synthesis is a frontier topic in chemistry and chemical engineering.

Over the past several decades, a variety of methods have been applied to achieve the goal of directly producing enantiopure chiral chemicals. The area received a boost when it was found that an appropriate modification of the classical catalysts could significantly improve the catalytic performance in terms of selectivity and activity [3]. A good enantioselective catalytic system should contain two basic

functions: an activating function, which is the actual catalysis performance; and a controlling function, which controls the enantioselectivity of the reaction [4].

Homogeneous chiral catalysis has been long investigated because of several considerable advantages, such as remarkable selectivity and activity, low sensitivity to poisoning, and quick heat transfer during the reaction. Such kinds of catalysts are usually complexes, which contain a metal ion center interacting with an organic ligand. The earliest examples of using homogeneous chiral metal complex catalysts were reported in the 1960s. Nozaki *et al*. produced *cis* and *trans* isomers of ethyl 2-phenyl cyclopropanecarboxylate from ethyl diazoacetate in the presence of bis[N-(R)-α-phenylethylsalicylaldiminato]Cu(II)(I), obtaining a 72% optical yield [5]. Horner *et al*. reported that hydrogenation of α-ethylstyrene and α-methoxystyrene with phosphine-Rh complex catalyst could produce (S)-(+)-2-phenylbutane, and (R)-(+)-1-methoxy-1-phenylethane, with optical yield of 7-8% and 3-4% respectively[6]. Knowles and co-workers obtained 15% optical purity for hydrogenation of α-phenylacrylic acid with $RhCl_3(PPhMePr)_3$ homogeneous complex catalyst [7].

Among the later studies concerning homogeneous catalysts, it has been found that chiral phosphine complexes with transition metals with low oxidation states are a promising way to promote enantioselectivity. It has been generally accepted that low-valent Ru, Rh, or Ir with phosphorus are the most active and versatile catalysts [8]. It is reported that 2, 2'-Bis (diarylphosphino)-1, 1'-binaphthyl (BINAP) is one of most effective chiral ligands. For example, Noyori reported that a homogeneous cationic Rh-BINAP complex catalyst can produce amino acids from α-(acylamino) acrylic acids with e.e. up to 100% [9]. Later, they achieved an e.e. of 96% using

Rh(I)-BINAP complex in catalyzing the isomerization of allylic amines to enamines [10]. A variety of other homogeneous chiral catalysts have been developed over the years, and it remains an active area of research [8, 11, 12]. Nevertheless, homogeneous catalysts retain some significant weaknesses in terms of their application in industry, such as difficulties associated with the high cost of separation, the challenge of recovery and reuse of the chiral catalyst, and the product contamination caused by metal leaching [13]. Table 1.1 shows a list of advantages and disadvantages of homogeneous and heterogeneous catalyst respectively.

Table 1.1 Comparison of homogeneous and heterogeneous catalysts [14]

	Heterogeneous	Homogeneous
Catalyst form	Solid, often metal or metal oxide	Metal complex
Mode of use	Fixed bed or slurry	Dissolved in reaction medium
Solvent	Usually not required	Usually required – can be product or byproduct
Selectivity	Usually poor	Can be tuned
Stability	Stable to high temperature	Often decompose < 100°C
Recyclability	Easy	Can be very difficult
Special reactions	Haber process, exhaust clean up etc.	Hydroformylation of alkenes, methanol carbonylation, asymmetric synthesis etc

Over the past several decades, researchers have been committed to the development and improvement of transition metal-based heterogeneous catalysts in almost all industries [4, 8, 15]. However, successful applications of heterogeneous enantioselective catalysts have been limited. The most convincing way of developing enantioselective heterogeneous catalysts is the surface modification of conventional metal catalysts by adding optically active compounds (i.e. modifiers). It has been found that synthesis in the presence of chiral auxiliaries (i.e. a modified catalyst) is

most attractive in the sense that a small amount of optically active catalyst can produce a large quantity of product. Figure 1.1 shows some of most important chiral modifiers that scientists have developed for enantioselective heterogeneous catalysis, most of which are naturally occurring chemicals. Basically speaking, these chiral auxiliaries for enantioselective synthesis are in three main groups: alkaloids, hydroxy and amino acids [16].

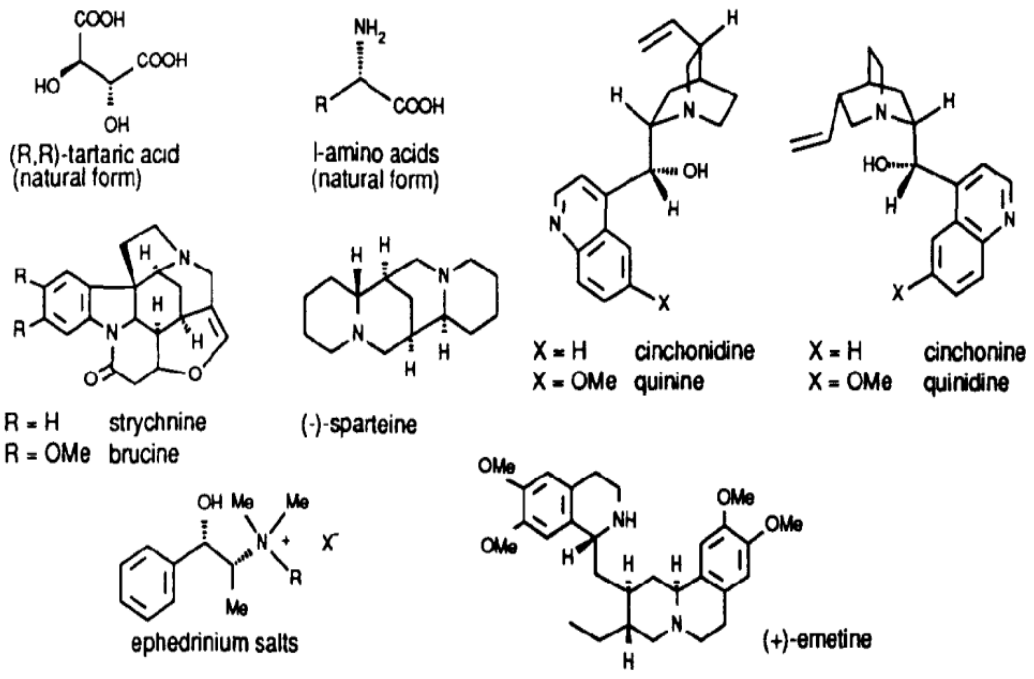

Figure 1.1 Structures of most important chiral modifiers for heterogeneous metallic catalyst [4]

However, such heterogeneous enantioselective catalysts are still lagging behind homogeneous catalysts in terms of performance, mechanistic insight and scope of reactions [17]. These modified catalysts are very specific with respect to the substrate, which means the combination of catalytically active metal and appropriate modifier only ensures the enantioselectivity of a small group of substrates [18]. To

optimize such heterogeneous catalysts, the activating and controlling parts need to match each other to work effectively. For instance, tartaric acid is a good modifier for Ni but not with Pt, whereas cinchona alkaloids interact well with Pt, Rh, and Pd but not for Ni and Ru [19].

At present, successful applications are mostly confined in narrow range of C=O and C=C asymmetric hydrogenation. In general, there are three well-studied systems according to previous work:

(i) Hydrogenation of β-ketoester and β-diketone with tartaric acid modified Ni catalysts [20-28].

(ii) Hydrogenation of α-ketoester and α, β-diketone and other activated carbonyl compounds with cinchona-alkaloid modified Pt catalysts [21, 29-41].

(iii) Hydrogenation of C=C in α, β-unsaturated carboxylic acids with cinchona-alkaloid modified Pd catalysts [21, 42-57].

The general reactions for such systems are shown in Figure 1.2:

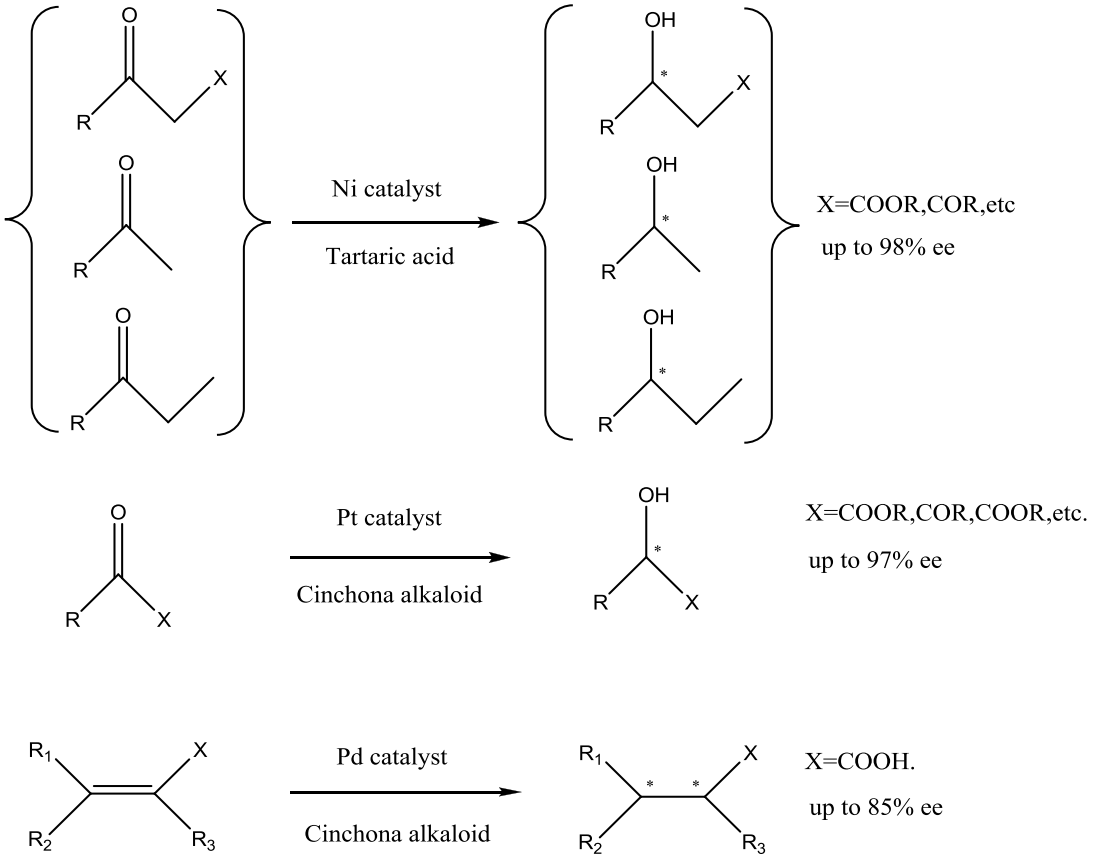

Figure 1.2 General reactions of three well-developed heterogeneous enantioselective hydrogenation systems [33]

In these systems, the source of chirality is an organic compound, which strongly adsorbs on metal surface and provides a chiral environment for hydrogenation in the following step.

The next section is a review of the relevant literature, in which the current state of knowledge regarding the enantioselective hydrogenation with homogeneous and heterogeneous catalysts is introduced. This is followed by a discussion of the experimental methodologies, the results and discussion of the research performed, and the concluding remarks.

2. Literature Review

This section contains four parts. The first part is the current knowledge regarding asymmetric hydrogenation based on homogeneous catalysts. Some classic reaction systems are introduced. Part two presents a discussion of heterogeneous catalytic hydrogenation. The basic mechanism that governs the C=O reduction and some recognized models of substrate-modifier complex are introduced. In addition, C=C bond hydrogenation with cinchona-modified metal catalysts is reviewed, with the most important features of the reaction system being pointed out. The third part discusses the various conformations of cinchona alkaloid modifiers and their adsorption on metal surfaces. Such behavior of the modifier significantly affects the performance of the catalyst for enantioselective hydrogenation. Finally, some background of the surface vibrational technique of attenuated total reflection infrared (ATR-IR) spectroscopy is introduced.

2.1 Asymmetric Hydrogenation-Homogeneous Catalysis

Driven by the high requirement of nonracemic, chiral chemicals, the development of methods to produce enantio-pure chemicals is of particular interest in both academic and industrial research labs. Asymmetric synthesis has been recognized a promising way to produce enantiomerically pure compounds, which have been widely applied to production of pharmaceuticals and agrochemicals (see books and reviews [58-60]). Among all methods, homogeneous transition metal based catalyst,

during the past 40 years, play an important role due to their outstanding efficiency (e.g., high activity and great e.e. value).

2.1.1 Chiral Ligand

The chiral ligand is actually the key part during the asymmetric reaction (see Figure 2.1). In the late 1960s' and early 1970s', Knowles and Sabacky's group reported that CAMP and DIPAMP were effective ligands on Rh for asymmetric reduction of α-acylaminoacrylic acid, affording the e.e. values up to 90% [7, 61, 62]. Meanwhile, another diphosphine ligand- DIOP, discovered by Kagan and Dang, was found to be active with Rh(I) in reduction of β-substituted α-acylaminoacrylic acid, giving 70-80% optical yields [63, 64]. These chemicals are believed to be the first synthesized optical active ligands in chiral production via this method. Later, many other phosphorus-containing ligands were discovered, including Fryzuk and Bosnich's CHIRAPOS [65, 66], and Fiorini and Giongo's PNNP [67, 68].

Another ligand is BINAP, which was discovered by Noroyi and co-workers in 1980 [9]. Complexes of this ligand with Ru, Rh, and Pd showed remarkable efficiency in a wide range of enantioselective transformations (e.g., olefin, ketone) [69]. The superior adaptability and activity of BINAP made it very popular, and various BINAP-derivatives were subsequently synthesized in many laboratories. Eventually, Noyori's prominent work on BINAP and chirally catalyzed hydrogenation was recognized by the Nobel Prize in 2001.

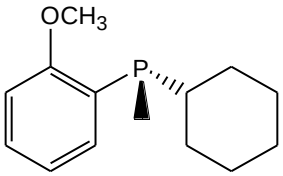

(S)-CAMP

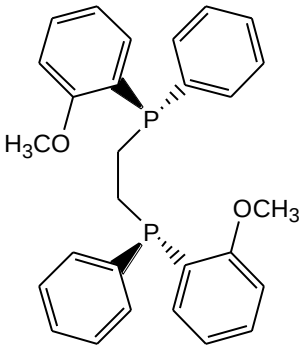

(S,S)-DIPAMP

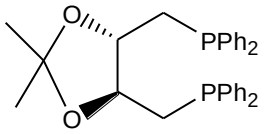

(S,S)-DIOP

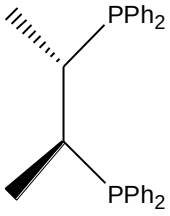

(S,S)-CHIRAPHOS

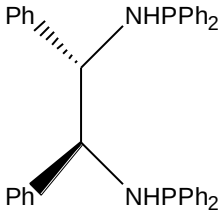

(S,S)-PNNP

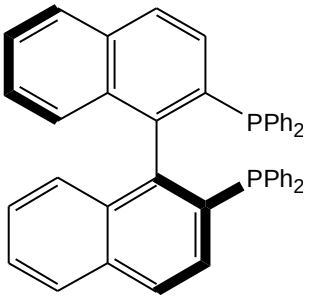

(S)-BINAP

Figure 2.1 Classic chiral ligands used in homogeneous catalyst

2.1.2 Typical Reaction

Asymmetric hydrogenation through homogeneous catalysis has been extensively studied and successfully applied in a wide range of industries in producing chirally pure chemicals. Basically, there are three types of classic reactions, which are C=O, C=C, and C=N bond reduction. This section briefly summarizes the current scope of knowledge in this area.

2.1.2.1 C=O asymmetric reduction

At present, successful applications are mostly confined to ketones and ketoesters. In general, there are three well-studied systems according to previous work (see Figure 2.2):

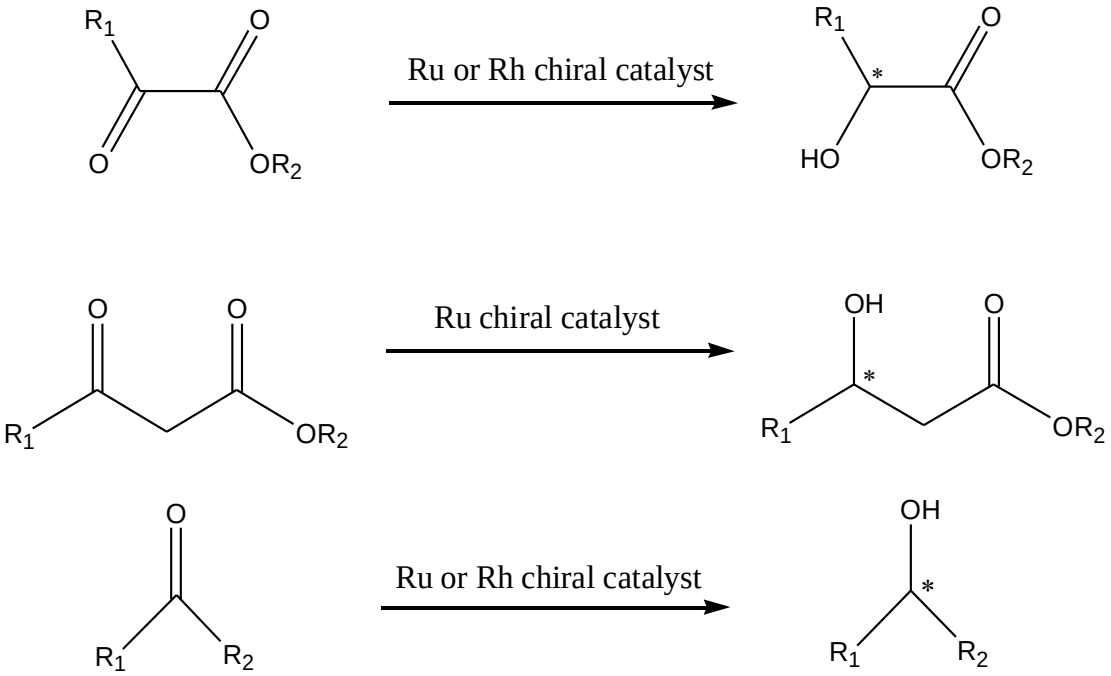

Figure 2.2 Typical studied systems of homogeneous catalyzing of C=O reduction

I. Hydrogenation of functionalized ketone

Chiral functionalized alcohols play an important role in the area of organic chemistry and biology. Hence, efficient production of such chirally pure enantiomers is one of the challenges in synthetic chemistry. Among several methods, asymmetric hydrogenation from functionalized ketones (e.g., ketoesters) is promising. Many Rh or Ru complex catalysts have been investigated in the study of asymmetric hydrogenation of α-ketoesters. For example, Rh-MCCPM in THF [70], Rh-Cy, Cy-oxoProNOP in Toluene [71, 72] produced high e.e. values (>87%) under mild

conditions (T< 20 ℃, P_{H2}<50 atm). Takaya worked with Ru-BINAP [73] and Ru-BICHEP [74] in alcohol system, which also exhibited good enantioselectivity under room temperature.

In contrast, asymmetric hydrogenation of β-ketoester has been extensively studied, especially with Ru complex catalysts. For example, a variety of substrates have been examined with Ru-BINAP [75-77]. In general, most studies were carried out in an alcohol solvent, with temperatures lower than 80 ℃ and H_2 pressures lower than 50 atm. The e.e. values were at least 97%. Other complexes, such as Ru-BPE [78], and Ru-PHANEPHOS [79] were also found to have similar performance.

II. Hydrogenation of unfunctionalized ketones (e.g., aliphatic and aromatic ketones)

Asymmetric hydrogenation of unfunctionalized ketones usually shows only moderate performance in comparison with functionalized substrate. This has been generally explained as resulting from the lack of a second coordination site to the metal catalyst that decrease the enantioselectivity [80, 81].

For example, Marko and co-workers used Rh-DIOP [82] and Rh-BDPP [83] complexes in catalyzing the asymmetric hydrogenation of an aromatic ketone - acetophenone. The corresponding e.e. values were about 80%. An Ir complex has also been studied, however, the enantioselectivity was poor with 50% [84]. In the late 1990's, Noyori's group found that the [$RuCl_2$-(diphosphine)-(1,2-diamine)] catalyst family exhibited the best catalytic performance in hydrogenating unfunctionalized aromatic ketone [85, 86].

Meanwhile, for aliphatic unfunctionalized ketones, Rh-PennPhos [87] and Ru-BINAP [88] are two well-studied catalyst families, providing promising e.e. values that range from 75% up to 97%.

2.1.2.2 C=C asymmetric reduction

The study of C=C asymmetric hydrogenation has mainly focused on olefins. In general, there are three well-studied systems according to previous work (see Figure 2.3):

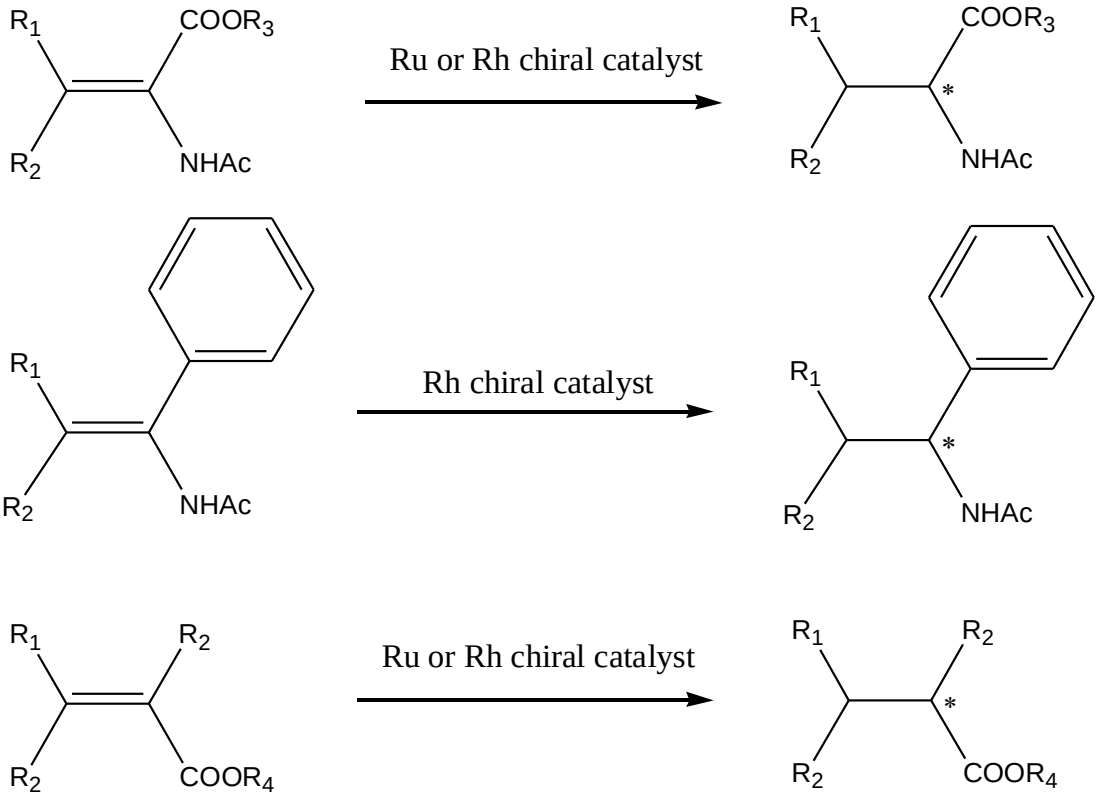

Figure 2.3 Typical studied systems of homogeneous catalyzing of C=C reduction

I. Hydrogenation of α and β - dehydroamino acids

The corresponding produced chiral amino acids are of particular importance in pharmaceuticals, and biochemistry in general. Hence, a large number of catalysts

have been tested in this system, with Rh complexes being most efficient under mild conditions (T<35 ℃, P_{H2}< 10 atm, e.e.> 97%).

II. Hydrogenation of Enamide

Similar to the case of dehydroamino acid, the asymmetric hydrogenation of enamide could be achieved by a Rh-complex catalyst, showing great performance in terms of e.e. value.

III. Hydrogenation of unsaturated carboxylic acid and ester

Another typical class of chemicals that has been targeted for chiral synthesis is unsaturated carboxylic acid and corresponding ester derivatives. Interestingly, itaconic acid and its ester were easily hydrogenated with Rh-ligand complex, while for tiglic acid, Ru catalysts proved to be very effective.

2.1.2.3 C=N asymmetric reduction

In comparison with the extensive studies of asymmetric hydrogenation of ketones (C=O) and olefins (C=C), the investigations of C=N reduction are lagging behind (see Figure 2.4). It is believed that the strong binding interaction of amine groups to metal catalysts is the reason for low activity and selectivity. Nevertheless, several Ir and Rh complex have been discovered to be potential candidates for catalyzing amine substrates.

I. Hydrogenation of Imine

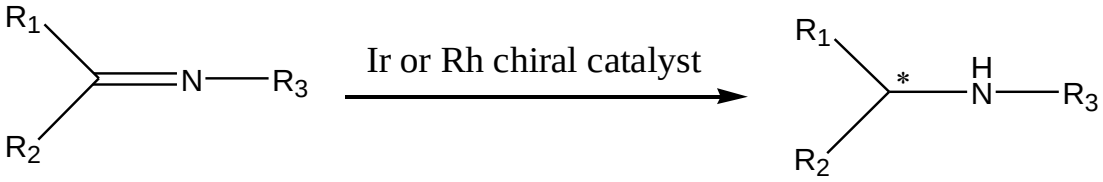

Figure 2.4 Typical studied system of homogeneous catalyzing of C=N reduction

For example, Rh-BDPP [89] and Ir-BINAPHANE [90] are found to be effective catalyst in hydrogenation of α-aryl N-alkylimine and N-arylimine, respectively. However, the reactions were always carried out in high H_2 pressure and long reaction times. Moreover, additives, such as I_2 and $N(Et)_3$ are necessary to improve activity and enantioselectivity.

To summarize the homogeneous catalysis methods for asymmetric hydrogenation, researchers have developed hundreds of metal-ligand complex systems. These have successfully been applied in a large variety of organic synthetic reactions, although there are still many limitations, such as expensive cost, difficult separations required for purity of product and recycling of catalyst. The immobilization of homogeneous catalysts has recently been the focus of much attention to address these concerns. Nevertheless, for quite a long time, homogeneous catalysis has proved itself a promising way forward, and has dominated in the area of many industrial applications.

2.2 Asymmetric Hydrogenation-Heterogeneous Catalysis

Catalysis technologies play key roles in the area of asymmetric synthesis, especially have been widely used in life science and biology [91, 92]. The growing market demand of enantio-pure chemical and more rigorous legislation regarding the environmental protection boost the fast developing of a novel technique-heterogeneous catalysis. The significant advantages of heterogeneous catalysts include easy separation, low cost, and efficient recycling of catalyst.

One promising strategy is to modify the active metal surface by adsorbing a suitable organic compound, which is usually called a chiral modifier (see review and

books [21, 93, 94]). In this way, the metal atom acts as catalytic center, while via the species interaction between adsorbed chiral modifier and reactant, the prochiral substrate is induced to take on some preferential surface orientation, leading to an enantioselective reaction.

A combination of surface spectroscopic techniques, computational modeling, and kinetic studies has been applied to these systems, aiming to interpret the intermolecular interactions and predict the catalytic behavior. Since the intermolecular interaction is always very sensitive and subtle, such "metal-modifier-reactant" combinations are very structurally specific with respect to the substrate. Hence, during the past decade of investigations, the development of heterogeneous catalytic reduction is still essentially limited to C=O and C=C bonds, and substrate scope is still relatively narrow. Nevertheless, a rational design of a suitable "metal-modifier-reactant" system is a great challenge and in high demand from both practical and theoretical standpoints.

2.2.1 C=O hydrogenation with cinchona-modified metal catalyst

A classic catalytic system for C=O asymmetric reduction is the hydrogenation of β-ketoesters and β-diketones with tartaric acid-Ni catalysts [95]. In general, the Raney-Ni catalyst was treated in a solution of tartaric acid, and sometimes NaBr was added as a second modifier. The corresponding active Ni catalyst, the so-called "Izumi catalyst", was found to show good enantioselectivity, ranging from 84 % - 99 % [96-98].

Another active catalyst is the Pt-cinchona alkaloid system, which was first discovered in 1979 for the asymmetric hydrogenation of α-ketoesters to α-hydroxy

esters [99]. Orito *et al.* originally reported that addition of cinchonidine to the reaction mixture preferentially induced the R-conformation of product, while cinchonine resulted in an excess of the S-conformation [99, 100]. Since then, considerable research efforts have been made to understand the mechanism that governs such catalytic reactions with the aim of developing the industrial applications. Several reviews have been published over the years summarizing this research [15, 17, 21, 30, 33, 101-104]. Usually ethyl or methyl pyruvates have been chosen as good probe molecules to produce lactates. The best e.e. (>97%) value that has been reported is ethyl pyruvate hydrogenation on Pt/Al_2O_3, pretreated with ultrasonication and modified with cinchonidine [105]. The presence of chiral modifier not only provides enantiodifferentiation, but also shows a ligand acceleration effect on the rate of reaction [106-108]. The latter effect leads to the remarkable feature that the reaction rate is improved by a factor of 2-100 [33] over the racemic reaction without modifier.

Adsorption of substrate may occur in two mirror-image configurations [36], as shown in Figure 2.5. Here the two C=O groups are in *trans* configuration because of the lower energy state. Without modifier, the two configurations of ketoester adsorb parallel to the metal surface with the same probability. Consequently, two hydrogen atoms adsorbed on the metal surface add onto the α-keto group from below the plane of substrate. The hydrogenation of prochiral carbon in α-keto group produces the chiral pyruvate molecules. However, since the amounts of two mirror-image configurations on the surface are equal, this process only produces a racemic product mixture. When the chiral modifier (e.g. cinchonidine) adsorbs on the metal surface,

an interaction between modifier and the substrate is introduced. Consequently, one of the two mirror images preferentially adsorbs on the surface, which results in the observed enantioselectivity for hydrogenation.

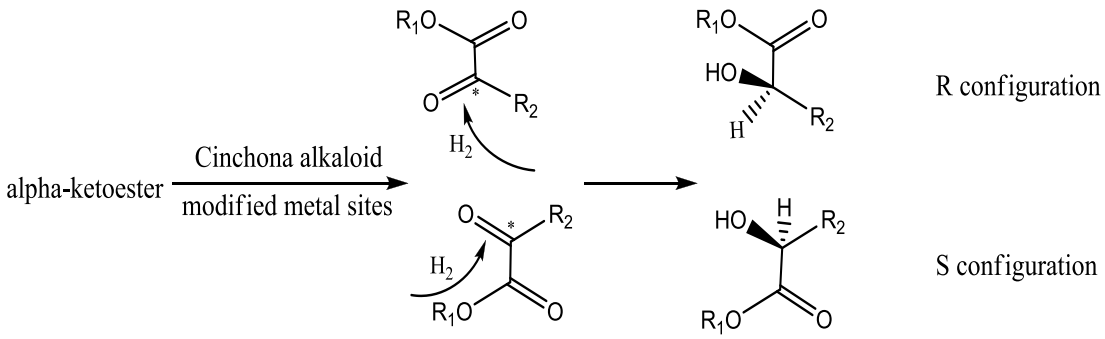

Figure 2.5 Schematic reaction of heterogeneous enantioselective hydrogenation of α-keto esters

Several models of the interaction between cinchonidine and substrates have been proposed based on both experimental and theoretical results. Wells *et al.* first built up a model in 1990 [40] and finally refined it in 1994 [36]. They proposed a 1:1 interaction between the cinchonidine and pyruvate ester, where the modifier is in the most stable conformation (open (3), see Figure 2.10 and Figure 2.11) and the substrate is in the *trans* conformation. Augustine and co-workers suggested a model involving a "bidentate" complex between N atom of quinuclidine moiety and O atom in CD and two carbonyl groups of pyruvate, which formed a six-atom ring. Yet another model proposed by Margitfalvi was based on a shielding effect [109, 110]. In this scheme, the reactant can only adsorb on the Pt surface by its unshielded side, favoring the predominant formation of one enantiomer [33]. Finally, Baiker *et al.* proposed a model based on theoretical modeling, which suggested a hydrogen bonding interaction between a protonated cinchonidine at the quinuclidine nitrogen

and the oxygen of the α-carbonyl of the pyruvate substrate [111-113]. This modifier-substrate complex is then suggested to be the precursor of one of the enantiomers. This calculation prediction was in agreement with previous experimental results [114]. Figure 2.6 demonstrates the four commonly mentioned models of those described above.

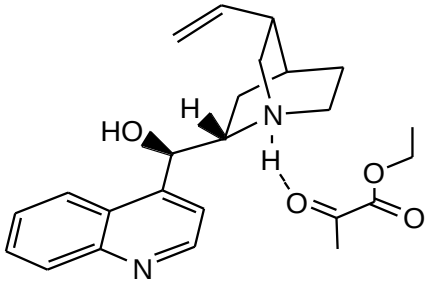

Wells' model

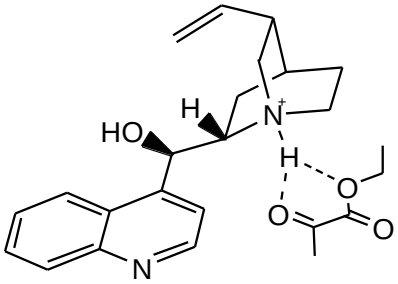

Baiker's model

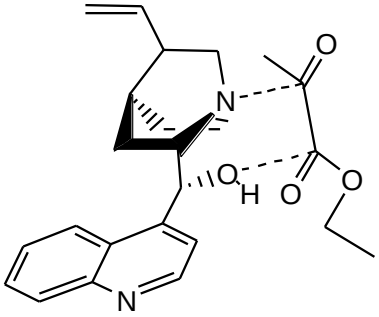

Augustine's model

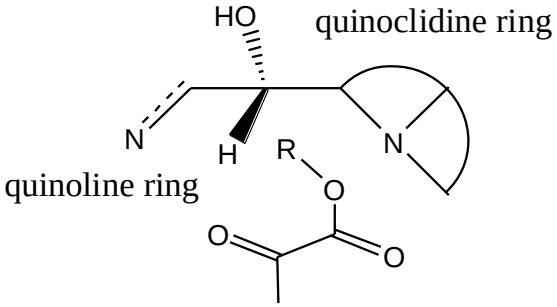

Margitfalvi's model

Figure 2.6 Classic α-ketoester-cinchonidine complex models

2.2.2 C=C hydrogenation with cinchona-modified metal catalyst

Compared with excessive studies for enantioselective hydrogenation of α-ketoesters and ketones on cinchona-alkaloid modified metal catalysts, there are fewer reports on hydrogenation of substrates containing a C=C bond. Hydrogenation of α-acetamidoacrylic acid and α-acetamidocinnamic acid over 5 wt% Pd on charcoal modified with 1-sparteine and 1-ephedrine was reported in 1971, with a very poor catalytic performance of 0.5%-4.5% e.e. [115]. In 1993, Corma *et al.* introduced rhodium and nickel complexes with N-based chiral ligands into zeolites for hydrogenation of N-acyldehydrophenylalanine derivatives. It was discovered that the zeolite had a cooperative effect on the reaction rate and selectivity, yielding an enantiomeric excess as high as 99% [116]. Figure 2.7 shows the schematic equation of such reaction. By heterogenization of such transition metal complexes, the catalyst can be recycled without losing activity and selectivity.

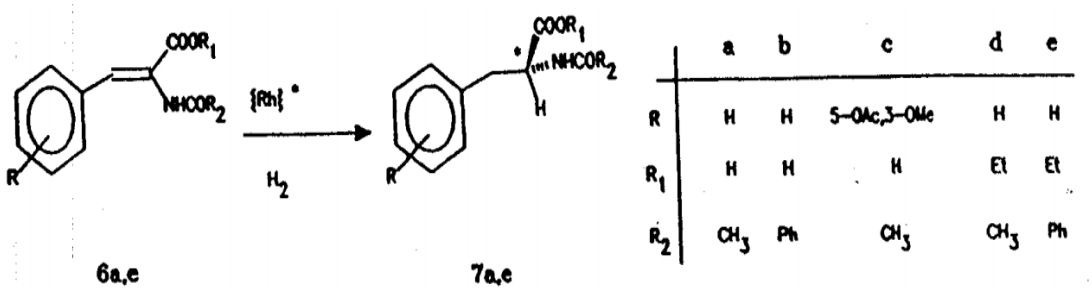

Figure 2.7 Schematic reaction of hydrogenation of N-acyldehydrophenylalanine derivatives [116]

Hydrogenation of the C=C bond in isophorone in a MeOH solution over modified Pd catalyst has been investigated in the presence of dihydrovinpocetine (DHVIN), a vinca-type alkaloid, as the modifier [16]. The highest e.e. (up to 38%) was achieved on Pd black under reaction conditions of 40 bar H_2 pressure and a

modifier/AcOH/substrate/solvent weight ratio of 1/5/35/400, where AcOH is an additive. A schematic equation of such reaction system is shown in Figure 2.8.

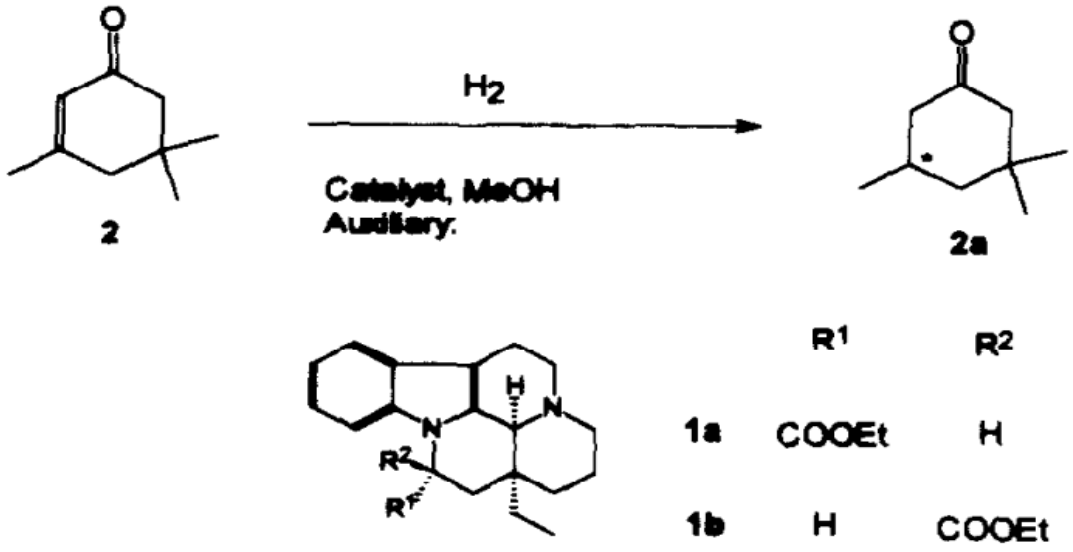

Figure 2.8 Schematic reaction of hydrogenation of isophorone [16]

To the best of our knowledge, the first report of enantioselective hydrogenation of a C=C bond with cinchona-modified catalyst was in 1985 [117]. Among several works since then, aliphatic and aromatic alkenoic acids are the two main types of probe molecules that have been investigated. Several groups have been working in this area. Nitta *et al.* mainly studied (E)-α-phenylcinnamic acid as the substrate, and have investigated reaction variables that affect the activity and enantioselectivity, such as polarity of solvent [50, 56, 57, 118], support texture [53, 54, 57, 119], preparation method of catalyst [53, 57], transition metal loading [52, 53], hydrogen pressure [120, 121], modifier structure [122, 123], substrate structure [42, 48, 124, 125], additives [118, 126], reaction and pretreatment temperature [119, 127] and other factors. Baiker and the co-workers have also been very active [128-143],

together with Bartok *et al.* [43, 46, 47, 144-147], Vaccari *et al.* [148, 149], and Garin *et al.* [150, 151].

Several main features and conclusions of C=C bond hydrogenations with cinchona alkaloid-modified metal catalysts are summarized below:

(i) Catalysts made by a precipitation method show a higher activity than those made by impregnation method, probably due to the detrimental effect of remaining anions (e.g. chloride) from the precursor [57].

(ii) Ni and Pt catalyst systems are much less effective for hydrogenation of C=C bonds compared to C=O hydrogenation [4, 152]. On the other hand, Pd is superior for catalyzing hydrogenation of C=C bonds in α, β-unsaturated carboxylic acids, although the selectivity is still relatively low [103, 120, 131, 143].

(iii) Both enantioselectivity and activity are strongly solvent dependent. For aromatic unsaturated compounds, increasing the dielectric constant (ε_r), (which partly reflects polarity of solvent), always leads to higher enantioselectivity. A contrary observation is that increasing the polarity of solvent leads to a decrease of the e.e. for 2-methyl-2-pentenoic acid [143]. Generally speaking, aromatic and aliphatic substrates have opposite behavior with respect to polarity of the solvent. This is most likely due to the different mode of adsorption on catalyst surface in the presence of π electrons from the aromatic ring. Polar solvents with higher solubility for aromatic substrate are preferable. Moreover, the addition of a small amount of water is also very effective for hydrogenation of aromatic substrate in terms of both enantioselectivity and activity [56]. This

is explained by the water affecting the desorption of product, which is proposed to be rate determining step of the selective reaction on the modified sites.

(iv) Reaction rates on unmodified Pd catalyst are much faster (ca. 10 times) than on cinchona-modified catalysts for C=C hydrogenation [126]. This is completely different than the hydrogenation of α-ketoester with cinchona-modified Pt, where reaction rates are enhanced dramatically with modifier present [153].

(v) The absolute configurations of the C8 and C9 positions in the modifier primarily determines the sense of enantioselective hydrogenation of C=C bond, which is similar to the hydrogenation of α-ketoesters [103]. Introducing methoxy group at C9 of cinchona alkaloid has a significant effect on both the sense and value of e.e. while alkylation of N atom of quinoclidine moiety has very little effect [122]. This phenomenon is also quite contrary with the hydrogenation of α-ketoesters with cinchona-modified Pt, where alkylation of N atom completely shuts down the enantioselectivity [114].

(vi) Nonporous or large pore size supports are favorable, due to the space needed to allow both modifier and substrate interaction on the metal surface, and to allow the formation of an intermediate complex that is required for enantioselectivity. In addition, alumina and titania supported catalysts are more favorable [57].

(vii) Unlike the promotion effect in the hydrogenation of α-ketoesters on cinchona-modified Pt catalyst, adding acid is not effective in promoting hydrogenation of unsaturated carboxylic acid contains C=C bond [122]. It is explained that the added acid interferes the acid-base interaction of substrate with modifier. On the other hand, addition of amine can increase the activity, with benzyl amine (BA)

being one the most effective additives (0.5-1.0 molar equivalent to the substrate) [126]. It is suggested that reactions on modified sites accelerate in the presence of BA due to effective desorption of hydrogenated molecules from such sites [118].

(viii) The effect of hydrogen pressure with respect to reaction rate and enantioselectivity is complicated. For example, the e.e. for hydrogenation of (E)-α-phenylcinnamic acid decreases with increasing hydrogen pressure up to 5MPa. However, for (E)-2-methyl-2-pentenoic acid, e.e. values slightly enhance along with increasing H_2 pressure up to 4 MPa [121]. Meanwhile, hydrogen pressure dependence of reaction rate is always explained in terms of adsorption of various substrates on both modified and unmodified sites.

2.3 Conformational and Adsorption Study of Cinchona Alkaloids

The interaction between chiral modifier and substrate is the key part in the enantioselective hydrogenation of C=O and C=C bonds. Since the steric structure of modifier plays an important role in interacting with substrate, it is necessary to introduce the behavior of modifier in terms of conformation and adsorption.

2.3.1 Conformational behavior of cinchona alkaloids

Cinchona alkaloids are plentiful in nature. They are isolated from the bark of several species of Cinchona and Remeyia trees [154]. Among the modified transition metal systems used to accomplish asymmetric induction, the cinchona alkaloid occupies a central position [155]. Figure 2.9 illustrates the structure of cinchona alkaloid and the derivatives.

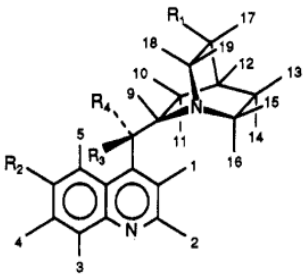

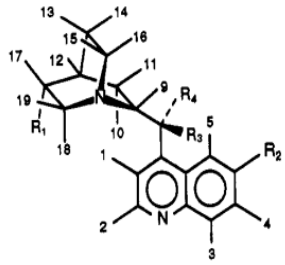

	R_1	R_2	R_3	R_4
quinine	C_2H_3	OCH_3	OH	H
cinchonidine	C_2H_3	H	OH	H
dihydroquinine	C_2H_5	OCH_3	OH	H
dihydrocinchonidine	C_2H_5	H	OH	H
epiquinine	C_2H_3	OCH_3	H	OH
benzoylquinine	C_2H_3	OCH_3	OBz	H
(p-Cl)- benzoyldihydroquinine	C_2H_5	OCH_3	pClBzO	H
chloroquinine	C_2H_3	OCH_3	Cl	H
deoxycinchonidine	C_2H_3	H	H	H

	R_1	R_2	R_3	R_4
quinidine	C_2H_3	OCH_3	OH	H
cinchonine	C_2H_3	H	OH	H
dihydroquinidine	C_2H_5	OCH_3	OH	H
dihydrocinchonine	C_2H_5	H	OH	H
epi quinidine	C_2H_3	OCH_3	H	OH
epidihydroquinidine	C_2H_5	OCH_3	H	OH
(p-Cl)-benzoyldihydroquinidine	C_2H_5	OCH_3	pClBzO	H
acetyldihydroquinidine	C_2H_5	OCH_3	OAc	H
(dimethylcarbamoyl)dihydroquinidine	C_2H_5	OCH_3	OCONMe	H
methoxydihydroquinidine	C_2H_5	OCH_3	OMe	H

Figure 2.9 List of cinchona alkaloid and the derivatives [154]

Addition of such kinds of molecules into an enantioselective catalyst system leads to preferential formation of an enantiomer. Their characteristics of intimate interaction and recognition are crucial to the success of being used as modifier. The first attempt to achieve asymmetric induction with these alkaloids was made in 1912 [156]. Benzaldehyde was reacted with hydrogen cyanide in the presence of quinine as a catalyst, to yield cyanohydrin with an e.e. of 20%. Over the past several decades, theoretical modeling [106, 157-160], along with experimental studies (NMR, NOESY, X-Ray, *etc.*) [154, 156, 161, 162], have revealed that cinchona alkaloids exhibit a very rich conformational behavior. The mechanism of asymmetric catalysis strongly depends on these various conformations. While a few groups [106, 157, 163] have performed theoretical investigations on conformational behavior of cinchona alkaloids, many of these studies ignored the solvent effects. In order to probe the intimate details of the mechanism of action of the cinchona alkaloids, a thorough understanding of their preferred conformation in solution is needed [158].

For example, Baiker *et al.* took solvent effects into consideration when investigating the conformational behavior of cinchonidine. Through NMR experiments and ab-initio calculations at the Hartree-Fock (HF) level using the 6-31G** basic set, it was found that conformations of cinchona alkaloids strongly depend on solvent [162]. Some of the most stable structural conformations, energies, and dihedral angles are shown in Figure 2.10, Figure 2.11, and Table 2.1, respectively. In general, "Open (3)" is most stable in apolar solvent, while "Closed (1)" and "Closed (2)" are more stable in polar solvents. The terms "Open" and "Closed" are commonly used when discussing different conformations. "Open" indicates that the quinuclidine N points away from quinoline ring, while "Closed" refers to the quinuclidine N pointing toward the quinoline ring. Kellogg, Wynberg and co-workers also showed via a molecular mechanics study that cinchona alkaloids can in principle adopt four different conformations: two "Open" conformations and two "Closed" conformations [156, 158].

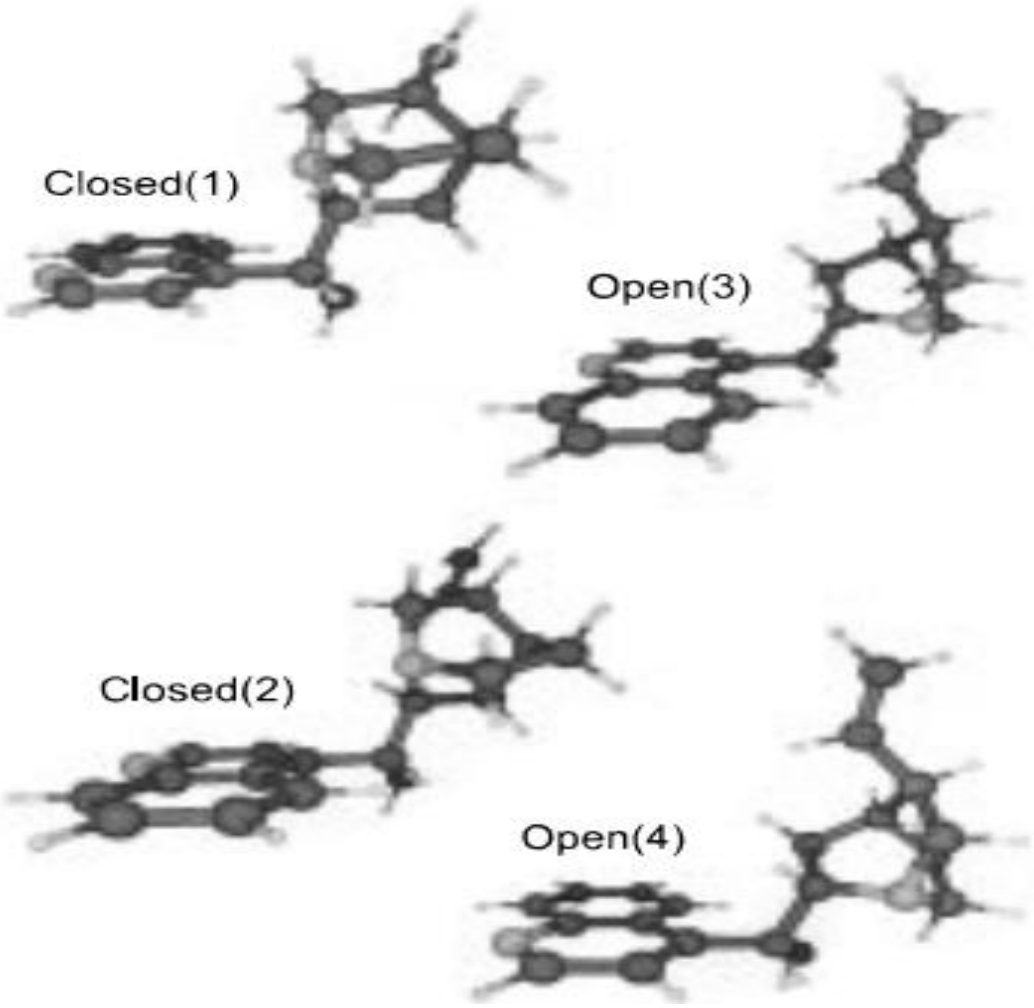

Figure 2.10 Four most stable conformations of cinchonidine based on HF level with 6-31G** basis set [162]

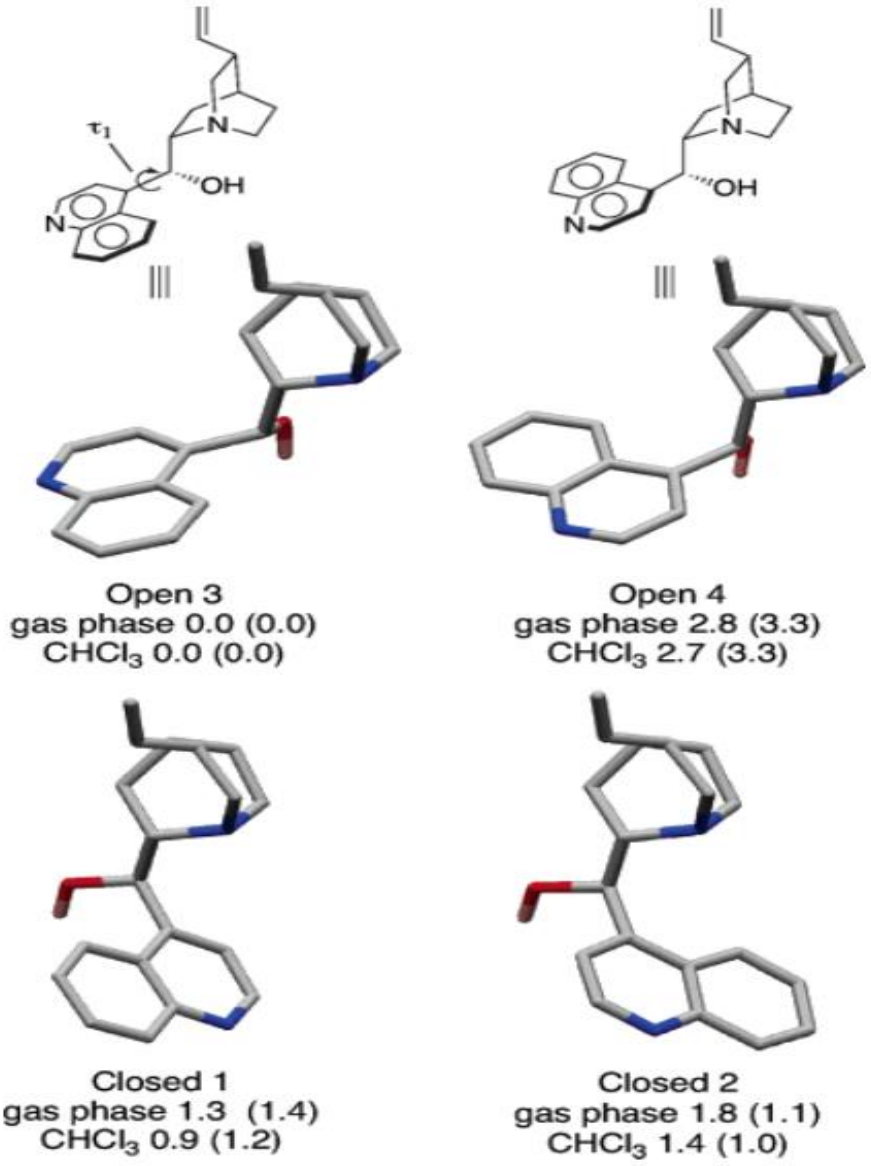

Figure 2.11 Structures and relative energies (kcal/mol) of low energy cinchonidine conformations B3LYP/6-31+G*/PCM (AMBER*/GB/SA/[$CHCl_3$]) [164]

Table 2.1 Calculated dihedral angles for several conformers of Cinchonidine[a] [162]

	Closed(1)	Closed(2)	Open(3)	Open(4)	Open(5)	Open(6)
τ_1	−107.0	80.4	101.4	−89.3	85.7	−98.7
τ_2	57.5	65.3	153.6	150.1	−48.6	−54.9
τ_3	−176.8	−172.5	−78.3	−77.5	76.2	74.0

[a] τ_1: $C_3-C_4-C_9-C_8$, τ_2: $C_4-C_9-C_8-N$, τ_3: $H_9-C_8-C_9-H_8$ (see Figure 1). Complete optimization is Performed at the ab initio Hartree−Fock level using a standard 6-31G** basis set.

In 2008, Baiker and co-workers revisited their previous study [165], and obtained similar results. According to systematic studies, three structural elements are crucial for determining the function of the cinchona alkaloids as chiral modifiers: (i) an anchoring part represented by flat aromatic ring system, which is believed to be responsible for adsorption onto the metal surface; (ii) the absolute configuration of C8 and C9, which controls the sense of chirality; (iii) a basic nitrogen atom that interacts with prochiral substrates [30, 166]. Among those studies, two important parameters appeared to have a central role in controlling the behavior of alkaloids: dihedral angles τ_1(C3-C4-C9-C8), and τ_2(C4-C9-C8-N) [162]. A systematic order of atom numbers and three dihedral angles of cinchonidine are shown in Figure 2.12, and this order will be used for the rest of proposal and later research.

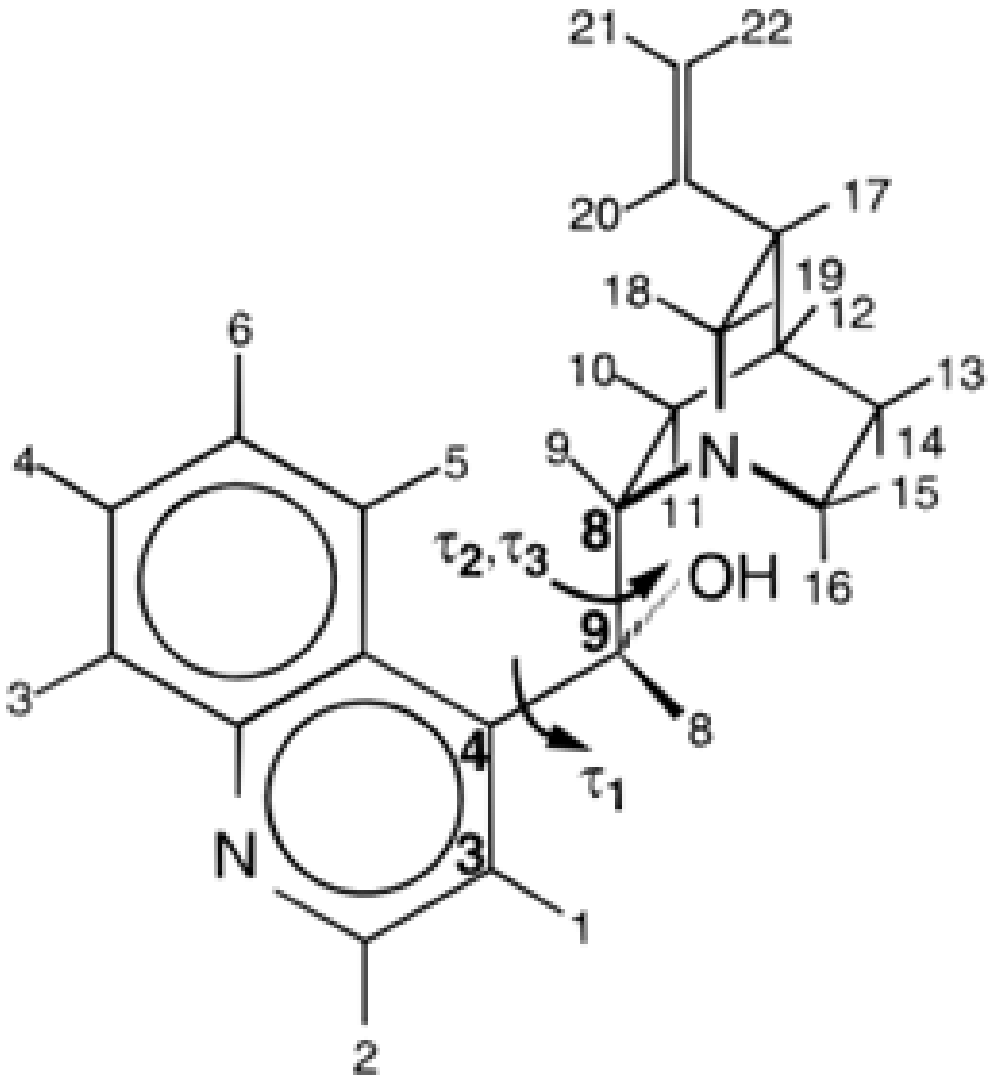

Figure 2.12 Cinchonidine atom numbering and definition of τ_1 τ_2 τ_3 dihedral angles [162]

2.3.2 Adsorption of cinchona alkaloids on metal surfaces

To better understand the mechanism that governs the enantioselective catalytic reaction, the adsorption behavior of the modifier on metal surfaces has been investigated. The adsorption of 10, 11-dihydrocinchonidine (DHC) on Pt (111) was studied by use of X-ray photoelectron spectroscopy (XPS) and low-energy electron

diffraction (LEED) under UHV condition [36, 113, 167]. Wells *et al.* found no absorbate-induced LEED pattern for dihydrocinchonidine or quinoline, at either room temperature or higher temperature. This showed that the adsorption of such molecules and likely related alkaloids on Pt (111) is not ordered [36, 167]. Wells *et al.* also used mass spectroscopy (MS) and ^{1}H NMR to show that H-D exchange occurred at the hydroxyl group, the H atom at C9 and all positions of quinoline system, but not within the quinuclidine ring system [168]. The most rapid exchange occurred at the H-1 and H-3 positions, while the slowest occurred at H-5 (see in Figure 2.12).

Such UHV-based studies indicated that the quinoline moiety of the molecule was lying parallel to the metal surface through a π-electron interaction at room temperature, and became tilted at 323K [169]. However, up until the end of the last century, there was no information regarding the surface of chiral-modified metals under conditions approaching those of the actual reaction conditions (i.e. liquid phase, elevated H_2 pressures). Development of *in-situ* spectroscopic techniques has made it possible to begin to address this situation over the past decade and moving forward. For example, attenuated total reflection infrared (ATR-IR) spectroscopy has made it possible to detect the adsorption of cinchona alkaloids on supported Pt, Pd and Au under reaction condition [166, 170-175]. Williams and co-workers investigated polycrystalline Pt surfaces using surface enhanced raman spectroscopy (SERS) to study cinchonidine adsorption in ethanol solvent [176]. Wang *et al.* also utilized *in-situ* STM to study the adsorption of cinchonidine on Cu (111) in an aqueous solution of 0.1M $HClO_4$ and 0.1mM cinchonidine, and showed that the

modifier could form a long-range ordered adlayer on top of Cu surface [177], in contrast to the previous UHV studies on Pt(111).

To summarize the *in-situ* studies available to date, the quinoline moiety is the responsible function group for the adsorption on the metal surface. This adsorption behavior is strongly concentration (i.e. coverage) dependent in the presence of solvent. There are three regimes depending on the solution concentration: (i) at low concentration (10^{-6}~10^{-7}M), a flat-lying mode prevails in which the long axis of the quinoline moiety is parallel to the surface; (ii) at higher concentration (~10^{-5}M), the quinoline rings tilt with the increasing concentration/coverage, with two other species (α-H abstracted and N lone pair bonded cinchonidine) observed. (iii) at high concentration (10^{-4}~10^{-3}M), all three species coexist on the surface, and a slow transition occurs from α-H abstracted cinchonidine to more N lone pair bonded cinchonidine at increasing cinchonidine concentration [172]. The suggested adsorption mechanism of cinchonidine as described above is shown in Figure 2.13.

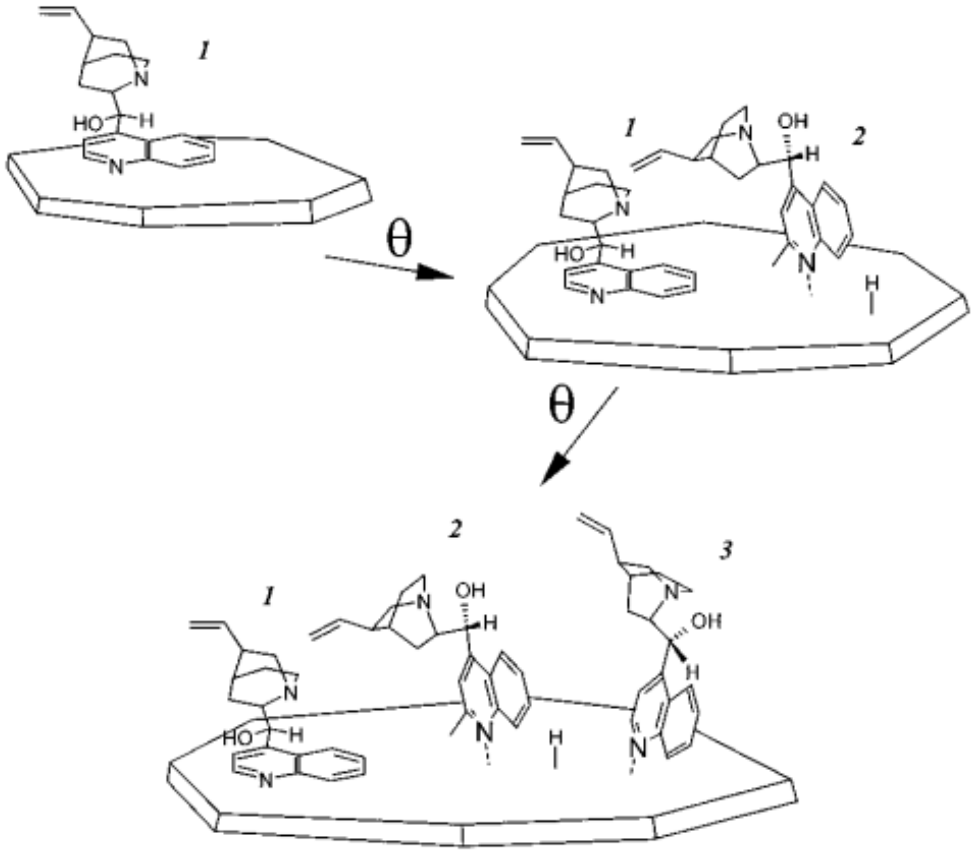

Figure 2.13 Suggested Adsorption Mechanism of Cinchonidine on Pt/Al_2O_3 at 283K from ATR-IR (θ is surface coverage, species 1: π-bonded, 2: α-H abstracted, 3: N lone pair bonded) [172]

2.4 Spectroscopic Technique

Fourier transform infrared (FT-IR) spectroscopy has been proved to be an effective approach to characterize molecular components in solid, liquid, and gas phases, providing valuable information about chemical forces between atoms, and vibrational frequencies of molecules [178]. Attenuated total reflection infrared (ATR-IR) spectroscopy is one of the most powerful tools available currently for study of solid-liquid interfaces, and has been developed in the area of heterogeneous catalysis since the late 1990s [179, 180]. ATR-IR provides a means of examining the

solid sample without changing the characteristics of the surface. This most attractive feature allows us to investigate *in-situ* the sample at the interface while avoiding (or at least diminishing) the signal from bulk liquid.

Consider a two-phase system containing an interface, where one side is an internal reflection element (IRE) with higher refractive index (n_1), and the other side a thin film contacting the crystal element with a lower refractive index (n_2). In ATR-IR, an infrared beam is passed through the IRE with an angle that is at or greater than the critical angle, θ_c, where

$$\sin(\theta_c) = n_2 / n_1 \qquad \text{Equation 2.1}$$

With this arrangement, the beam will undergo total internal reflection at the interface. Every time that the IR beam reflects from the interface, an evanescent electric field (radiation) is produced at that spot and penetrates into the sample, decaying exponentially with distance into the rarer medium. The radiation is absorbed within the sample, and an absorption spectrum of the sample is obtained.

Since the goal of ATR-IR is to measure a catalyst sample at the interface, and avoid (or decrease) pure bulk liquid, the sample should be at least three times thicker than the penetration depth (d_p). This is quantity defined as the depth required that the strength of electric field decays to e^{-1} (37%) of its value at the surface. The value of d_p is always on the order of a micrometer for mid-infrared measurements.

$$d_p = \frac{\lambda}{2 * \pi * n_1 * (\sin^2 \theta - n_{21}{}^2)^{1/2}} \qquad \text{Equation 2.2}$$

In the equation above, λ is the wavelength of the IR beam, n_{21} is the ratio of n_2 over n_1, and θ is the incident angle. The penetration depth (d_p) of a system can therefore be controlled by either changing the angle of incidence (θ) or the

composition of the crystal element. Typical crystals for ATR-IR are made of zinc selenide (ZnSe), germanium (Ge), zinc sulfide (ZnS), silicon (S), and diamond, *etc*, and all have different refractive indices. In the research described in this dissertation, ZnSe has been chosen.

ATR-IR is currently one of the very few available techniques that allows for *in-situ* investigation of solid/liquid interfacial processes and phenomena. Information about the nature of adsorbed species can be readily acquired, often together with details of orientation of adsorbate, adsorption/desorption equilibrium, and kinetics [179]. For the past 25 years, a huge amount of literature concerns the utilizing the ATR-IR technique to *in-situ* investigate interfacial phenomena have been published. As to the full theory and applications of ATR-IR regarding the surface and interface in more detail, the reader is referred to several review articles [178, 179, 181]. Figure 2.14 depicts that IR beam route within the IRE.

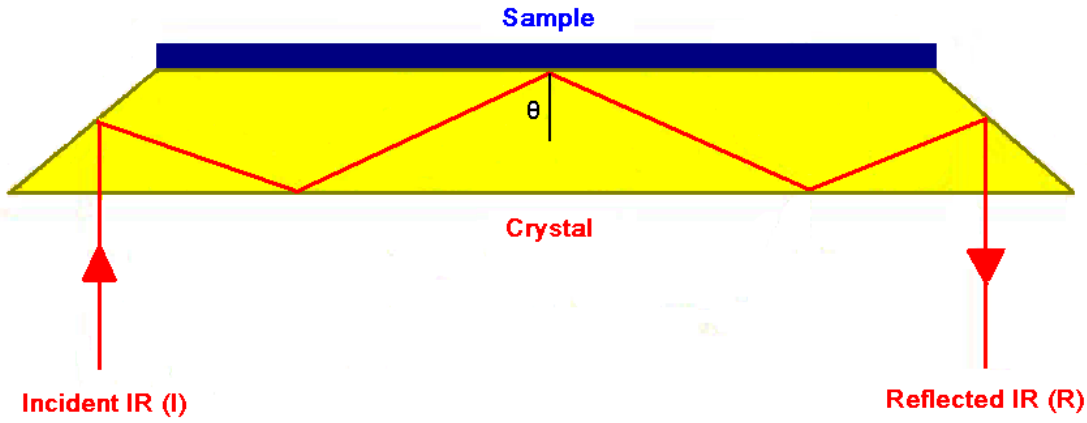

Figure 2.14 Description of beam route within the IRE

3. Experimental

3.1 Materials

Trans-2-methyl-2-pentenoic acid (Figure 3.1, 98%, SAFC), cinchonidine (CD, Figure 3.1, 98.0%, Fluka), 2-methyl-2-pentene (98%, Aldrich), dichloromethane (99.9%, Sigma-Aldrich), methanol (99.9%, Alfa-Aesar), 1, 4-Dioxane (99.9%, Sigma-Aldrich), 5 wt% Pd/γ-Al_2O_3 powder (Alfa-Aesar), $PdCl_2$ (99.9%, Alfa-Aesar), $Pd(NO_3)_2$ (99.9%, Alfa-Aesar) and γ-Al_2O_3 powder (99.5%, BET surface area=45m^2/g, diameter=37nm, Alfa-Aesar) were used as received. H_2 (UHP), N_2 (UHP), He (UHP), Ar (UHP), O_2 (UHP), CO (UHP), 1% CO/He (UHP), 10% O_2/He (UHP), 10% H_2/Ar (2000Psi), and 20% H_2/N_2 (2000Psi) were supplied by Airgas. Deionized water (18 MΩ) was obtained using a Barnstead water system with nano-pure and B-pure filter.

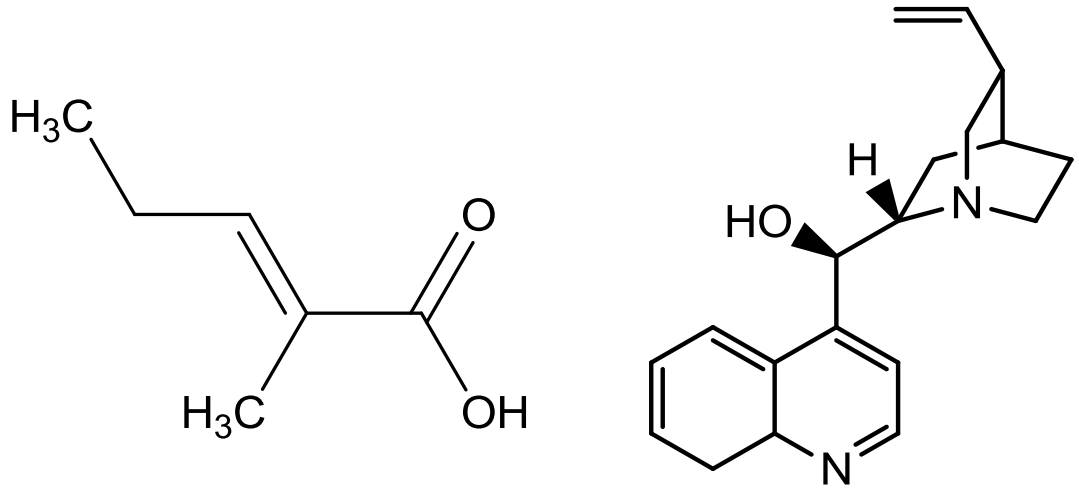

Figure 3.1 Structure of *trans*-2-methyl-2-pentenoic acid (left) and cinchonidine (right)

3.2 Catalyst Preparation

A 1 wt% Pd/γ-Al_2O_3 catalyst was synthesized using wetness impregnation method with H_2PdCl_4 as precursor. The Al_2O_3 support with small particles size (37 nm) was chosen based on known compatibility with ATR-IR experiments [182]. Supports with larger particle sizes (e.g. >1 nm) led to a poor adhesion of the catalyst film on the ATR element. The dried impregnated catalyst was calcined in a furnace with air at 400 ℃ for 4 hours. Then, a sample was measured with H_2-chemisorption, the remaining catalyst was reduced in H_2 for 1 hour at 300 ℃, followed by cooling down in a He flow. After reduction, the catalyst was washed with excess DI water to remove any ions and impurities (at least more than 2 L DI water to wash 1 g catalyst) and was measured by high-resolution transmission electron microscopy (HR-TEM). Figure 3.2 is a sketch of the procedure of making catalyst and measurement.

Figure 3.2 Sketch of procedure of making catalyst and measurements

3.3 Catalyst Characterization

3.3.1 Atomic Absorption Spectroscopy

Atomic absorption spectroscopy (AAS) was used to determine actual Pd metal content of the synthesized catalyst. The deposited Pd particles were removed from the support by dissolving ca. 0.1g catalyst samples in a digestion solution in Teflon vials. The digestion solution contains 6-7 ml of aqua regia (volume ratio

$HCl:HNO_3$=6:1). Then, the capped vials were put into Precision Scientific Econotherm laboratory oven, while the temperature was kept at 130 ℃ for 5 hours. Next, the vials were removed from the oven and the caps were loosened immediately to avoid contraction on the Teflon vials and were cooled to room temperature. These solutions were then diluted to 25 ml using DI water. The samples were allowed to settle down overnight. Then, 5 ml of the top solution was transferred with a pipette and placed in a 40 ml disposable centrifuge vial. The solutions were diluted with blank solution (contains 5% HCl, and 0.5 wt% La) into 30 ml. At least three samples of the catalyst were digested and measured with AAS.

Samples were analyzed by using a Perkin Elmer AAnalyst-400 Atomic Absorption Spectrometer. Pd calibration standards were made from a purchased 1000 ppm Pd stock solution (Sigma Aldrich) containing 5% HCl. The calibration curves were obtained for 0, 1, 2, 5, and 10 ppm Pd solutions. The calibration curves were verified by the use of a check standard from a different source (5 ppm). As to the preparation of blank solution, see Appendix.

3.3.2 H_2-Chemisorption

A pulse H_2-chemisorption analysis can determine the active surface area, metal dispersion, and the average particle size by applying measured doses of reactant gas to the sample. The gas reacts with each active site of Pd particles until all sites have been occupied. Once all the active sites have completely reacted, the discretely injected gas volumes emerge from the sample tube unchanged. The amount of chemisorbed gas is the difference between the total amount of reactant gas injected and the amount that emerged from the sample.

H_2-chemisorption studies were performed with an AutoChem II 2920 chemisorption analyzer from Micromerities. The H_2 and O_2 applied in the experiments passed through moisture traps and O_2 scrubbers (Restek). Approximately 0.1 g of catalyst was loaded in a fix-bed quartz reactor. The catalysts were reduced in pure H_2 flow at 200 ℃ for 1 h, and then purged with Ar for 1 h. The chemisorption experiments were performed when the sample was cooled down to 40 ℃ with 10% H_2/Ar at a flow rate of 50 cm^3 STP/min. During the H_2 chemisorption, the H atoms adsorbed on both surface site, and perhaps in the bulk phase. Then, 10% O_2/He was applied to replace all the surface species, while not the bulk H (β-hydride). Finally, H_2 was applied again to titrate the surface-adsorbed O atoms. The stoichiometry was assumed to be 2 Pd sites per each H_2 chemisorbed. In this way, the total amount of surface adsorbed atoms can be determined. Figure 3.3 shows this O_2-H_2 titration.

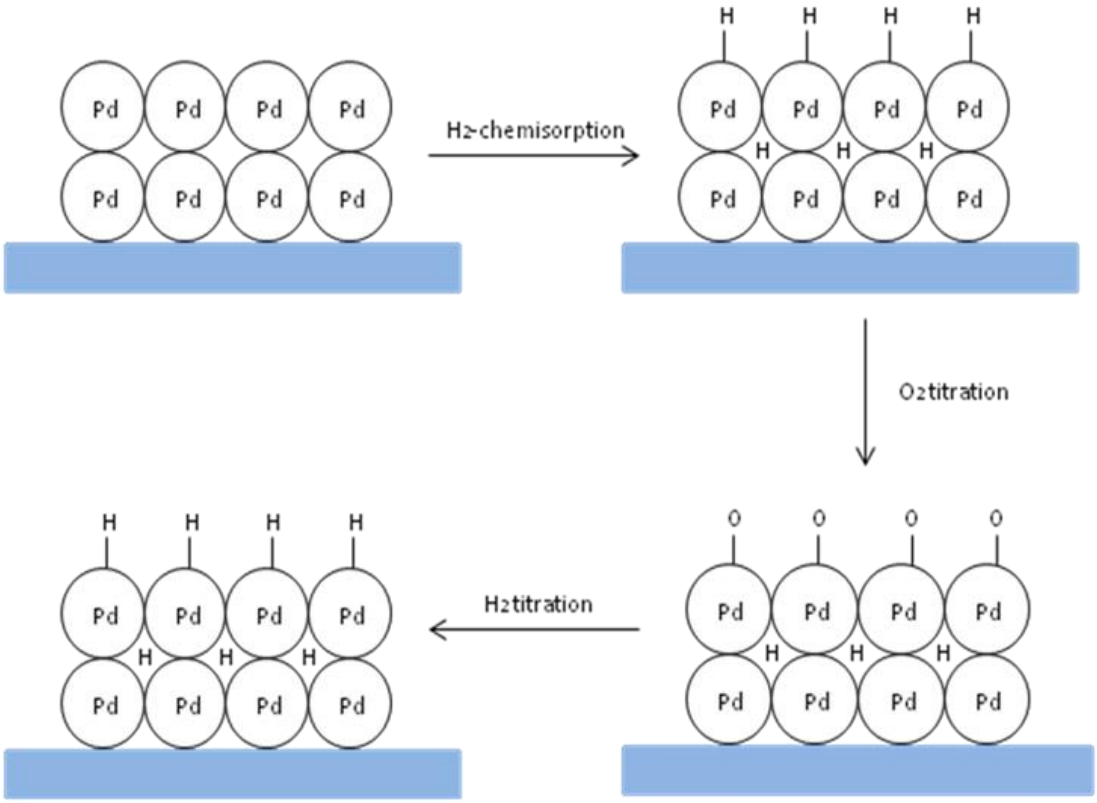

Figure 3.3 Schematic view of H_2-chemisorption and O_2 titration

Figure 3.4 shows the detailed steps within the H_2-chemisorption, together with the state of Pd in every step. Dispersion and thus estimated particle size are calculated at the steps with light blue background.

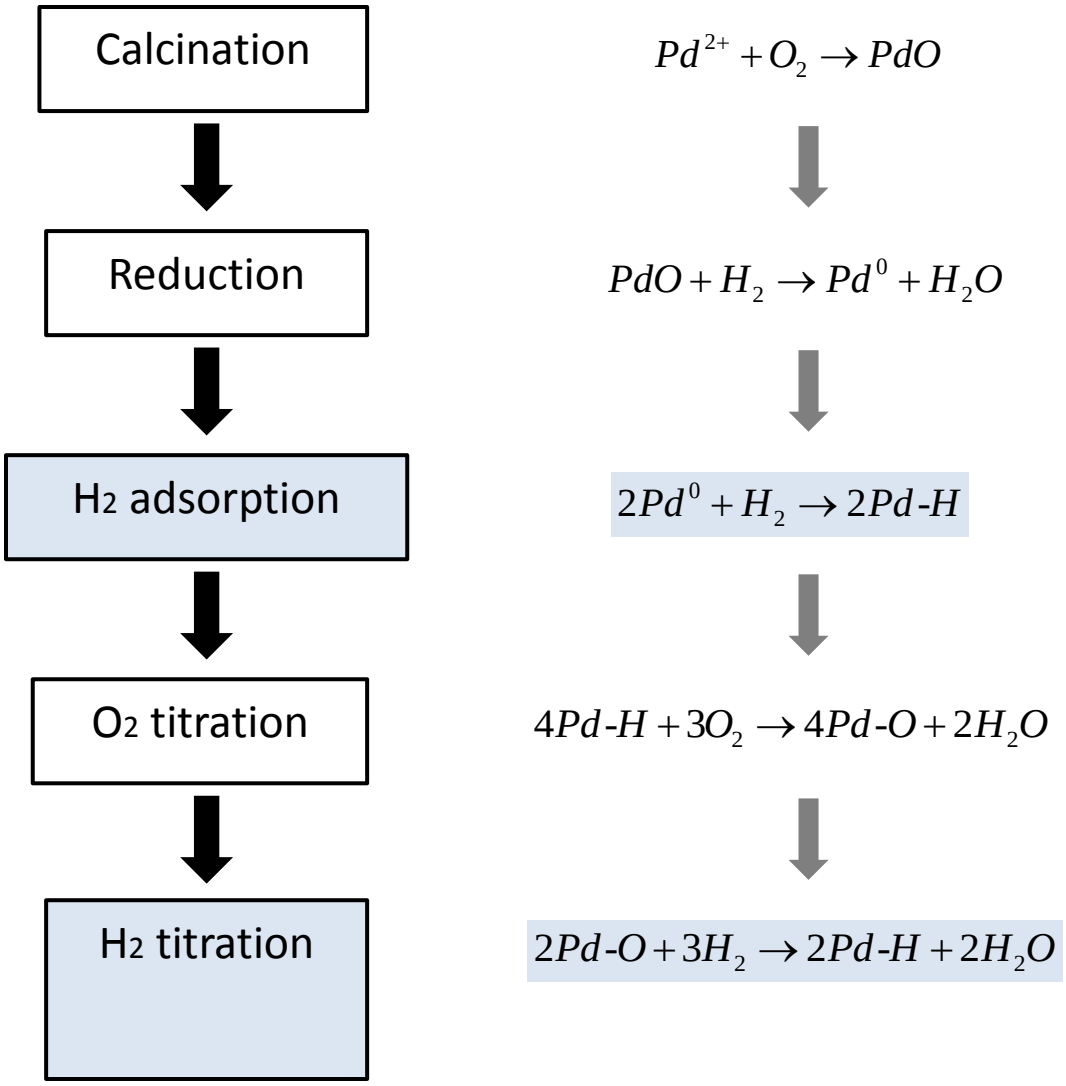

Figure 3.4 Depiction of steps of H_2-chemisorption and various Pd states

To test the influence of pretreatment temperature on metal dispersion and particle size, the catalysts were reduced again in H_2 at 300 ℃ and 400 ℃ respectively, and the titration procedure repeated. Several equations have been applied to the data collected in the chemisorption measurements, and to calculate the metallic dispersion values. They are:

1) Percent dispersion (PD) is calculated by

$$PD = 100(\frac{V_s \times SF_{calc}}{SW \times 22414})GMW_{calc}$$ Equation 3.1

where V_s is H_2 volume sorbed (cm^3 at STP), SF_{calc} is calculated stoichiometry factor, SW is sample weight (g), and GMW_{calc} is gram molecular weight (g/g-mole).

2) The stoichiometry factor (SF_{calc}) is calculated by

$$SF_{calc} = GMW_{calc} \times \sum_i (\frac{F_i \times SF_i}{W_{atom,i}})$$ Equation 3.2

where SF_i is stoichiometry factor for metal i, $W_{atom,i}$ is gram molecular weight of metal i (g/g-mole), and F_i is the fraction of sample weight for metal i.

3) The gram molecular weight (GMW_{calc}) formula is

$$GMW_{calc} = \frac{1}{\sum_i (\frac{F_i}{W_{atom,i}})}$$ Equation 3.3

4) The active particle size (APS) is calculated by the following equation

$$APS = \frac{6}{D_{calc} \times \frac{SW}{GMW_{calc}} \times 6.023 \times 10^{23} \times SA_{calc}}$$ Equation 3.4

where D_{calc} is the calculated metal density (g/cm^3), and SA_{calc} is the calculated specific surface area (per gram of metal).

5) The metal density (D_{calc}) is estimated by:

$$D_{calc} = GMW_{calc} \times \sum_i (\frac{F_i \times D_i}{W_{atom,i}})$$ Equation 3.5

where D_i is density of metal i.

6) The calculated specific surface area (SA_{calc}) formula is

$$SA_{calc} = GMW_{calc} \times \sum_i \left(\frac{F_i \times SA_i}{W_{atom,i}}\right) \qquad \text{Equation 3.6}$$

where SA_i is cross-sectional area of metal i.

3.3.3 High-Resolution Transmission Electron Microscopy (HR-TEM)

HR-TEM measurements were carried out in the Electron Microscopy Center at University of South Carolina by using JOEL 2100F electron microscope operating at 200KeV. The supported Pd catalysts were ultrasonically dispersed in ethanol solution prior to their deposition onto a copper grid covered by carbon support film. Then, the mounted samples were analyzed using a dry methodology where the grid was physically exposed.

The particle size distributions were obtained by measuring a minimum of 250 randomly selected particles from at least 15 different micrographs. Each particle was measured in both x- and y-direction lengths, and then those values were averaged. The length was measured in unit of pixels, and then converted into nm by calibrating the scale bar at each image. Finally, Anderson's standard equations were used to calculate for volume-area mean diameter [183].

$$D_{avg} = \frac{\sum_i^n n_i D_i^3}{\sum_i^n n_i D_i^2} \qquad \text{Equation 3.7}$$

Where D_{avg} is average particle size, n_i is the number particles and D_i is the measured diameter.

3.3.4 FT-IR of CO Adsorption

Spectroscopic techniques have been successfully applied in examining the adsorption of CO on transition metal catalysts [184-186]. The adsorption of CO in gas phase (mostly under UHV condition) has been investigated extensively [187, 188]. Moreover, CO adsorption at solid-liquid interfaces has been examined for both metal electrode-aqueous solution system [189, 190] and with ATR-IR. As a result, CO is a good probe molecule to examine the quality of Pd/Al_2O_3 catalysts at solid-liquid interfaces with ATR-IR spectroscopy.

The gas phase FT-IR studies for CO adsorption were performed with a Nicolet 4700 spectrometer equipped with a KBr beam splitter and a liquid nitrogen-cooled MCT detector. The spectra were collected with 64 scans and 4 cm^{-1} resolution. A 10 cm long cylindrical gas flow transmission cell, made of stainless steel, was used in the study. The cell was equipped with a flowing water-cooling system, gas inlet/outlet, thermocouple, and pressure gauge, with both ends were capped with IR-transparent NaCl windows. Estimately, 50mg of sample catalyst was pressed into a pellet (at pressure of ca. 3 Metric Tons for 40 seconds) with diameter of ca. 12mm using a Carver Laboratory Press, and loaded in sample holder. Then the sample holder was put in the flow cell (close to thermocouple) and sealed. A heating tape was wrapped around the cell allowing heating the sample. The temperature profile was programmed by an Omega CN 76000 temperature controller. A side view of flow cell for gas phase CO adsorption study is shown in Figure 3.5.

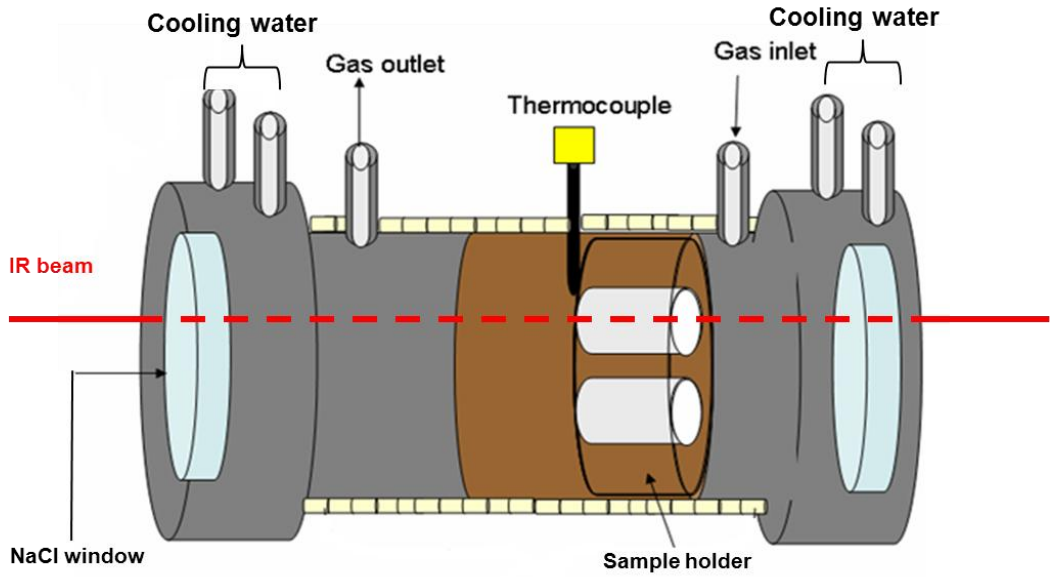

Figure 3.5 Schematic of flow cell for gas phase CO adsorption

Prior the exposure of catalyst pellet to CO, the sample was *in-situ* reduced according to the following activation protocol: First, He flow was introduced into the cell to flush away the air in the system. Then H_2 pretreatment was applied at 300 ℃ for 1 hour. Finally, the flow cell was naturally cool down to room temperature in a He flow followed with a background spectrum collection. After that, a 1% CO/He mixture was flowed through the catalyst pellet for 40 min to reach a surface saturation of adsorbed CO molecule, followed by He for an additional 15 min to purge CO gas phase in the system and remove weakly bonded CO species. Meanwhile, the FT-IR spectra were continuously collected until there was no further change of observed peak features.

3.4 Thin Film Preparation

Before film preparation, the ZnSe internal reflection element (IRE) was cleaned with a polishing cloth in 0.3 and 0.05 μm alumina suspensions and flushed with deionized water. Catalyst powders were prepared for ATR-IR studies by deposition as a thin film on a ZnSe internal reflection element. Specifically, 25 mg of Al_2O_3 or Pd/Al_2O_3 powder was mixed with 20 ml DI water in a glass bottle to form a suspension. The suspension was placed into an ultrasonic bath to sonicate overnight to decrease any agglomeration in solution. Then, the suspension was dropped onto a 70×10×3 mm ZnSe internal reflection element (Spectral Systems, 60 degree) to form a uniform liquid layer and dried out under room conditions (20 ℃ and 1 atm air). This step is repeated 4 times, leading to a powder film with ca. 10±2 μm thickness, which was measured using an Olympus XX microscope with an 80X long working objective. The coated ZnSe was rubbed off in a section, and then the relative difference in height between the top of the film and the ZnSe surface was measured using the fine adjustment of the microscope. The fine adjustment knob was calibrated using quartz coverslips of known thickness. This thickness ensures that all of the infrared electric field is attenuated within the thin film, since the penetration depth is on the order of 1-3 microns depending on the infrared wavelength. The stability of the film under liquid flow has been demonstrated previously [182]. The resulting Al_2O_3 and Pd/Al_2O_3 films were stable on the ZnSe element in the presence of flowing solvent (e.g., CH_2Cl_2 and MeOH) for at least 24 hours.

3.5 ATR-IR Spectroscopic Study

Reactant/solvent mixtures and pure solvent were stored in different three-neck round-bottom flasks with magnetic stirrers. Teflon tubing was used due to chemical resistance to both the solvent and reactants/products. A home-made aluminum flow cell was used together with an ATR accessory (ThermoNicolet) for *in-situ* spectroscopic measurements. The flow cell had a channel of 1.1 cm^3 to let liquid pass over the surface of the element, and was gasket-sealed with an O-ring. The different liquid solutions were pumped with a flow rate of 20 ml/min into the flow cell according to a scheduled time-concentration profile by using Labview software (see Figure 3.6). The schematic of the flow cell accessories and ATR-IR system have been discussed elsewhere [182]. A flow chart of ATR-IR system was depicted in Figure 3.7 with an insertion of the detailed view of flow cell accessories.

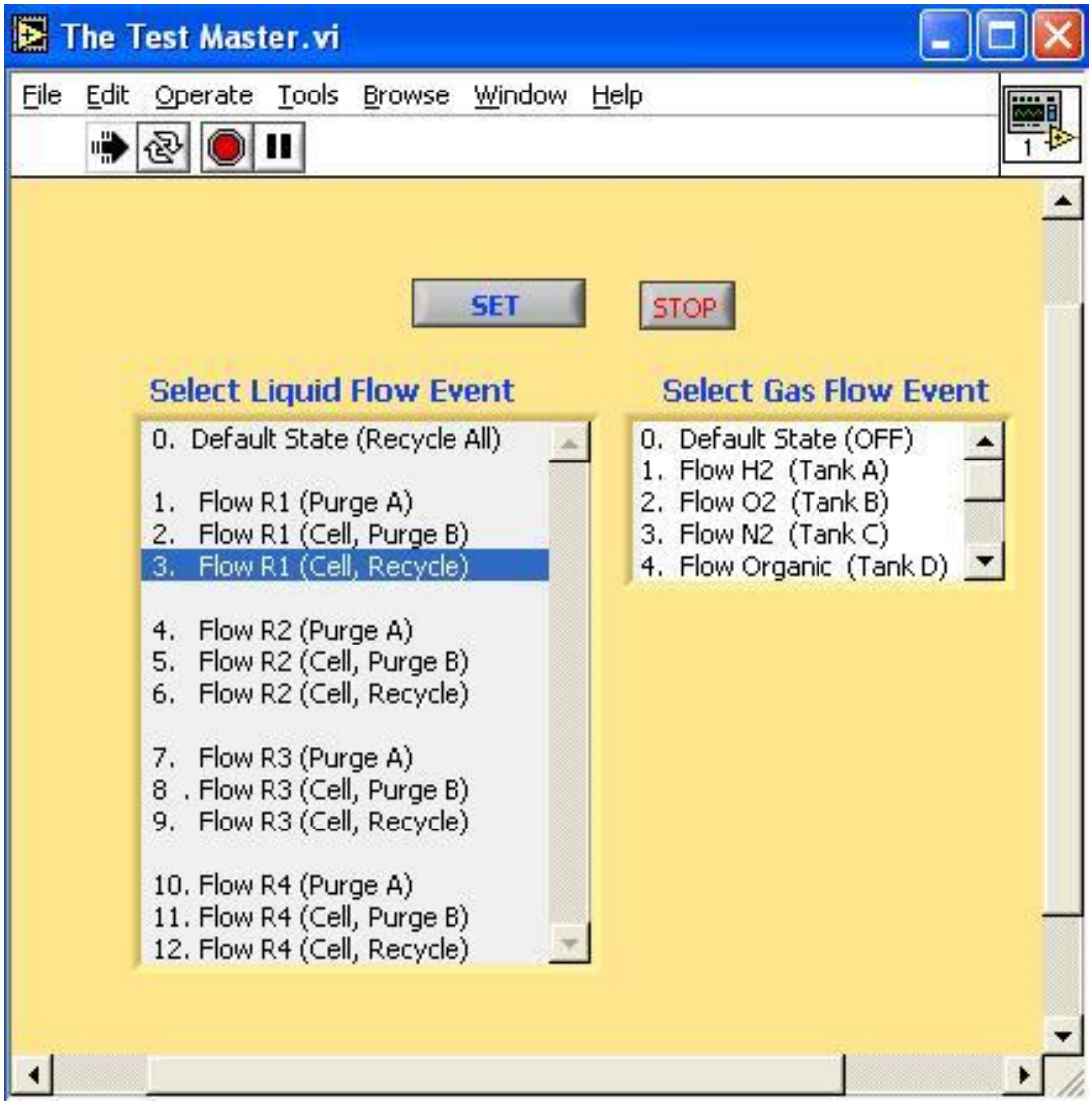

Figure 3.6 Screenshot of Labview software

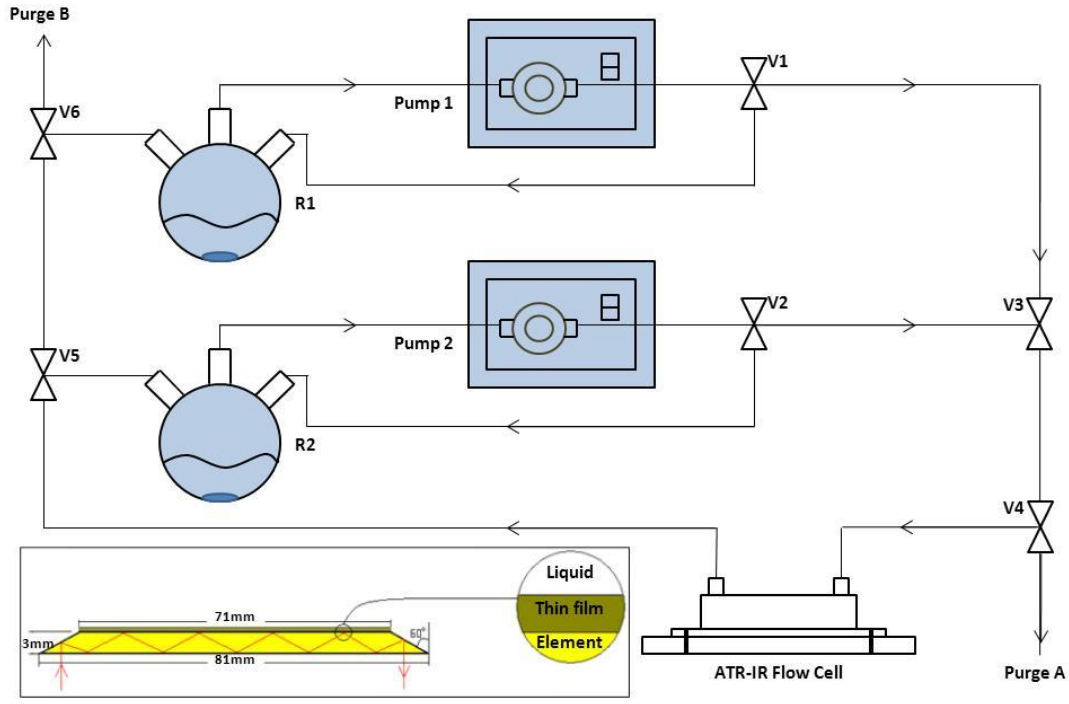

Figure 3.7 Description of flow chart of reaction system with side view of flow cell and accessories

In-situ ATR-IR spectra were obtained by using a Nicolet 670 Fourier transform infrared spectrometer with a liquid nitrogen-cooled MCT detector. Before collection, pure solvent was flowed through the flow cell for at least 2 hours in order to remove any contaminants and let the system reach a stable signal. The background was then collected in the pure solvent flow. Spectra consisted of 128 scans with 4 cm^{-1} resolution, and were recorded every two and half minutes. All experiments were performed at room temperature (20 ℃). The flow of acid solution and pure solvent through the cell were controlled by switching the valves in the system.

3.6 Batch Reaction System

Hydrogenation reactions of MPeA were carried out in a stainless steel EZE-Seal® batch reactor with 100 ml capacity from Autoclave Engineers, which is equipped with a K-type thermocouple, a pressure gauge and a stirring motor from Leeson SpeedMaster. In addition, water pipes ensure that the motor remains cool. Finally, a six-port valve and gas pipeline allow for purging of the gas and sampling of the liquid reaction mixture. This batch reactor can withstand the reaction temperatures from -29 ℃ to 450 ℃, with gas pressures up to 3300 Psi. A picture and schematic of the batch reactor system are shown in Figure 3.8 and Figure 3.9 respectively. A detailed description of 6-way valve is also shown in Figure 3.10.

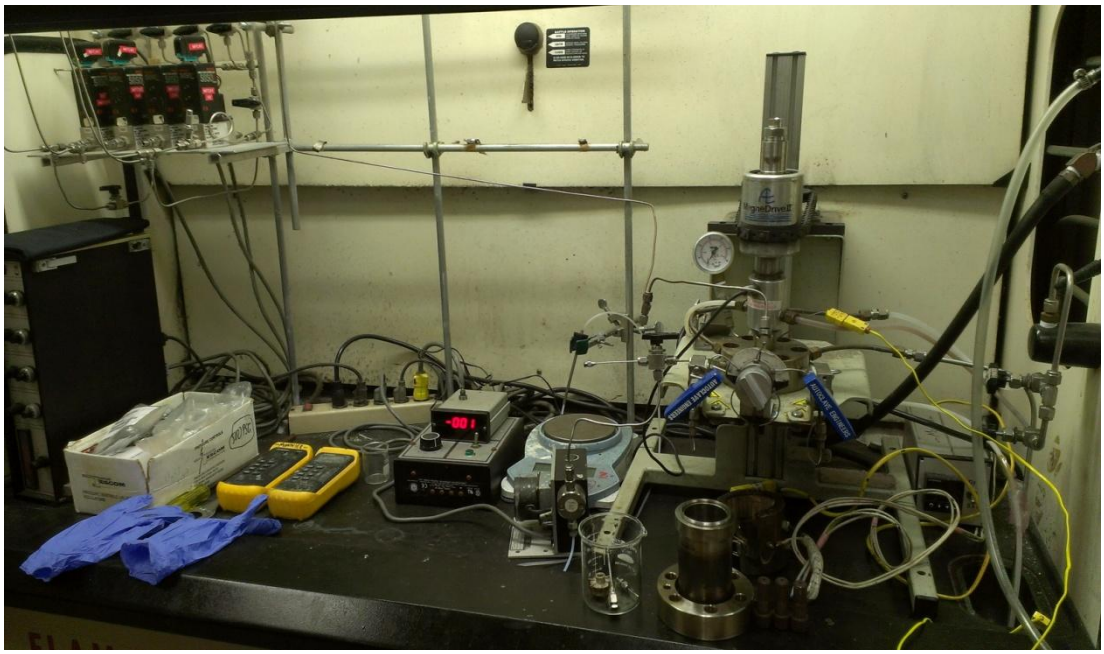

Figure 3.8 Picture of Autoclave reactor system

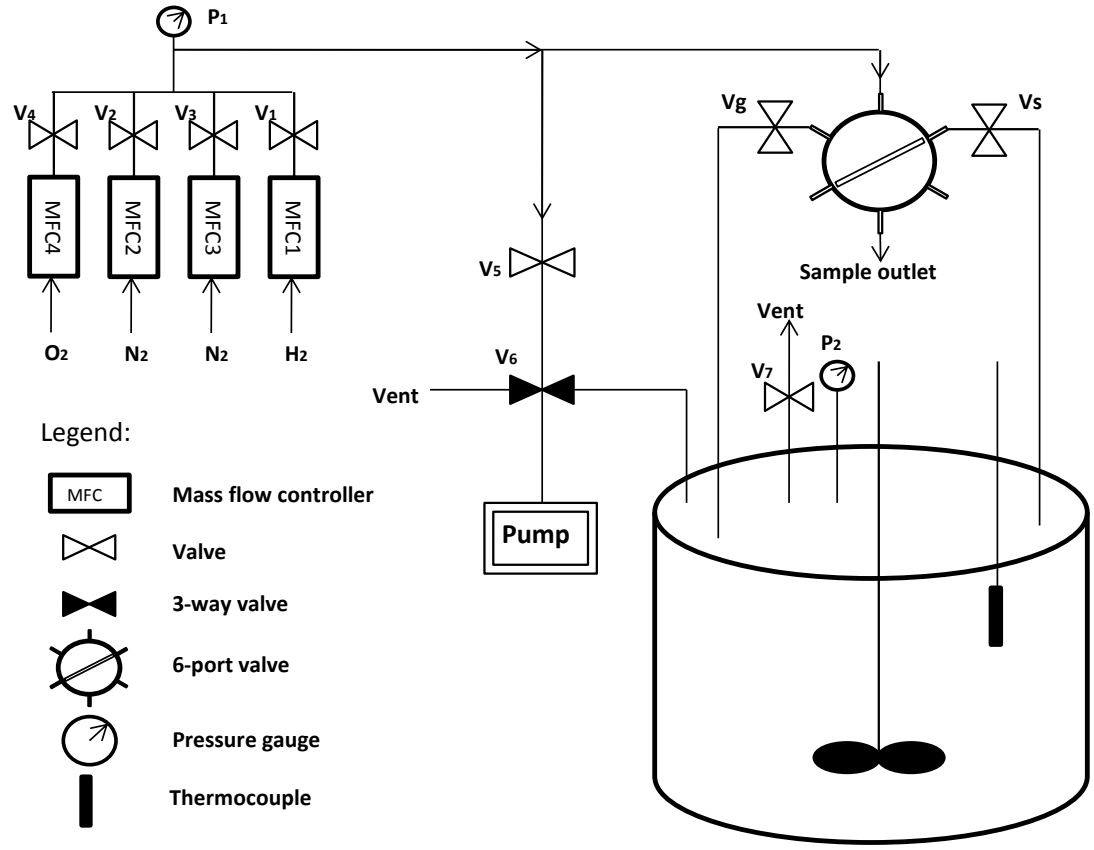

Figure 3.9 Schematic of hydrogenation reaction system

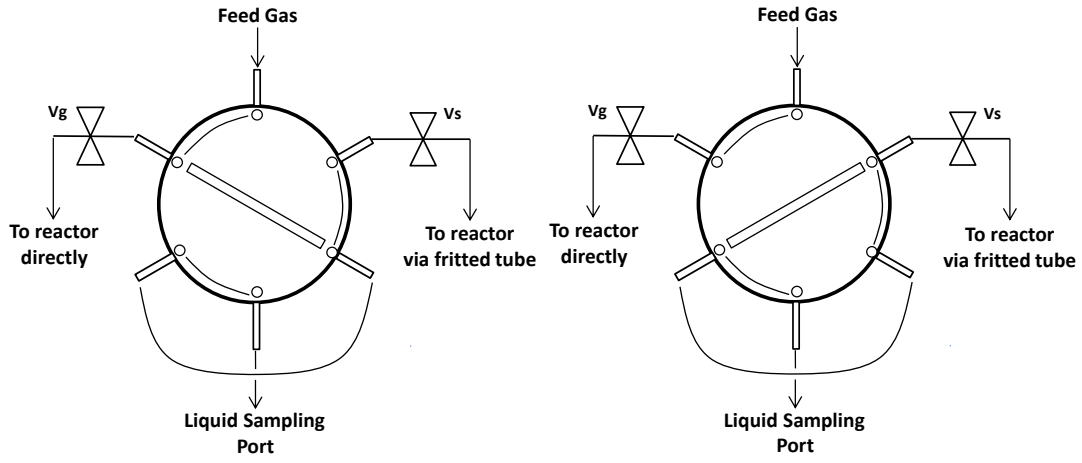

Figure 3.10 Detailed description of 6-way valve

In a typical reaction, the reactor was loaded with 60 ml solvent, 700 µl substrate (MPeA), and 0.05g catalyst. For enantioselective hydrogenation, 0.088g modifier (CD) was added into the reactor. In this way, the modifier/reactant ratio is fixed at ca. 1/20, which is a typical ratio for this kind of asymmetric hydrogenation [144]. After sealing, a leak check using 200 psi N_2 was performed three times, followed by three pressure/vent cycles in order to remove any residual oxygen from the system. The water-cooled stirring motor was set at a rate of 1000 rpm based on rate measurements made at varying speeds, and was chosen to ensure that reactions were carried out free of external mass transfer limitations. The reaction was then initiated by an introduction of H_2 into the reactor. The temperature of the liquid in the reactor was monitored with the thermocouple in real time during the reaction, and had a maximum deviation of 1-2 ℃.

3.7 Gas Chromatography (GC) Analysis

The samples collected from the batch reactor at different reaction times were injected automatically with a Hi-Tech 300A liquid auto sampler from Overbrook Scientific. The quantitative analysis of the product mixture was performed using a Hewlett Packard 5890 Series II gas chromatograph with a flame ionization detector (FID), equipped with an HP-chiral-20B capillary column (30 m length, 0.25 mm ID, 0.25 µm film, 30-250 ℃, part number: 1909G-B233) from Agilent J&W Technologies. According to the literature, the (S)-product of 2-methylpentanoic acid is in excess [145], and the enantiomeric excess (e.e.) value was calculated with the equation: e.e.(%)=100*([S]-[R])/([S]+[R]). A multi-step temperature profile for analyzing the reaction mixture was developed for best performance in separating the

chemicals and is shown in Figure 3.11. To be specific, the column was initially set as 40 ℃ when the sample was injected. After 1 min, the temperature was increased to 110 ℃ at a ramp of 10 ℃/min, followed by 10 min holding time. Then, a second ramp of 20 ℃/min was applied until the column reached 240 ℃ for 5 min. Generally speaking, the solvent (MeOH) peak appears at ca. 1.67 min, the internal standard (CH_2Cl_2) peak shows at ca. 2.08 min, two peaks of enantiomer products show up at ca. 14.8 min and 15.5 min, respectively, and the substrate (MPeA) peak comes out at ca. 18.5 min. The gas chromatography was printed out with a Hewlett Packard 5890 Series Integrator.

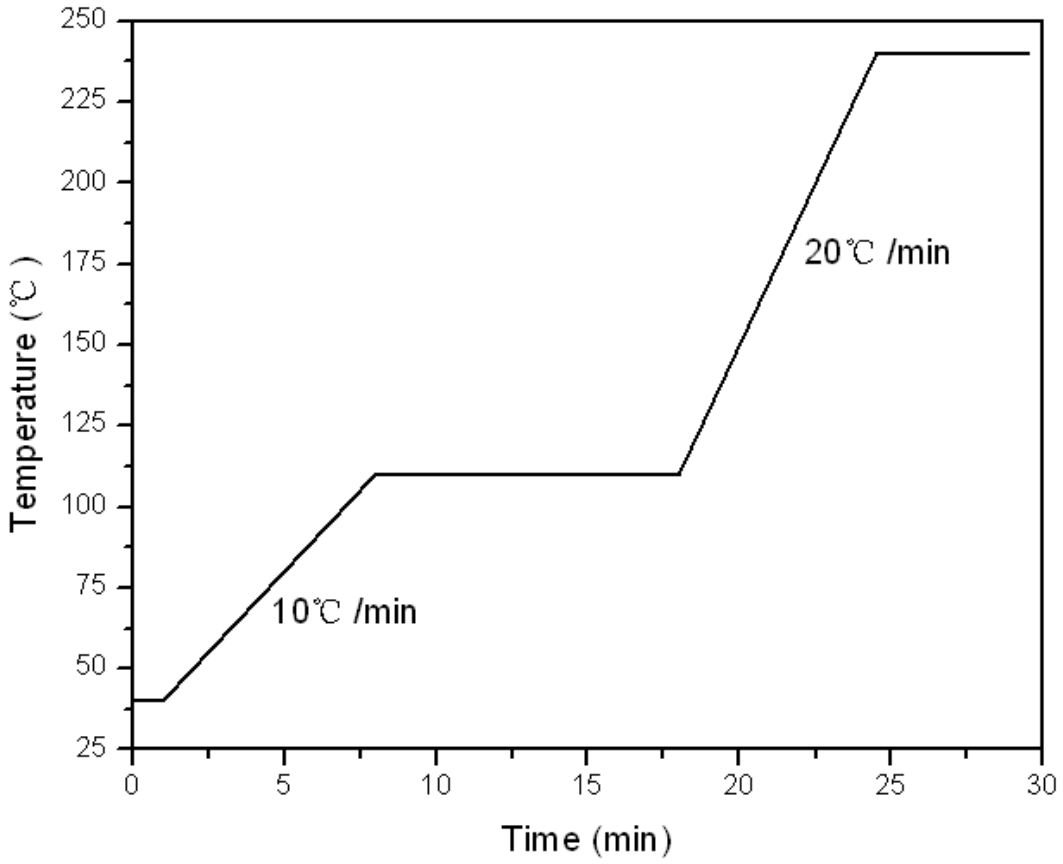

Figure 3.11 Temperature profile used in GC analysis

4. Results and Discussion

4.1. Catalyst Characterization

4.1.1. Atomic Absorption Spectroscopy

The metallic Pd content of the prepared catalyst was determined by a Perkin Elmer AAnalyst-400 Atomic Absorption Spectroscopy. The measured results were 99% of the calculated value, which indicated that the synthesized Pd/Al_2O_3 catalyst contains 0.99 wt% of Pd.

4.1.2. H_2-Chemisorption

A series of catalysts made with different procedures were measured with H_2 chemisorption in order to estimate the influence of the following factors on the metal dispersion and particle size distribution: Pd loading weight percent, Pd precursor, H_2 pretreatment temperature, washing, and calcination.

Figure 4.1 shows the H_2 chemisorption-derived dispersions for catalysts made in different ways and with different pretreatments.

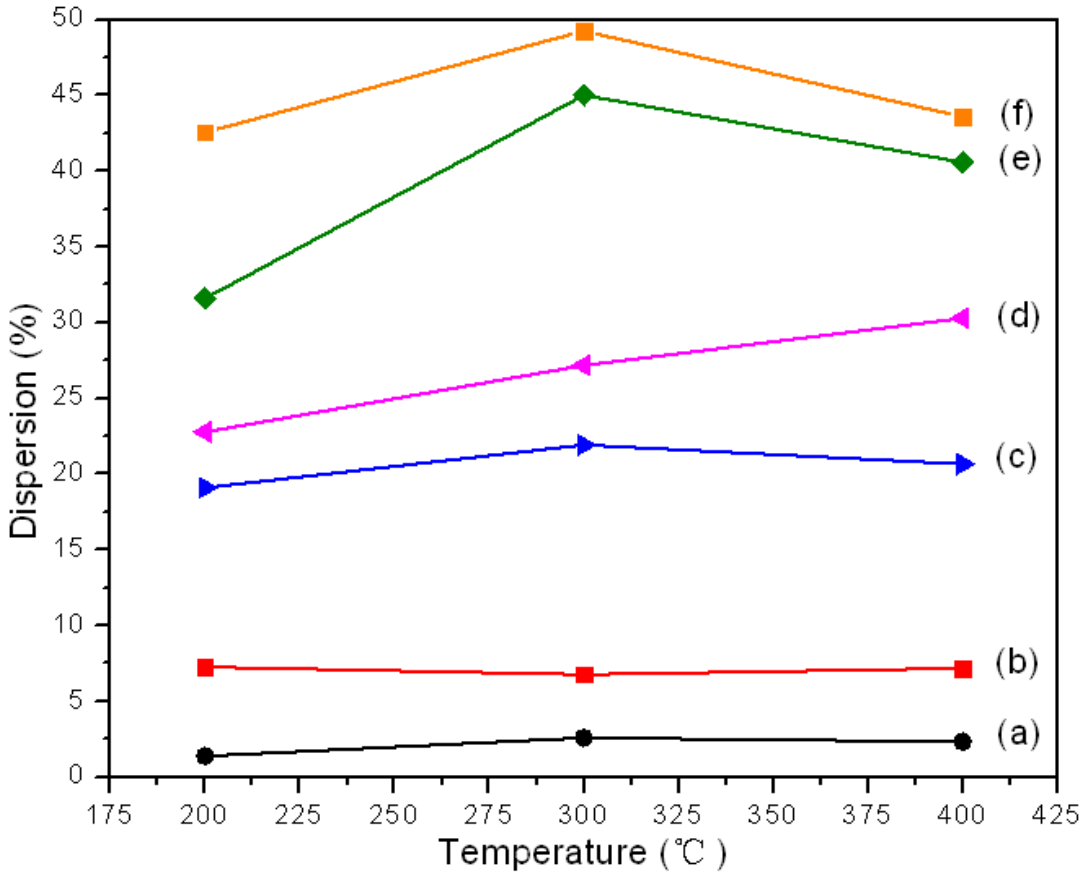

Figure 4.1 Results of H_2 chemisorption for series of catalysts made under different conditions and pretreatments. (a) 2.5 wt%, $Pd(NO_3)_2$ precursor, no calcination, washing. (b) 2.5 wt%, $PdCl_2$ precursor, no calcination, washing. (c) 2.5 wt%, $PdCl_2$ precursor, calcination, washing. (d) 1 wt%, $PdCl_2$ precursor, no calcination, no washing. (e) 1 wt%, $PdCl_2$ precursor, no calcination, washing. (f) 1 wt%, $PdCl_2$ precursor, calcination, washing.

Several conclusions can be made based on the trends in the plots:

1) Higher loading weight percentage of Pd leads to a lower dispersion (see pair of (b) vs. (e)). This is due to the increased tendency of Pd particles to agglomerate into larger particles.

2) Calcination of the catalyst is beneficial to obtain a higher dispersion (see pairs of (b) vs. (c), (e) vs. (f)). Calcination is helpful to thermally decompose the precursor, while addition of a washing step with DI water allows for the anions in the precursor to be removed.

3) Washing the catalyst also leads to higher dispersion of particles (see pair of (d) vs. (e)). This step of pretreatment is believed to be able to remove precursor ions.
4) $PdCl_2$ is believed to be a better precursor rather than $Pd(NO_3)_2$ for this Al_2O_3 support, although the reason for this is not entirely clear (see pair of (a) vs. (b)). Goodwin and co-workers revealed that for any silica support, $PdCl_2$ precursor resulted in small particle sizes and higher dispersion catalysts [191]. However, Xiao *et al.* reported that $Pd(NO_3)_2$ has a much lower decomposition temperature than that of $PdCl_2$ (473 K vs. 773 K), and that $Pd(NO_3)_2$ is superior to $PdCl_2$ in making $Pd/\alpha\text{-}Al_2O_3$ catalyst [192]. Such contradictory results indicate that the dispersion of catalyst is influenced by a combination of effects such as metal-support interactions, preparation method, *etc.*.
5) High reduction temperatures (> 400 ℃) are not suitable for obtaining catalysts with good dispersion, likely due to the sintering effect on Pd particles during the reduction.

According to the conclusions, the catalyst that with highest dispersion ((f) in Figure 4.1) was chosen for use in ATR-IR experiment.

The purchased commercial 5 wt% Pd/Al_2O_3 catalyst, which was used for batch reaction, was also measured with H_2-chemisorption experiment. The results lead to ca. 14% dispersion with ca. 8 nm averaged particle size.

4.1.3. HR-TEM

Catalyst prepared in wet impregnation method with the highest dispersion from H_2-chemisorption was also measured with HR-TEM for further analysis. Figure 4.2 (a) shows a representative HRTEM micrograph of the produced 1 wt% $Pd/\gamma\text{-}Al_2O_3$

catalysts. It can be seen that the Pd nanoparticles are well dispersed on the Al_2O_3 support. A statistical evaluation based on counting at least 400 particles over a series of TEM images yields a volume-surface mean diameter (VSMD) of 2.7 nm for the Pd clusters (Figure 4.2 (b)). The corresponding dispersion of the catalyst was about 42% dispersion, which was similar to that obtained by H_2 chemisorption measurements.

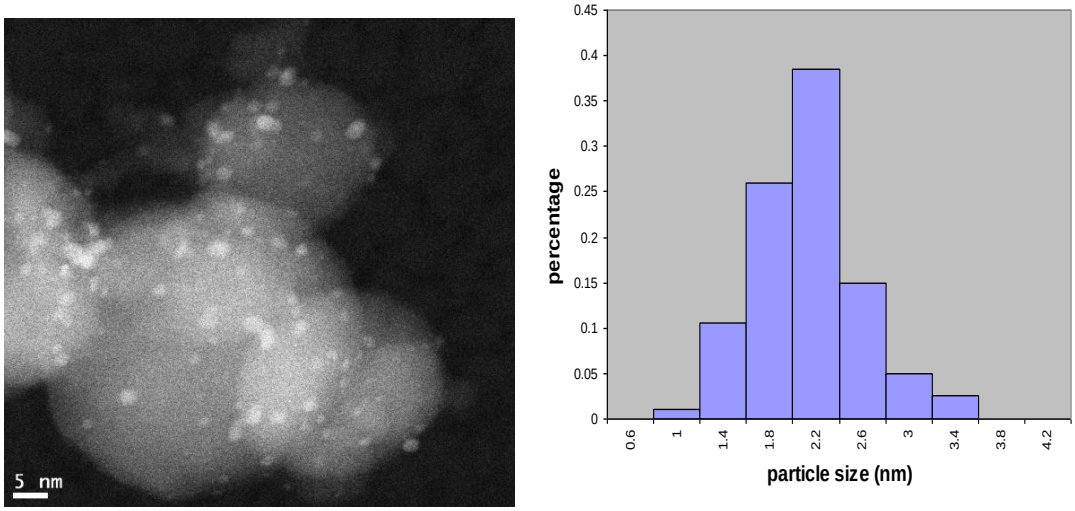

Figure 4.2 HR-TEM image and particle size distribution of 1 wt% Pd/γ-Al_2O_3 catalyst. (a) A typical HR-TEM image of produced 1 wt% Pd/γ-Al_2O_3 catalyst. (b) Particle size distribution histogram of produced 1 wt% Pd/γ-Al_2O_3 catalyst. Each Bar in the histogram represents the percentage of Pd particles with diameters ±0.2nm of average bin size, e.g., particles with diameters in 1.4±0.2 nm take 10%.

4.1.4. CO Adsorption

The adsorption of CO on Pd in gas phase was first examined with transmission FT-IR, with results shown in Figure 4.3. A background is collected first in purging He for 1 hour at room temperature to remove the residual gas and impurities, followed by exposure to 1% CO in He for 40 min. For adsorbed CO species, the stretching bands are observed in 2000-2150 cm^{-1} and 1800-2000 cm^{-1}. In the region of 1800-2000 cm^{-1}, there are several peaks overlapped with each other so that the

definite designation is difficult unless the Pd surface structure is known. Generally, the region of 1800-1920 cm^{-1} is assigned to CO adsorption on three-fold hollow Pd (111) sites [193]. Peaks in 1900-2000 cm^{-1} are attributed to bridged CO adsorption [194]. For regime of 2000-2150 cm^{-1}, it has been assigned to linearly bonded CO on Pd and Pd^{+} sites [195].

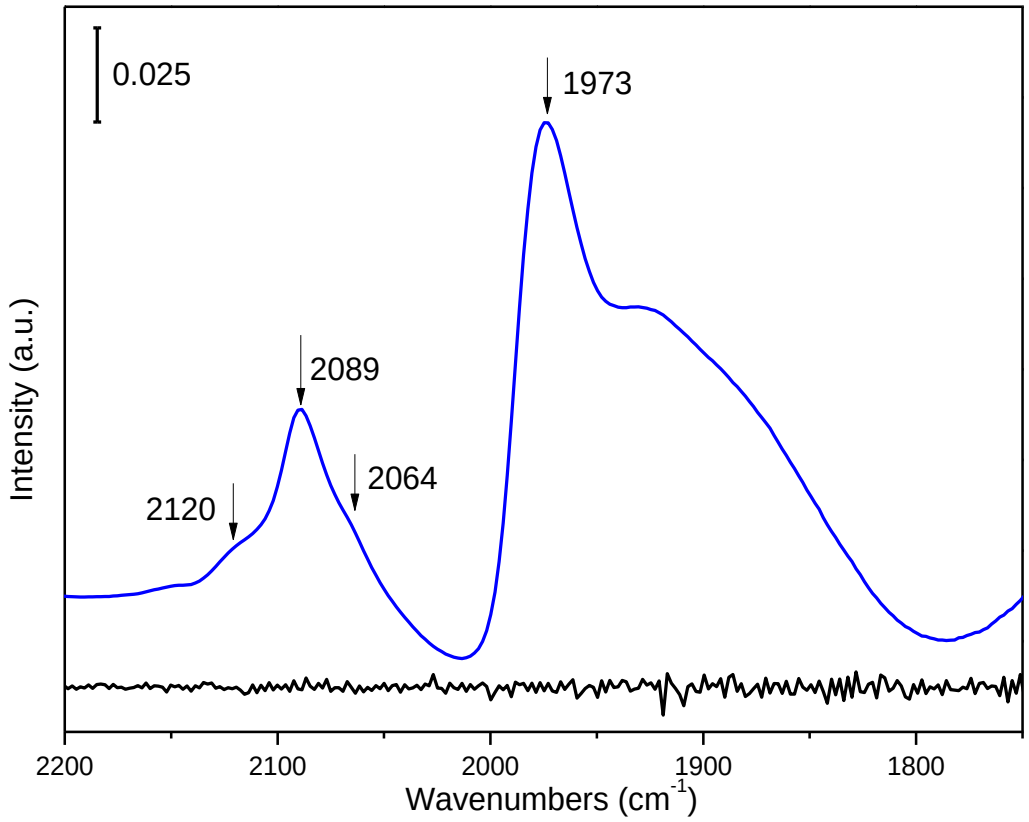

Figure 4.3 CO adsorption on Pd in gas phase measured with transmission FT-IR

Figure 4.4 shows ATR-IR spectra obtained for CO adsorption in liquid H_2O (top) and in CH_2Cl_2 (bottom). The solvents used in the experiments were N_2-pretreated in order to remove any dissolved O_2, and were used for the background spectrum. A spectrum for CO adsorption is collected after bubbling CO into solvent for 90 min. Two peaks appear at 1932 and 2064 cm^{-1} for CO adsorption in water. A blue-shift

about 10 cm^{-1} wavenumbers is observed in the case of CH_2Cl_2, with the positions at 1940 and 2078 cm^{-1}, respectively.

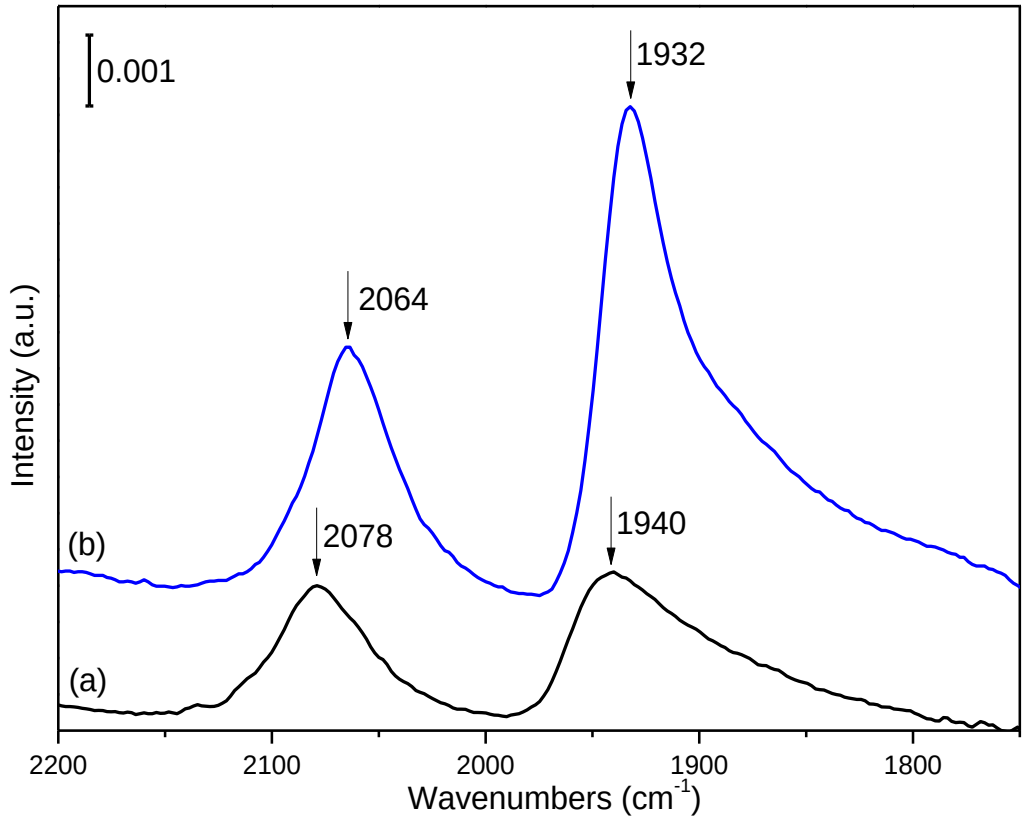

Figure 4.4 CO adsorption on Pd from ATR-IR experiment in solid-solution system with different solvent (a) CH_2Cl_2, and (b) H_2O

4.2. In-situ ATR-IR Spectroscopic Study

Carboxylic acids exhibit very fascinating properties that have made them the central concepts of many experimental and theoretical studies [196-198]. In the bulk carboxylic acid phase, hydrogen bonding can occur between two -COOH groups of two neighboring acid molecules and consequently produce a dimer. The "C-H---O" and "O-H---O" type non-covalent bonds determine many physical and chemical properties in reactions [199]. It has been reported that some simple carboxylic acids

(i.e. formic acid) can form the cyclic dimer [200], and the “open-chain” dimer [201]. Figure 4.5 indicates these two types of dimers. Also, an equilibrium between monomer and dimer is present in gas phase, where the dimer is more stable by 14 kcal/mol [202]. Sander and the co-workers reported that the cyclic type dimer is more stable than “open chain” type with an energy differential of 6 kcal/mol [203].

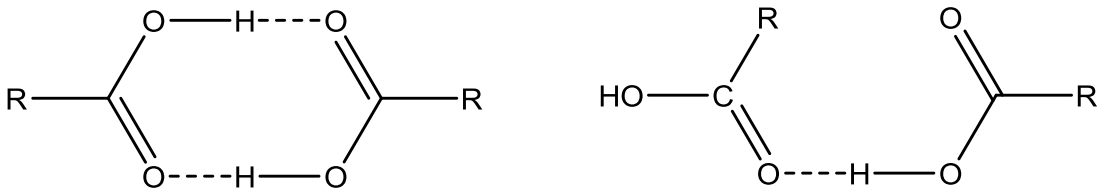

Figure 4.5 Structures of dimeric units of carboxylic acid

ATR-IR has been used to investigate *in-situ* the adsorption of acid substrates on vary surfaces, such as bare ZnSe element, Al_2O_3, and Pd/Al_2O_3. In order to fully interpret the spectra obtained, a deconvolution procedure was performed identifying adsorbed species on the support and metal.

4.2.1. Adsorption of substrate acid on bare ZnSe element, Al_2O_3, and Pd/Al_2O_3

For the present study, the synthesized 1 wt% Pd/Al_2O_3 catalyst was used. The thin film-coated element was exposed to a standard acid concentration-time step profile, as shown in Figure 4.6. Every step lasts 1 hour in order to obtain enough data (ca. 22 spectra per step) to facilitate spectral analysis. The last spectra obtained in each of the 7 steps were typically chosen for curve fitting analysis. Prior to examining adsorption behavior of the substrate acid, the bulk liquid ATR-IR spectra were obtained and analyzed using curve fitting.

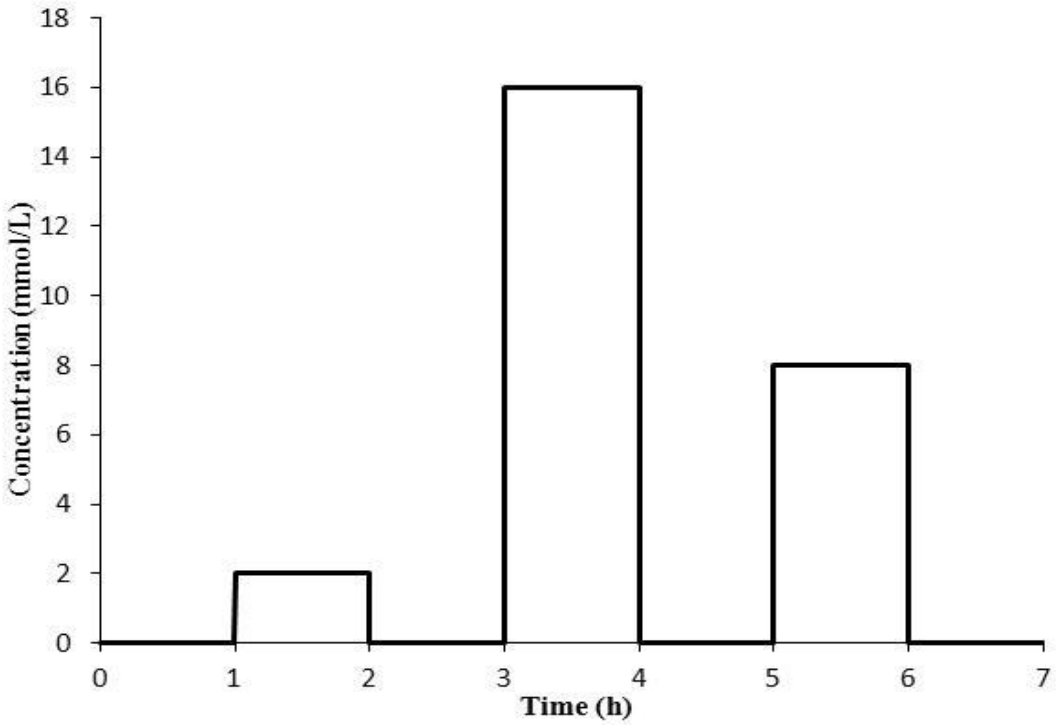

Figure 4.6 Acid concentration-time profile used during liquid flow ATR-IR experiments

Figure 4.7 shows *in-situ* ATR-IR spectra obtained from MPeA/CH_2Cl_2 solution flowing on a bare ZnSe element at the indicated concentrations according to the concentration-time profile (see Figure 4.6). Several clear peaks between 1550 and 1750 cm^{-1} appear when the acid is present in solution, and their intensities increase (to varying degree) with increasing concentration. However, these peaks disappear upon purging with pure solvent, indicating that they arise from the solution-phase acid and not from any acid adsorbed on the ZnSe. These peaks are confidently assigned to the C=O stretching vibrations of acid dimer and monomer species, respectively[128]. The dimer refers to a cyclic structure where two acid molecules interact through H-bonding between the H atom in the hydroxyl group and O atom in the carbonyl group. The clear 1647 cm^{-1} peak arises from the C=C stretching mode

in the unsaturated acid, and includes contributions from both dimer and monomer species[128]. The very weak feature at ca. 1606 cm^{-1} is designated as asymmetric stretching mode of COO^- [204], likely resulting from a small amount of acid decomposition on the ZnSe crystal. The small feature observed between 1400-1450 cm^{-1} is consistent with large solvent features at 1433/1422 cm^{-1}. Thus it is attributed to incomplete background subtraction of the very large solvent absorbance.

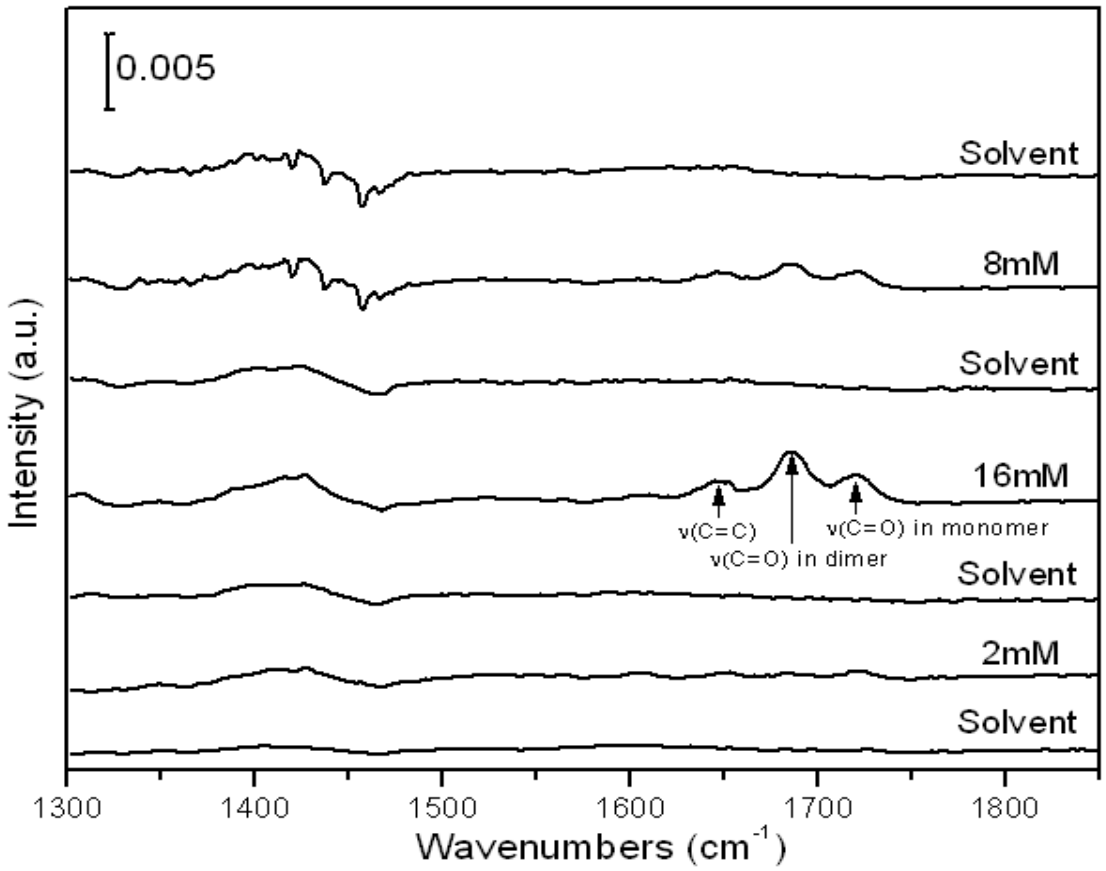

Figure 4.7 Stacked ATR-IR spectra acquired during alternating pure CH_2Cl_2 solvent/MPeA solution flow on a bare ZnSe element

To gain a clearer picture of the relative amounts of dimer and monomer species in solution as a function of concentration, the spectra were deconvoluted using curvefitting. For example, Figure 4.8 shows the result of curvefitting the highest concentration (16 mM) spectrum (in Figure 4.7) in the region of 1500-1850 cm^{-1}.

Trace (a) consists of the individual peak fits, while trace (b) beneath is the overall curve-fit, together with the raw spectral data (open circles) as a comparison. Initially, the individual peak parameters (i.e. position, full width at half maximum (FWHM), and height) were chosen based on visual inspection of the experimental spectrum. Then the residual between the overall fit and raw spectrum was minimized by minimizing the square root of the sum of square errors in an iterative fashion. All the peaks were modeled by pure Gaussian line shapes. In addition, the initial fits were always applied to the spectrum obtained at the highest concentration in order to allow the most accurate determination of the individual peaks.

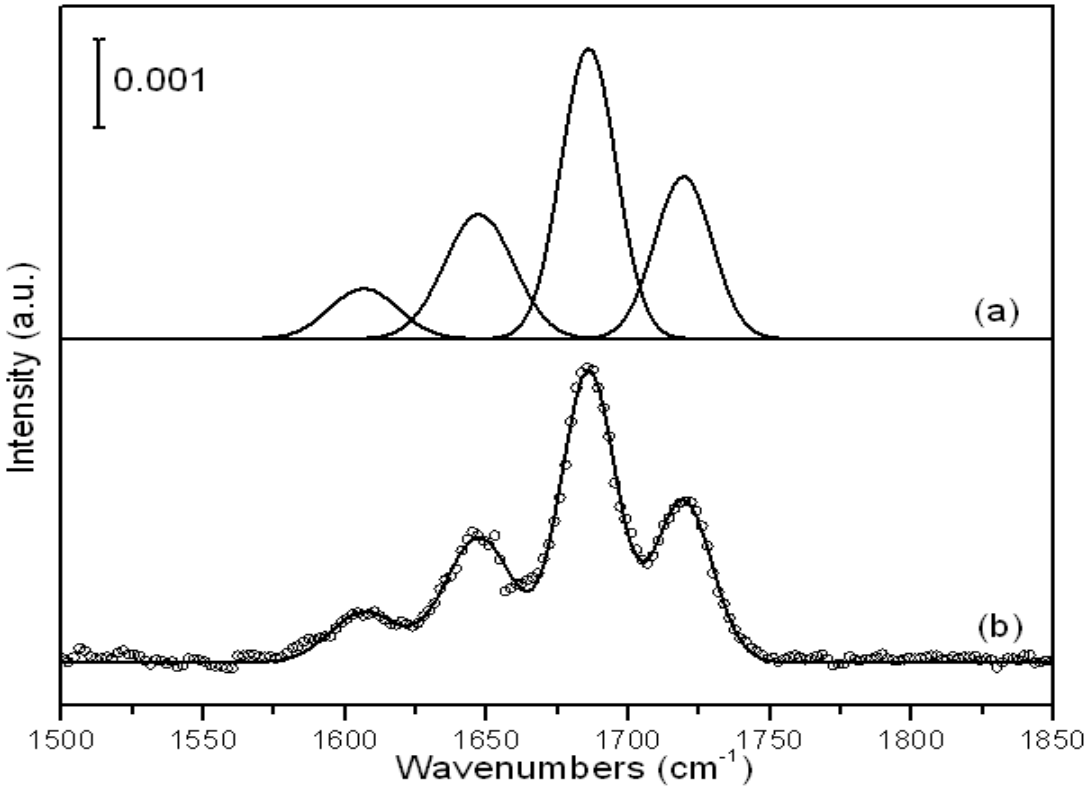

Figure 4.8 Spectral curve fitting results for MPeA solution (16mM) on bare element. (a) The individual peak fits. (b) The overall curve-fit, including the raw data (open circles).

Applying this same curve fitting procedure to MPeA solutions with different concentrations, yet keeping the position and FWHM constant, it is found that the ratio of peak intensity of C=O dimer/monomer is dependent on the acid concentration. This can be seen clearly in Figure 4.9, which plots the dimer/monomer intensity ratio versus concentrations on different surfaces. The open circles confirm that the equilibrium dimer-monomer distribution is strongly dependent on concentration [205]. This behavior is explained by the relatively stronger H-bonding interaction between acid molecules compared with the interaction between CH_2Cl_2 solvent and acid. Thus, as the concentration increases, the carboxylic acid monomers have higher possibility to form dimers.

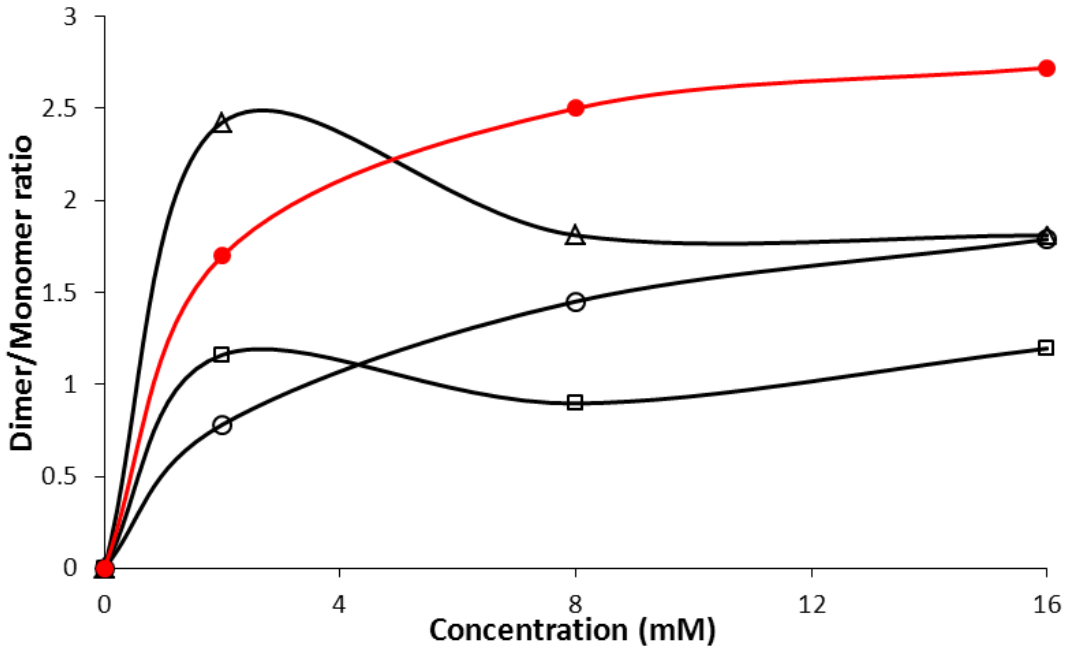

Figure 4.9 Concentration dependence of dimer/monomer IR peak ratio of MPeA in MeOH solution (red circles), in CH_2Cl_2 solution (open circles), adsorbed on Al_2O_3 (triangles), and adsorbed on Pd (squares)

Assuming that the penetration depth of the IR beam is constant over this range of concentrations, the ATR-IR signal should vary linearly with the concentration of the acid species in solution. Using this assumption, along with the concentration-dependent peak areas and the material balance on acid in solution, the equilibrium constant K_{dis} for dimer dissociation has been calculated to be ca. 0.025 mol/L in CH_2Cl_2 solvent, while it is 0.004 mol/L for the case of MeOH solvent. There are relatively few relevant comparisons in the literature available, and none for these acid-solvent combinations. For example, the value for acetic acid in benzene solvent has been found to be 0.036 mol/L at 20 ℃, while it has been reported to be 2.5E-4 mol/L in carbon tetrachloride [206]. It should be noted that the acid adsorption on the Al_2O_3 and Pd/Al_2O_3 surfaces (see below) is found to be largely irreversible under these conditions, and the absolute coverage of surface species are unknown. As such, similar equilibrium calculations are not possible in these cases.

After exploring the concentration-dependent behavior of the acid solutions over the bare ZnSe element, the adsorption behavior of MPeA on Al_2O_3 was examined. Figure 4.10 shows a typical set of *in-situ* spectra acquired during MPeA adsorption on Al_2O_3 using the same liquid-phase concentration profile. As for the bare element, peaks appear within the 1500-1850 cm^{-1} region when the acid is first introduced at the lowest concentration.

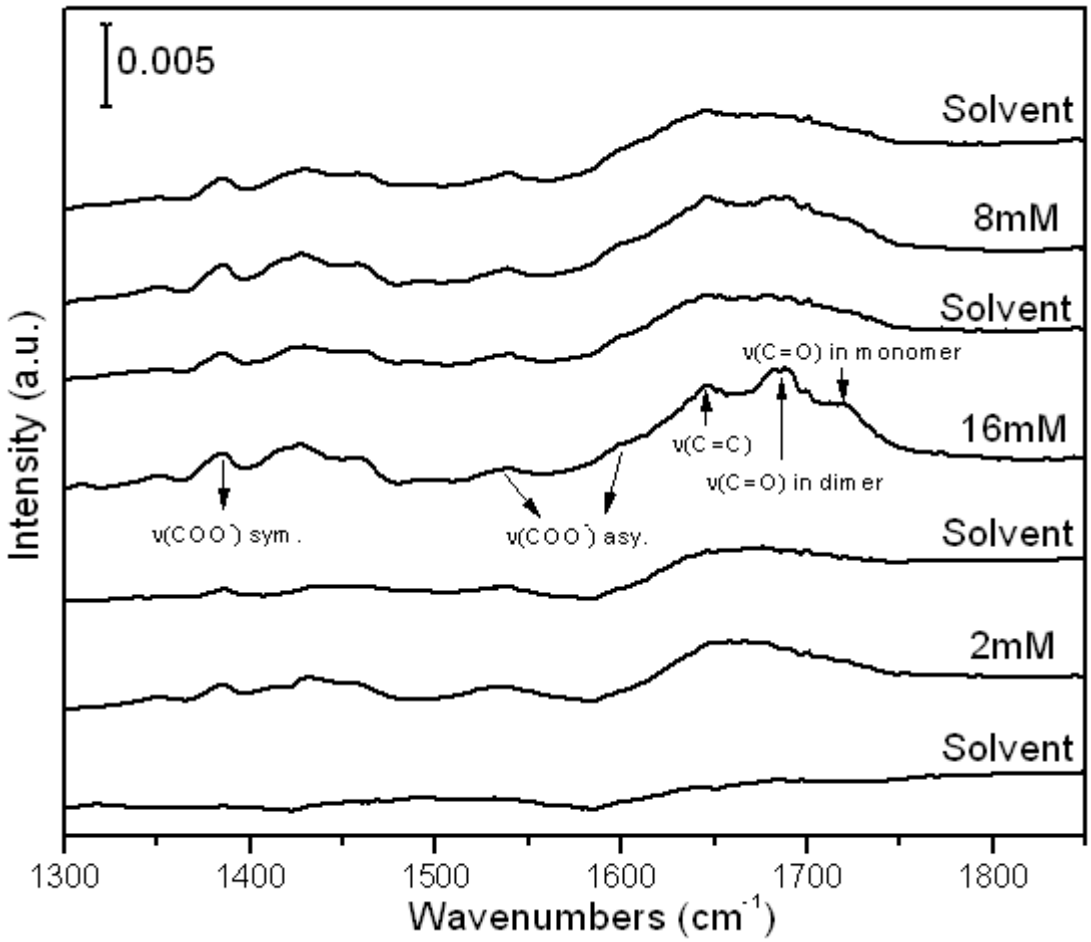

Figure 4.10 Stacked ATR-IR spectra acquired during alternating pure CH_2Cl_2 solvent/MPeA solution flow on Al_2O_3

However, the features are significantly broader and more intense than the previous case. Furthermore, the peaks are largely retained in the spectrum even after flushing with solvent for 1 hr, suggesting significant and strong adsorption on the Al_2O_3 film. While largely hidden at the lowest concentration, the sharper liquid acid peaks are clearly visible in the spectra obtained at higher concentrations. The broad peak envelope in the 1600-1750 cm^{-1} range consists of peaks associated with C=C streching, and C=O stretching from dimer and monomer species. However, several additional peaks are observed at 1538, 1425, 1385, and 1352 cm^{-1}.

To deconvolute the peaks present in Figure 4.10, the spectrum acquired under the highest concentration was curve fitted. In the analysis, it was assumed that the peaks associated with liquid phase acid were not affected by the presence of the support at the same concentrations. Thus, for liquid MPeA peaks, the peak positions, FWHM, and relative sizes (i.e. ratio of peak heights) were kept fixed at a given liquid-phase concentration, while the peak intensities were allowed to vary. For the remaining spectral features, these parameters were all allowed to vary. Figure 4.11 shows the resulting curvefitting results for the case of MPeA adsorbed on Al_2O_3 in 16 mM CH_2Cl_2 solution (see Figure 4.10). The individual and overall-fit from liquid phase MPeA is shown in trace (a), subject to the constraints as described above. It should be noted that liquid phase peak heights were found to be about 50 % of their value in the absence of Al_2O_3 film. This is consistent with the ca. 50 % void fraction of these thin powder films found previously[182]. Trace (b) shows the overall band envelope arising from adsorbed MPeA-related species on Al_2O_3 surface and the individual fitted peaks, while trace (c) is the overall fit by adding trace (a) and trace (b). Figure 4.11 shows excellent agreement between the experimental spectrum (open circles) and the overall curve fitted trace (c). Similar curvefitting was performed for the other spectra in Figure 4.10, and demonstrated that these peaks are sufficient and reasonable to fit all of the spectra. It should be noted that the peak widths in the liquid phase are between 20-25 cm^{-1}, while those of the adsorbed species vary from 30-50 cm^{-1}. Thus, there is very little ambiguity regarding the part of the signal coming from liquid versus the Al_2O_3 surface.

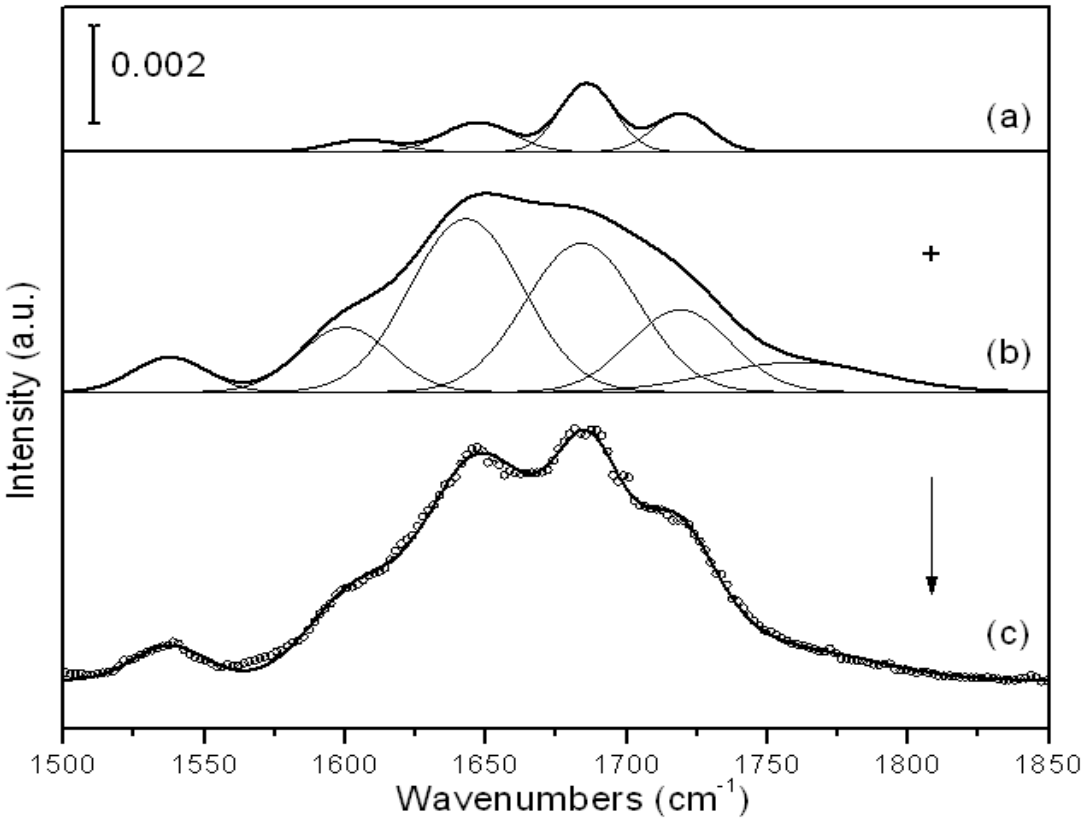

Figure 4.11 Spectral curve fitting results for MPeA solution (16mM) on Al_2O_3. (a) The peak contribution from the liquid phase. (b) The peaks from Al_2O_3 surface-adsorbed MPeA species. (c) The overall curve-fit by adding trace (a) and (b), together with raw data (open circles). See text for more details.

Inspection of the curve fit in Figure 4.11 reveals peaks at 1719 and 1684 cm^{-1}, which are assigned to C=O stretching vibrations of adsorbed monomeric and dimeric acid on the Al_2O_3 surface. The band at 1538 cm^{-1}, together with the one at 1385 cm^{-1} (from Figure 4.10) is assigned to COO^- asymmetric/symmeteric stretching vibrations of adsorbed carboxylates[132, 207, 208] . The peak at 1600 cm^{-1} is again designated as asymmetric stretching vibration of the COO^- group[204]. The peak at 1352 cm^{-1} is due to C-H deformation[209, 210]. Carboxylic acids can adsorb at metal or metal oxide surfaces through the carboxylate group acting as a ligand for vacant coordination sites of surface metal ions[207]. It has been demonstrated that the

adsorption of carboxylic group (COO^-) on such surface has three representative types of coordinations: unidentate, chelating bidentate, and bridging bidentate[211]. An empirical rule has been developed to determine the coordination type by measuring the peak separation $\Delta_{sep}=\nu_{as}(COO^-) - \nu_s(COO^-)$, where $\nu_{as}(COO^-)$ is the frequency of COO^- antisymmetric stretching mode, and $\nu_s(COO^-)$ refers to the symmetric stretching mode[197, 212, 213]. The band separations are expressed in the following order: unidentate (Δ_{sep} = 350-500 cm^{-1}) > bridging (Δ_{sep} = 150-180 cm^{-1}) > chelating (Δ_{sep} = 60-100 cm^{-1}) [207, 214]. Based on these rules, the Δ_{sep} values of ca. 153-215 cm^{-1} observed here suggest that these species are in a bridging coordination. Finally, the peaks at 1643 and 1425 cm^{-1} arise from the C=C stretch and $-C_2H_5$ deformation respectively, with both adsorbed molecular acid and carboxylate species contributing to their intensity [215].

Finally, the adsorption behavior of MPeA on Pd/Al_2O_3 surface was studied and the results shown in Figure 4.12. The same assumption and constraints were applied to peaks of acid on Al_2O_3 as were used for liquid acid in the curve fitting of MPeA adsorption on Pd/Al_2O_3 surfaces. In Figure 4.13, trace (a) and (b) are signals of MPeA from liquid phase and Al_2O_3-surface adsorbed species, respectively. Trace (c) shows the overall and individual peaks due to the adsorption on the Pd particle surface. At the bottom, trace (d) is the summation fit of traces (a), (b), and (c), which again is in good agreement with the experimental spectrum obtained (open circles).

As can be seen, similar peaks appear in the 1500-1850 cm^{-1} range as in the case of Al_2O_3. However, they appear to be larger in the case of Pd/Al_2O_3 (see curve fitting results in Figure 4.13). In addition, in the presence of Pd particles, several peaks are

detected in the region from 1330 cm^{-1} to 1450 cm^{-1} that are not so obvious in the cases of bare element and Al_2O_3 surface. Previous studies indicate that the peak at 1423 cm^{-1} arises from the deformation of the $-C_2H_5$ group, while the peaks observed at 1541 and 1613 cm^{-1} are again assigned as COO^- asymmetric stretch, the peak at 1388 cm^{-1} from the COO^- symmetric stretch, and the 1353 cm^{-1} band from C-H deformation of the substrate[216, 217]. Applying the empirical rule introduced above, the band separation in the current case is between 153 cm^{-1} and 225 cm^{-1}, which again indicates a bridging bidentate adsorption mode of the acid onto the Pd surfaces. Still, the presence of the C=O stretch of the dimer illustrates that some acid adsorbs on Pd in this form.

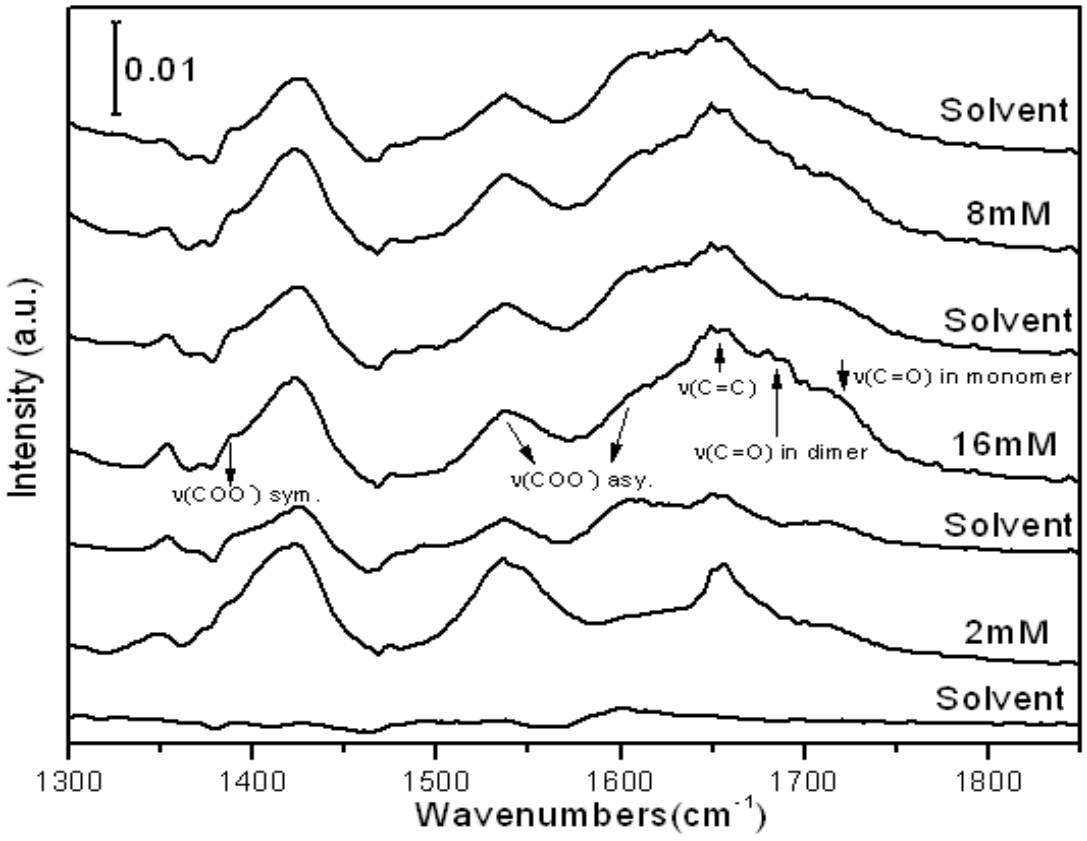

Figure 4.12 Stacked ATR-IR spectra acquired during alternating pure CH_2Cl_2 solvent/MPeA solution flow on Pd/Al_2O_3

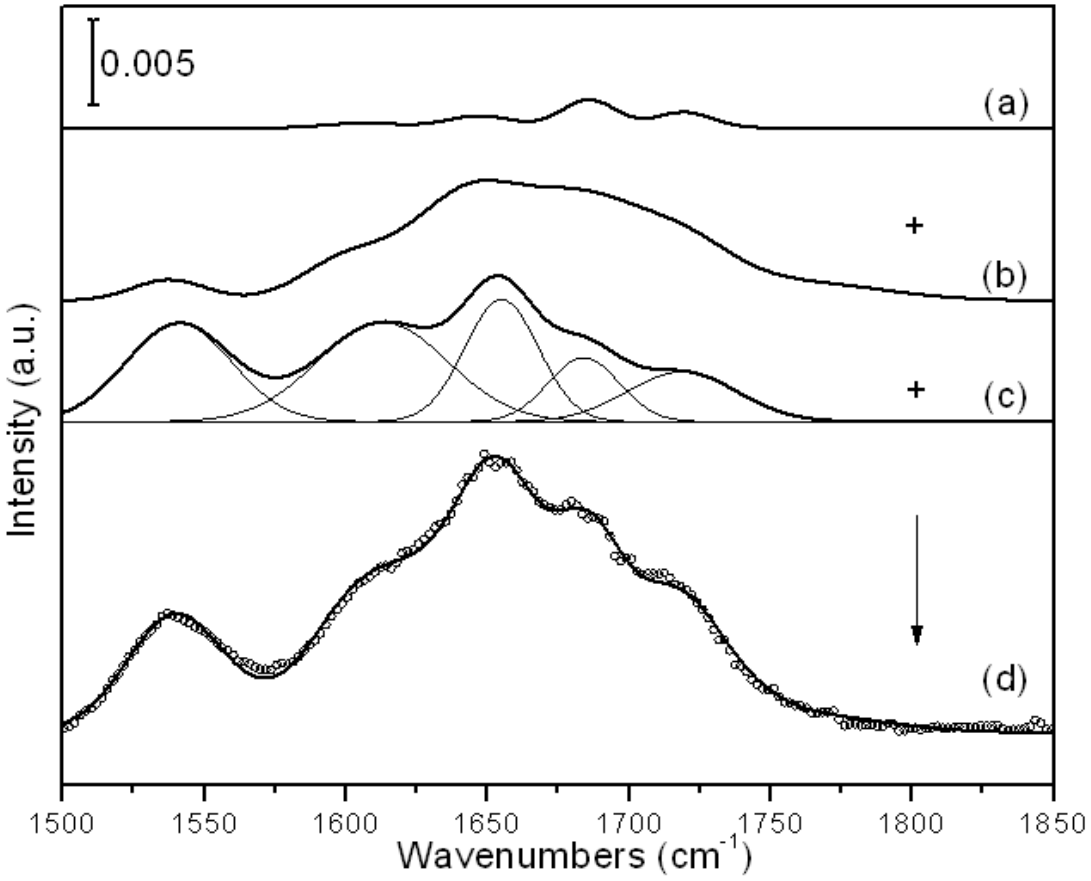

Figure 4.13 Spectral curve fitting results for MPeA solution (16mM) on Pd/Al_2O_3. (a) The peak contributions from liquid MPeA. (b) The peak contributions from Al_2O_3-surface adsorbed species. (c) The overall and individual curve-fits from Pd-surface adsorbed species. (d) The summation of trace (a), (b), and (c), along with the raw data (open circles). See text for more details.

It should be noted that while the bands present on Al_2O_3 and Pd are generally similar, there are small differences in peak positions and band widths. Most notable is the difference between C=C stretching modes, where in the case of Pd the band is upshifted from its liquid phase value by ca. 7 cm^{-1}, as opposed to Al_2O_3 where this band is downshifted by 4 cm^{-1}. In addition, the intensity ratios of the monomer/dimer bands to those of the carboxylate are very different for Al_2O_3 versus Pd, with the former exhibiting a larger relative amount of monomer/dimer species.

The adsorption of MPeA on different surfaces was also investigated in a typical polar solvent (MeOH) in order to examine the solvent effect on its behavior and for correlation with parallel kinetic studies. The concentration-time profile was kept same as it was applied in the MPeA/CH_2Cl_2 solution. In comparion with the case of CH_2Cl_2 solvation surrounding, only the spectra of highest acid concentration (16mM) were chosen. Figure 4.14 shows the ATR-IR spectra of MPeA solution (16mM) on bare element with CH_2Cl_2 and MeOH as solvents. For the case of MPeA/MeOH mixture, the bands are assigned as ν(C=O) in monomer at 1714 cm^{-1}, while the dimeric ν(C=O) stretch appears at 1687 cm^{-1}. The 1647 and 1438 cm^{-1} features are due to ν(C=C) and δ(C-H), respectively, from these species. Thus, the acid vibrational bands remain at the same position as it was in CH_2Cl_2, although the monomeric ν(C=O) became weaker than the latter case.

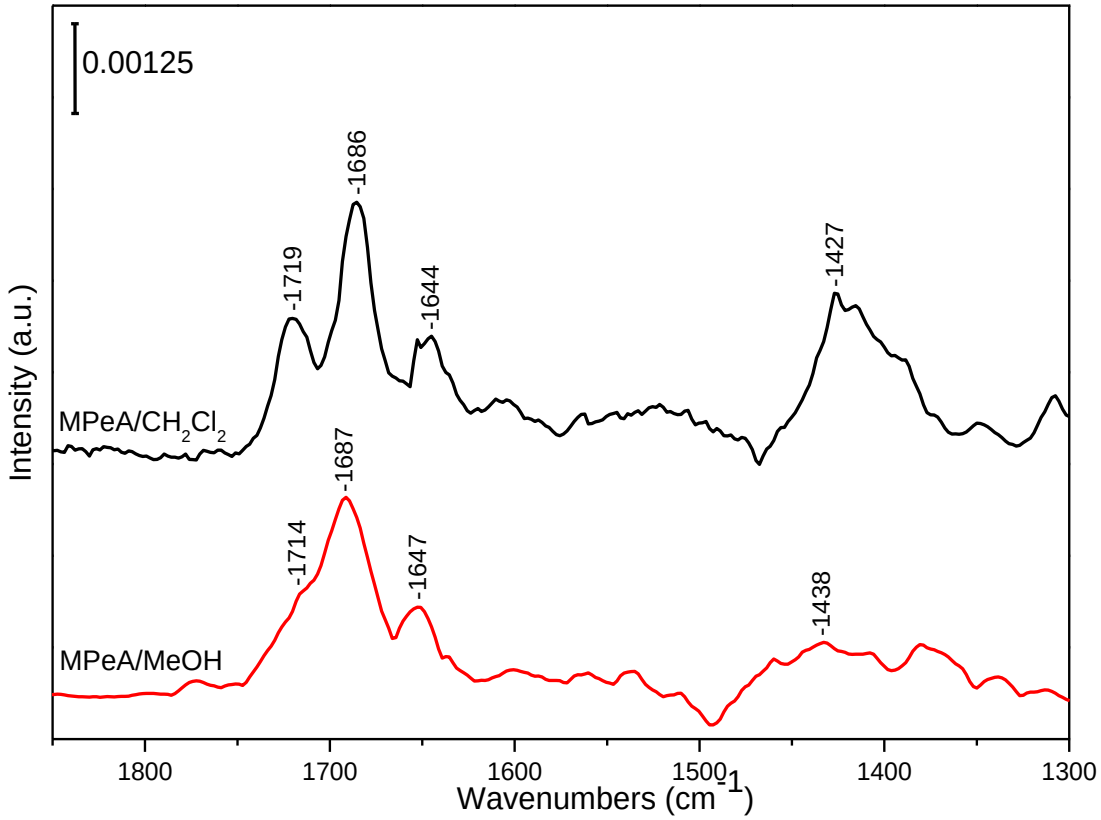

Figure 4.14 ATR-IR spectra of MPeA (16mM) in CH_2Cl_2 and MeOH solutions on bare element

Next, the adsorption of MPeA on the γ-Al_2O_3 surface in MeOH solution was studied as well. Figure 4.15 shows the spectra of adsorbed MPeA on the Al_2O_3 surface. The bands for adsorbed MPeA in CH_2Cl_2 solution were deconvoluted and assigned in our previous work [218] (see discussion of Figure 4.10 and 4.11). In short, the 1719 and 1684 cm^{-1} features are from the ν(C=O) stretches for monomer and dimer species, respectively. The 1643 cm^{-1} band is from the ν(C=C), while the shoulder at 1600 along with 1538 cm^{-1} are both assigned as $\nu_{as}(COO^-)$. The feature at 1385 cm^{-1} is due to $\nu_s(COO^-)$. In contrast, for the case of MeOH solvent, it is observed that the ν(C=O) stretches for both monomeric and dimeric species at ca.

1723 and 1692 cm^{-1} have weakened compared to the sharpened ν(C=C) band at 1655 cm^{-1}, and strengthened $\nu_{as}(COO^-)$ at 1621 and 1552 cm^{-1}, and $\nu_s(COO^-)$ at 1379 cm^{-1}. This indicates that with MeOH solvation, MPeA tends to more favorably form strongly adsorbed carboxylate on the Al_2O_3 surface, with less amount of molecular species, which is quite different from the case of CH_2Cl_2.

Moreover, it is noticed that the $\nu_{as}(COO^-)$ has a ca. 15-20 cm^{-1} blue shift, while $\nu_s(COO^-)$ is slightly red shift (ca. 6 cm^{-1}) in the presence of MeOH solvent. This is possibly due to H-bonding interaction between solvent molecule and solute. To be specific, the H atom in the hydroxyl group in MeOH interacts with O atom of carboxylate adsorbed at the surface. Therefore, the negative charge at $-COO^-$ could partly transfer, leading to a redistribution of electron density, which consequently affects the vibrational frequency.

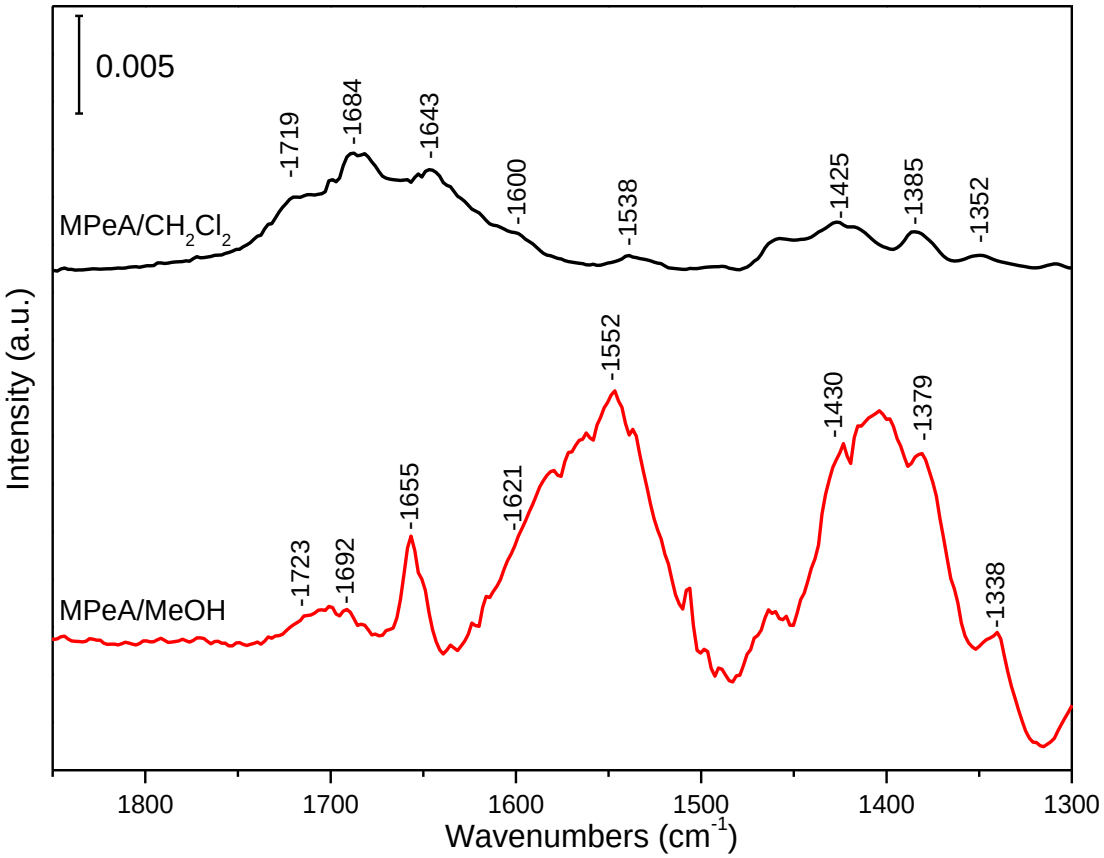

Figure 4.15 ATR-IR spectra of MPeA (16mM) in CH_2Cl_2 and MeOH solutions on γ-Al_2O_3 surface

Then, the spectra obtained during adsorption of MPeA/MeOH on Pd/Al_2O_3 were acquired and are summarized in Figure 4.16. Similar to the case of MPeA adsorption on Al_2O_3, the presence of MeOH as solvent dramatically affects the spectrum in terms of peak position and peak intensity. To be specific, the broadened peaks at 1500-1600 cm^{-1} and 1350-1450 cm^{-1} region indicate that MPeA tends to form carboxylate at the surface instead of molecular species.

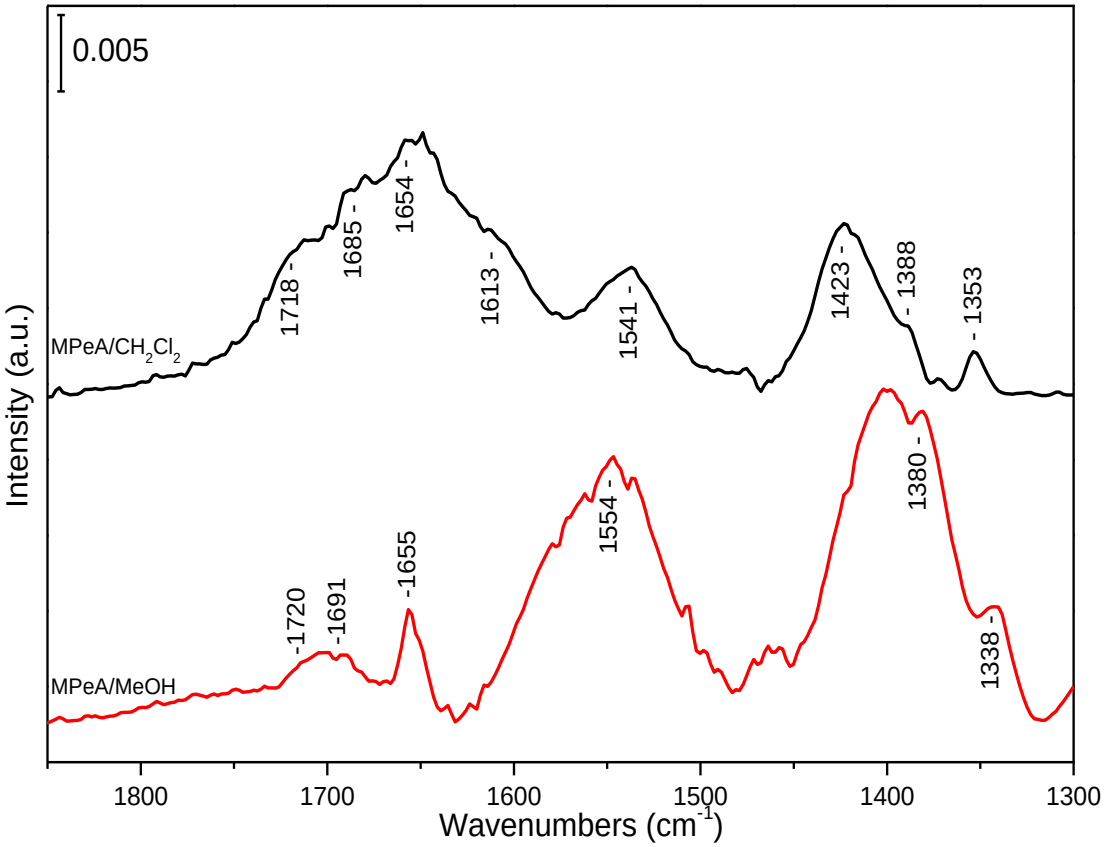

Figure 4.16 ATR-IR spectra of MPeA (16mM) in CH_2Cl_2 and MeOH solutions on Pd/γ-Al_2O_3 surface

Table 4.1 Peak Assignment of MPeA in liquid phase and adsorbed in MeOH and CH_2Cl_2

In solution MeOH (CH_2Cl_2)	On Al_2O_3 MeOH (CH_2Cl_2)	On Pd/Al_2O_3 MeOH (CH_2Cl_2)	Assignment
1714 (1719)	1723 (1719)	1720 (1718)	ν(C=O) (monomer)
1687 (1686)	1692 (1684)	1691 (1685)	ν(C=O)(dimer)
1647 (1644)	1655 (1643)	1655 (1654)	ν(C=C)
-	1621 (1600)	1623 (1613)	$\nu_{as}(COO^-)$
-	1552 (1538)	1554 (1541)	$\nu_{as}(COO^-)$
1438 (1427)	1430 (1425)	1433 (1423)	δ(C-H)
-	1379 (1385)	1380 (1388)	$\nu_s(COO^-)$
1339 (1350)	1338 (1352)	1338 (1353)	δ(C=C-H)

To summarize the results of the curve fitting analysis for MPeA in CH_2Cl_2 and MeOH solutions over the three surfaces, the band assignments of MPeA are listed in Table 4.1. The relationship between concentration and dimer/monomer ratio in different environments is revealed in Figure 4.9. The equilibrium behavior for bulk acid in CH_2Cl_2 and MeOH was explained earlier. For the cases of acid adsorbed on Al_2O_3 and Pd in CH_2Cl_2 solution, the dimer/monomer ratio is greater than that for the liquid phase, suggesting that adsorbed dimers are favored over monomers at lower liquid-phase concentrations (< 10 mM). This is likely due to the relatively larger surface concentrations of acid at these bulk concentrations, since the acid is strongly adsorbed. It is also possible that the formation of carboxylates decreases the sites needed to stabilize monomeric acid in favor of dimeric acid. It is unclear at present if the dimers adsorb directly from solution or form due to H-bonding of initially adsorbed monomers. At higher concentration, the distribution of acid species on the surface moves closer to that of the bulk phase in the case of alumina.

However, in the case of Pd, the distribution of acid continues to skew in the direction of monomer species. According to Davis and Barteau[29] in a study of propionic acid adsorption on Pd(111), carboxylic acid monomers are initially adsorbed through hydroxyl oxygen, and form dimers (and even catemers) at monolayer coverage at low temperatures (< 230K). However, such species decompose to form carboxylates and adsorbed monomers, eventually undergoing desorption as acid monomers near 273K or decarboxylation at much higher temperatures (i.e., > 373K). Thus, it is reasonable that at the present experimental temperature of 293K, the surface has a higher relative coverage of monomer species.

For ATR-IR study of MPeA in MeOH solution, the bulk phase exhibit similar peak position at similar intensity with respect to the case of CH_2Cl_2. However, for the adsorbate MPeA, the monomer and dimer C=O stretches do not exhibit strong band intensity while the carboxylate-related features show large intensity. Again, this indicates MPeA tends to adsorb on Al_2O_3 and Pd surface as carboxylate in presence of MeOH. This is possibly due to H-bonding between solvent and solute.

In summary, the adsorption behavior of MPeA in CH_2Cl_2 and MeOH solution on Al_2O_3 and Pd/Al_2O_3 was examined by ATR-IR spectroscopy for the first time in the present study. The MPeA molecules adsorb on both Al_2O_3 and Pd surfaces molecularly and dissociatively under the conditions examined. In the case of molecular adsorption, both monomer and dimer species are observed to adsorb, with the relative amount of monomer to dimer dependent on the surface and the liquid phase acid concentration. In the case of dissociative adsorption, the acid adsorbs predominantly in a bridged bidentate configuration. In the presence of MeOH solvent, the vibrations associated with adsorbed carboxylate exhibit a wavenumber shift, likely due to the H-bonding between solvent and acid molecule. The interplay between these surface species is expected to be an important factor in determining C=C bond hydrogenation activity on these Pd catalysts. Other ATR-IR investigations along these lines have focused on the interaction between this prochiral substrate acid and the chiral modifier cinchonidine on the Pd surface. The competitive nature of such adsorption and the mode of specific modifier-substrate interaction are of interest. These results are shown in Chapter 4, sections 2.3.

More broadly, the present results also provide further evidence that ATR-IR is an effective means to monitor the adsorption and desorption of acids at the solid-liquid interface from a molecular level. Coupled with extensive curve fitting to deconvolute the vibrational data, this approach has value beyond the currently considered catalytic system, especially for application to adsorption and surface reactions of biomass-derived acids and acid esters on solid catalysts.

4.2.2. Adsorption of cinchonidine on bare ZnSe element, Al_2O_3, and Pd/Al_2O_3

IR spectra of CD in bulk phase [173], liquid phase [219] and as an adsorbate on metals such as Pt [171] and Pd [220] have been studied extensively. In this present work, the peak assignment of CD follows previous work from our group [173] and others [172].

The commercial 5 wt% Pd/Al_2O_3 catalyst was used in the ATR-IR study of cinchonidine adsorption. The traces at the bottom of Figure 4.17 show the ATR-IR spectra from liquid CD solutions, with features observed at 1639, 1592, 1571, 1509, 1455, 1423, 1390, 1347 and 1324 cm^{-1} in CH_2Cl_2. It is also found that for the case of MeOH, most of vibrational band positions have only 1-3 cm^{-1} difference, which is negligible given the resolution of the measurement.

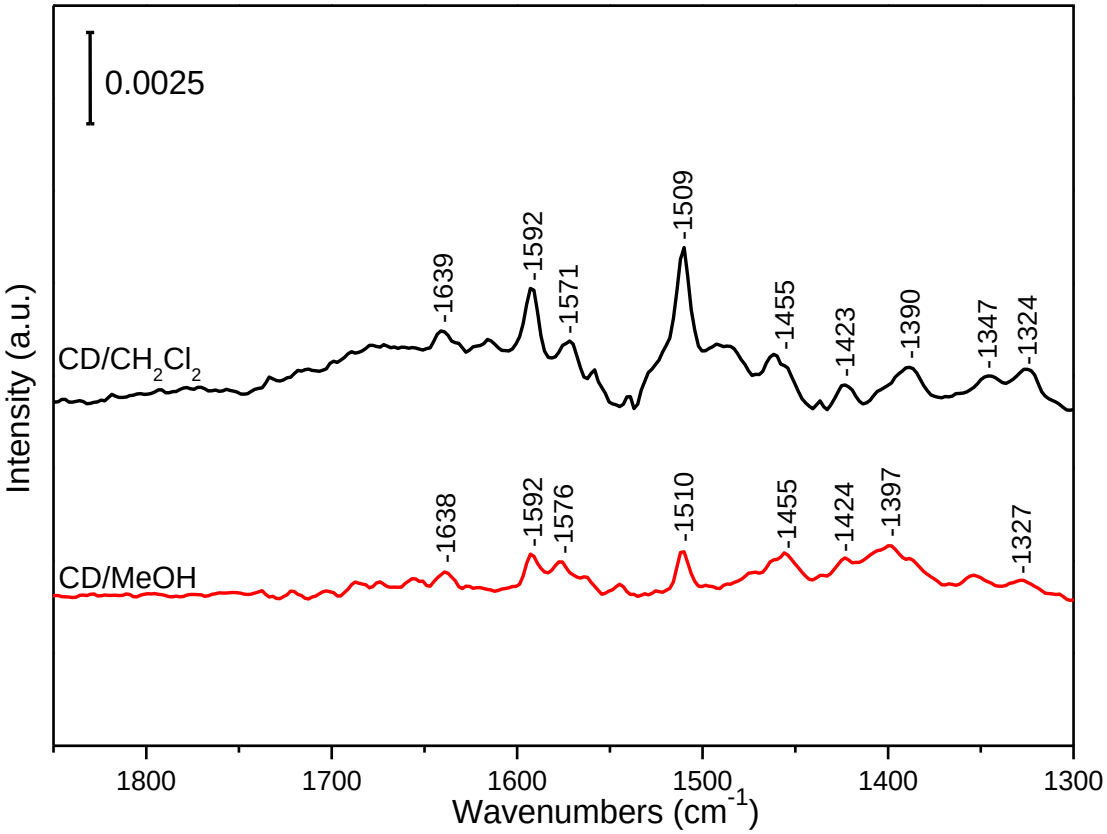

Figure 4.17 ATR-IR spectra of CD (10mM) in CH_2Cl_2 and MeOH solutions on bare element

The adsorption of CD on γ-Al_2O_3 surfaces was studied under the same concentration solutions followed by purging with pure solvent for 1 hour. Figure 4.18 shows the spectra of adsorbed CD on the Al_2O_3 surface. In contrast to Burgi's study [172], adsorption of CD on the Al_2O_3 surface is observed here, as shown in the Figure 4.18. This observation is supported by Li and co-workers [221] who investigated the adsorption and decomposition of ethyl pyruvate (EtPy) over chiral-modified Pt/γ-Al_2O_3 by using ethanol as solvent. The main bands are observed at 1636, 1590, 1569, 1507, 1463, 1422, and 1390 cm^{-1}, which is similar as the case of bare element. Moreover, comparing the spectra of CD adsorption on Al_2O_3 in Figure

4.18, the similar band shapes and positions indicate that the solvent has little effect on CD adsorption.

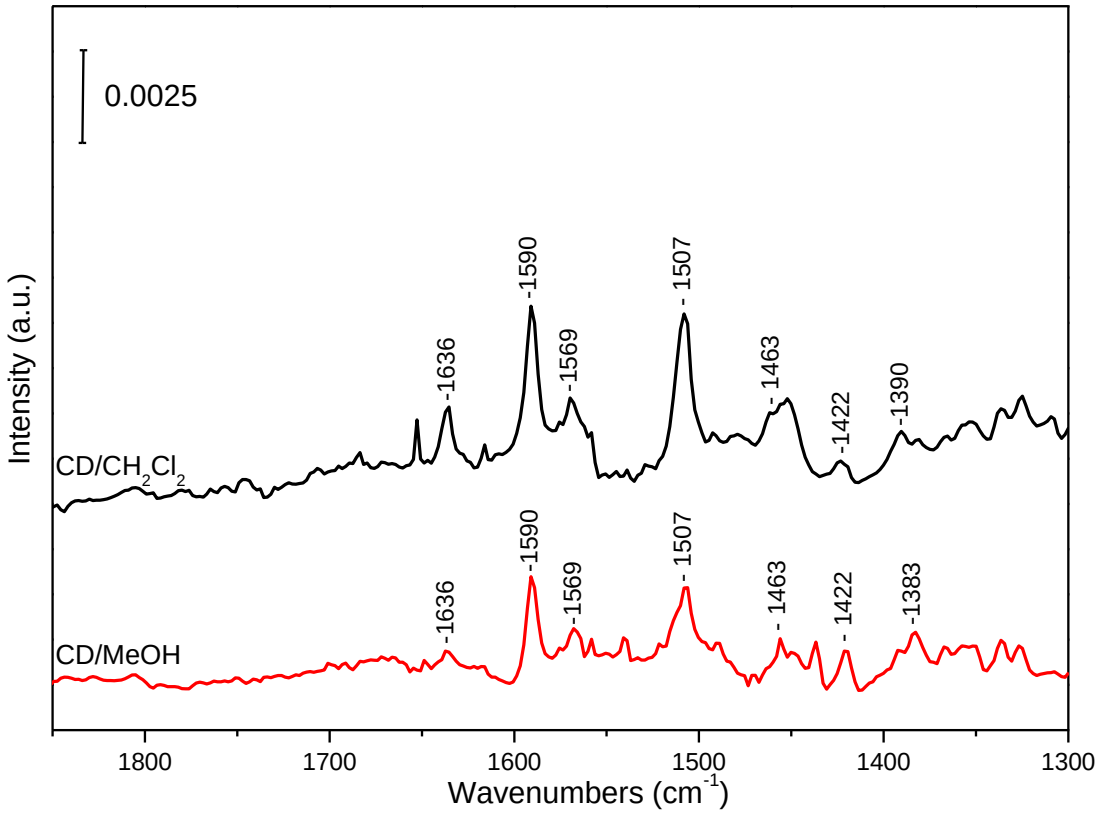

Figure 4.18 ATR-IR spectra of CD (10mM) in CH_2Cl_2 and MeOH solutions on γ-Al_2O_3 surface

Next, the spectra obtained during adsorption of CD on Pd/Al_2O_3 were acquired and are summarized in Figure 4.19. The adsorption of CD in the two solvents shows very similar spectra, with strong signal in the 1500-1600 cm^{-1} region due to in-plane quinoline ring stretch. This suggests a tilted orientation with respect to metal surface. Interestingly, for CD adsorption, the peak intensities in CH_2Cl_2 are always larger than those in MeOH (see Figure 4.17-4.19). According to Zaera and co-workers [222], the solubility of CD in MeOH (73 g/L) is almost 6 times as much as in CH_2Cl_2

(12 g/L). Considering a solubility-adsorption correlation, the greater ATR-IR signal in CH_2Cl_2 is due to more surface-covered CD in this solvent. It also should be noted that in CH_2Cl_2 solvent, the peak intensity of adsorbed CD in the presence of Pd particles is much greater than the case of just Al_2O_3. Given the low weight percent (5%) and metal surface area (<4 m^2 metal/$g_{catalyst}$) of Pd, this observation indicates that the CD is much stronger adsorbed on the metal. The similar band intensity in case of MeOH is again probably due to the high solubility of CD.

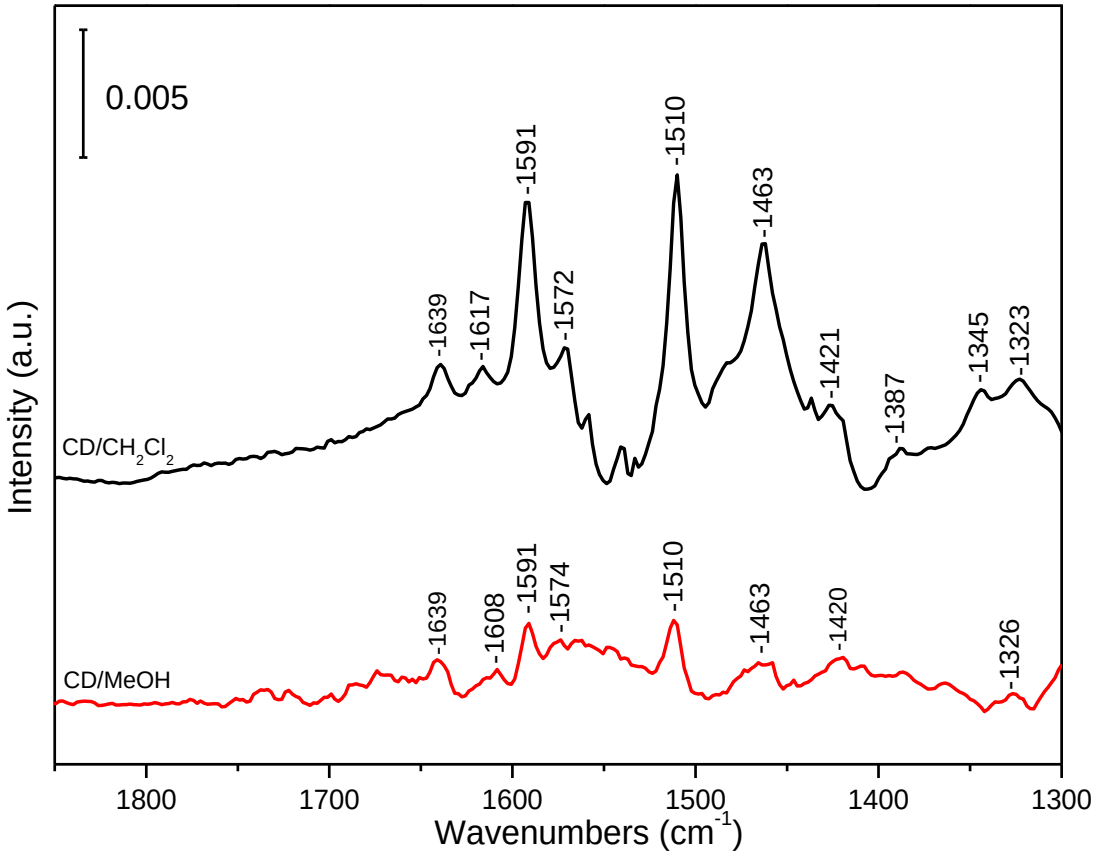

Figure 4.19 ATR-IR spectra of CD (10mM) in CH_2Cl_2 and MeOH solutions on Pd/γ-Al_2O_3 surface

The list of peak assignments of CD in solution and adsorbed on surfaces are provided in Table 4.2. In summary, for the case of cinchonidine adsorption, the

properties of solvents (i.e., polarity, H-bonding) do not significantly affect the adsorption geometry and orientation of adsorbate, although the band intensity varies due to different solubility.

Table 4.2 Peak Assignment of Cinchonidine in solid phase, liquid phase and as adsorbate

Solid	In solution		On Al_2O_3		On Pd/Al_2O_3		Assignment
	MeOH	CH_2Cl_2	MeOH	CH_2Cl_2	MeOH	CH_2Cl_2	
1635	1638	1639	1636	1636	1639	1639	C=C str
1617		1615		1617	1608	1617	Q ip def + QC-H ip bend
1591	1592	1592	1590	1590	1591	1591	Q ip def + QC-H ip bend
1568	1576	1571	1569	1569	1574	1572	Q ip def + QC-H ip bend
1508	1510	1509	1507	1507	1510	1510	Q ip def + QC-H ip bend
1462		1464	1463	1463	1463	1463	QN C(7)H_2 op scissor
1452	1455	1455		1451		1451	QN C(5)H_2 op scissor
1421	1424	1423	1422	1422	1420	1421	Q ip def
	1397	1390	1390	1390			C8-C9 str
1383	1386		1385		1386	1387	Q str + CH ip bend
1367			1364		1363		Q str + CH ip bend
1358			1360				C=C-C def
1336		1347		1337		1345	Q str + QN C(8)H wag
1326	1327	1324		1326	1326	1323	QN CH_2 wag + Q ip def
1307							QN CH and CH_2 wag

Comments: ip-in plane; op-out plane; Q-quinoline ring; QN-quinuclidine

4.2.3. Co-adsorption and intermolecular interactions of CD-Acid complex

Having explored the adsorption behavior of single component (substrate and modifier) on various surfaces, ATR-IR was used to investigate the intermolecular interaction between the acid and cinchonidine. The substrate-modifier interaction plays a key role in determining the complex intermediate structure and orientation with respect to the surface, providing insight into the reaction mechanism.

As shown in Figure 4.20, the CD concentration was fixed at 10 mM. The MPeA/CD ratio was adjusted by injecting MPeA into the reservoir, ranging from 0.5-2 equivalents with respect to CD. It can be seen that along with the increase in MPeA concentration, growing bands appear in the regions of 1360-1410 cm^{-1} and 1520-1560 cm^{-1}. As can be seen, altering the acid/modifier ratio does not affect either band position or shape, although the intensity varies. It is known that the peak at ca. 1390 cm^{-1} is due to the C_8-C_9 stretch of CD, where C_8 is the neighbor carbon atom of quinoclidine N atom, and C_9 is the chiral carbon atom of cinchonidine. The band at 1460 cm^{-1} is assigned as quinoclidine -CH_2 out-of-plane scissoring. However, the bands between 1520-1560 cm^{-1} do not belong to either MPeA or CD in CH_2Cl_2, indicating that they arise from a substrate-modifier interaction. The observations are supported by an FT-IR study of CD-tiglic acid interaction in liquid phase [128].

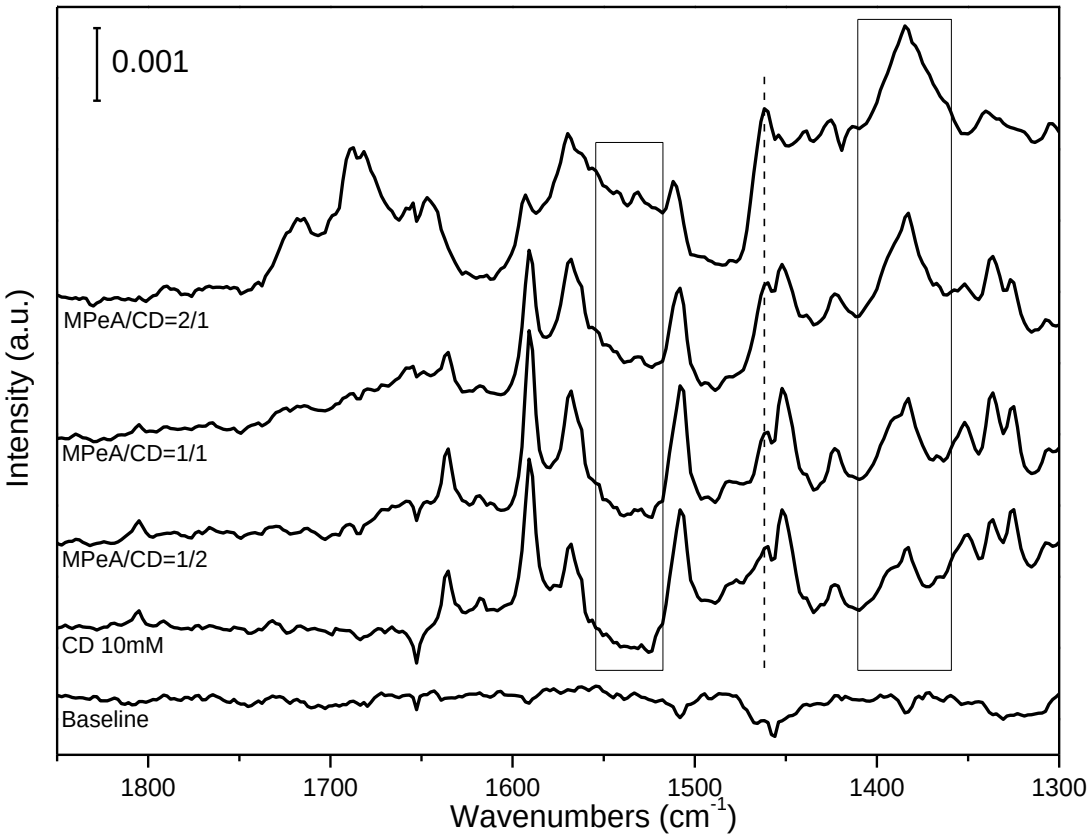

Figure 4.20 ATR-IR spectra of MPeA/CD at different ratio in CH_2Cl_2 solution on bare element

Moreover, it is found that up to a 1/1 MPeA/CD ratio, MPeA featured bands associated with dimer and monomers in solution are not observed. However, above this ratio, the expected bands (between 1670 and 1720 cm^{-1}) appear just as if acid were alone in solution. Such behavior suggests that the type of intermolecular interaction involves substrate with modifier in a 1:1 ratio. The complex prevents the acid from either forming a dimer or remaining in solution as a monomer species. Therefore, judging from the structure of CD and MPeA, such interaction is probably due to H-bonding between the -OH group from CD and the carbonyl group of the

acid, as well as the easily-protonated N atom of quinoclidine moiety of CD and the -OH group of the acid.

Next, the intermolecular interaction of the surface-adsorbed MPeA-CD complex was investigated. A spectrum of a 16 mM MPeA/CH_2Cl_2 mixture flowing over the catalyst surface was first obtained and is shown in Figure 4.21. Then, CD was stepwise added into the liquid mixture to reach various CD/MPeA ratios from 1:8 to 1:1. As the CD concentration was increased, the MPeA featured bands in the 1650-1750 cm^{-1} region decreased in intensity. Meanwhile, even at the smallest ratio (1/8), the peaks belonging to the quinoline ring of CD (1515, 1570, and 1590 cm^{-1}) start to arise. Moreover, these peaks keep increasing with increased CD concentration, indicating a relatively stronger adsorption of modifier compared to substrate acid. In addition, at 1460 cm^{-1} and in the 1360-1410 cm^{-1} and 1520-1560 cm^{-1} regions, the band intensities increased with addition of CD, suggesting the formation of an intermolecular interaction at the Pd/Al_2O_3 surface. By comparing Figures 4.20 and 4.21, clearly the intermolecular interactions show up at same region, although the intensity differs. This suggests that the acid-modifier complex exhibits a specific type of interaction, regardless of the ratio of two species, and whether the complex exists in solution or adsorbed at the surface.

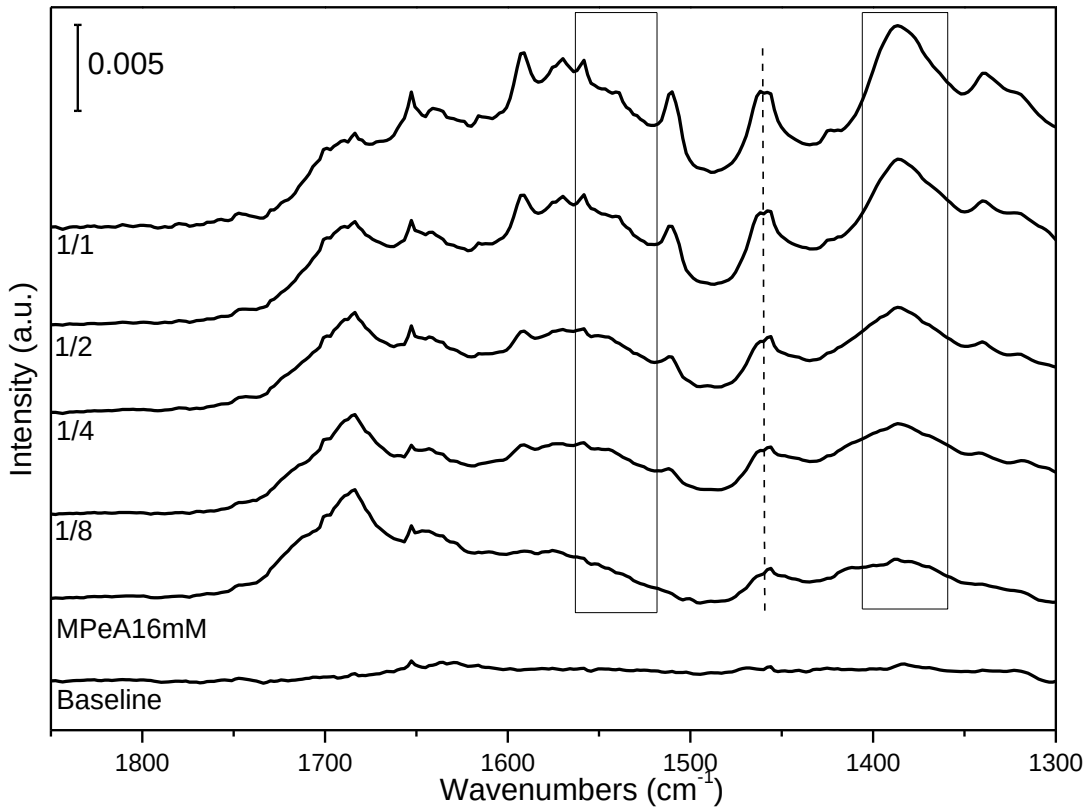

Figure 4.21 ATR-IR spectra of CD/MPeA at different ratio in CH_2Cl_2 solution on Pd/γ-Al_2O_3 surface

The same experiment was carried out in MeOH solvent. As can be seen in Figure 4.22, although the MPeA shows peaks in the region of 1360-1410 cm^{-1} and 1520-1560 cm^{-1}, shoulders and bands at 1510, 1574, and 1590 cm^{-1} due to quinoline ring deformation of the modifier could be observed with increasing CD, indicating a replacement of adsorbed substrate acid by modifier.

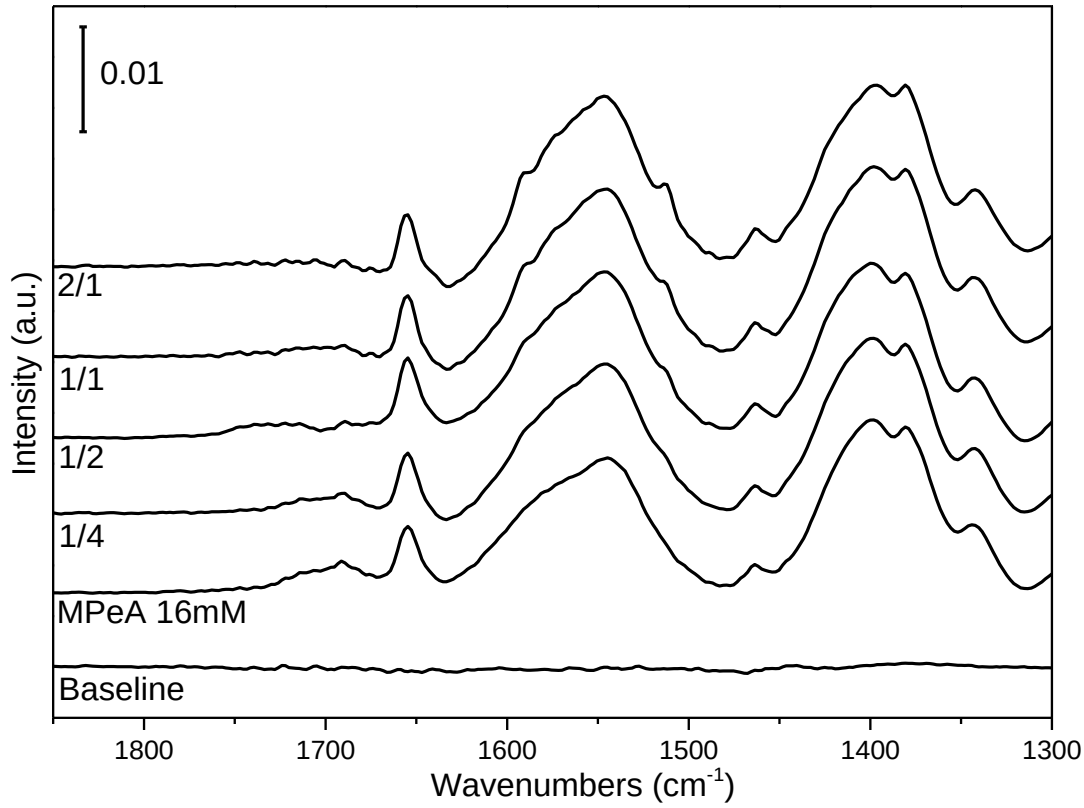

Figure 4.22 ATR-IR spectra of CD/MPeA at different ratio in MeOH solution on Pd/γ-Al_2O_3 surface

Finally, it is interesting to determine if the adsorption sequence will affect this interaction. To examine this, a series of experiments were carried out based on the following routine. The two species (20 mM substrate acid and 10 mM modifier) were introduced onto Pd/Al_2O_3 surface in sequential order with solvent flushing between the steps, followed by solvent purging. Then, the final obtained spectra were compared and shown in Figures 4.23 and 4.24 for CH_2Cl_2 and MeOH, respectively. As can be seen, the bands due to acid-modifier complex, although exhibiting slightly different intensity, show up at same region, demonstrating again a specific type of intermolecular interaction regardless of the adsorption sequence of acid and modifier.

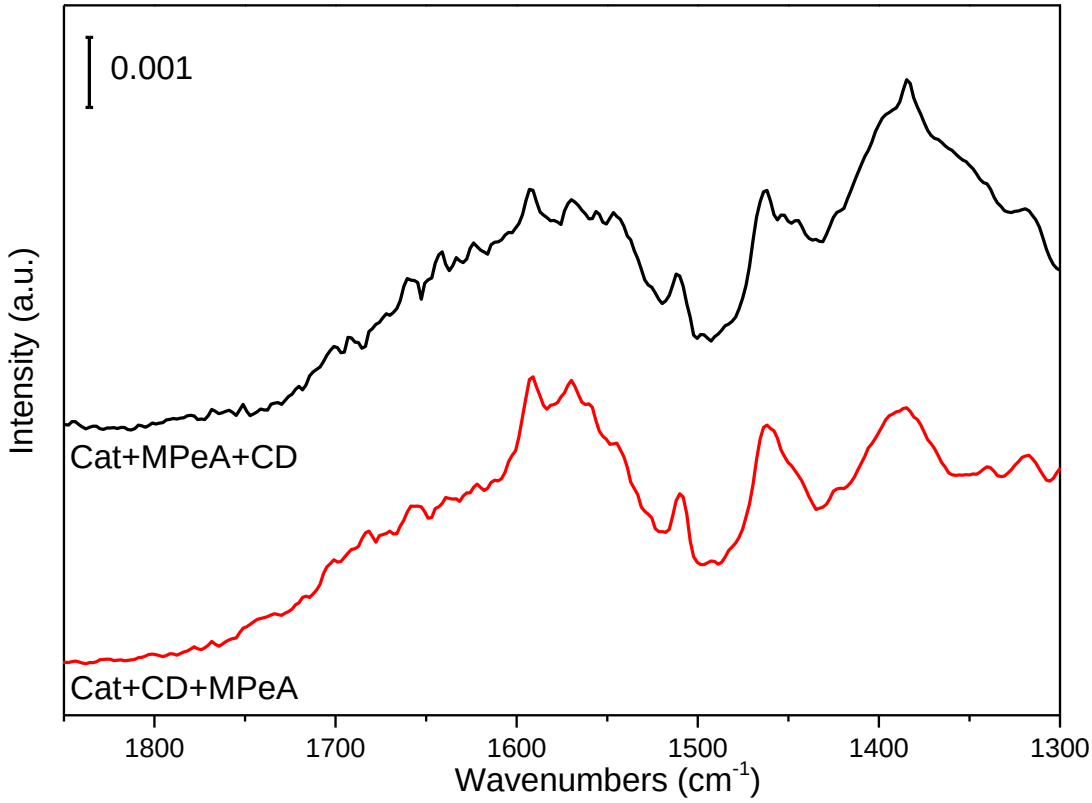

Figure 4.23 Sequential ATR-IR study of CD-MPeA interaction in CH_2Cl_2 solution on Pd/γ-Al_2O_3 surface

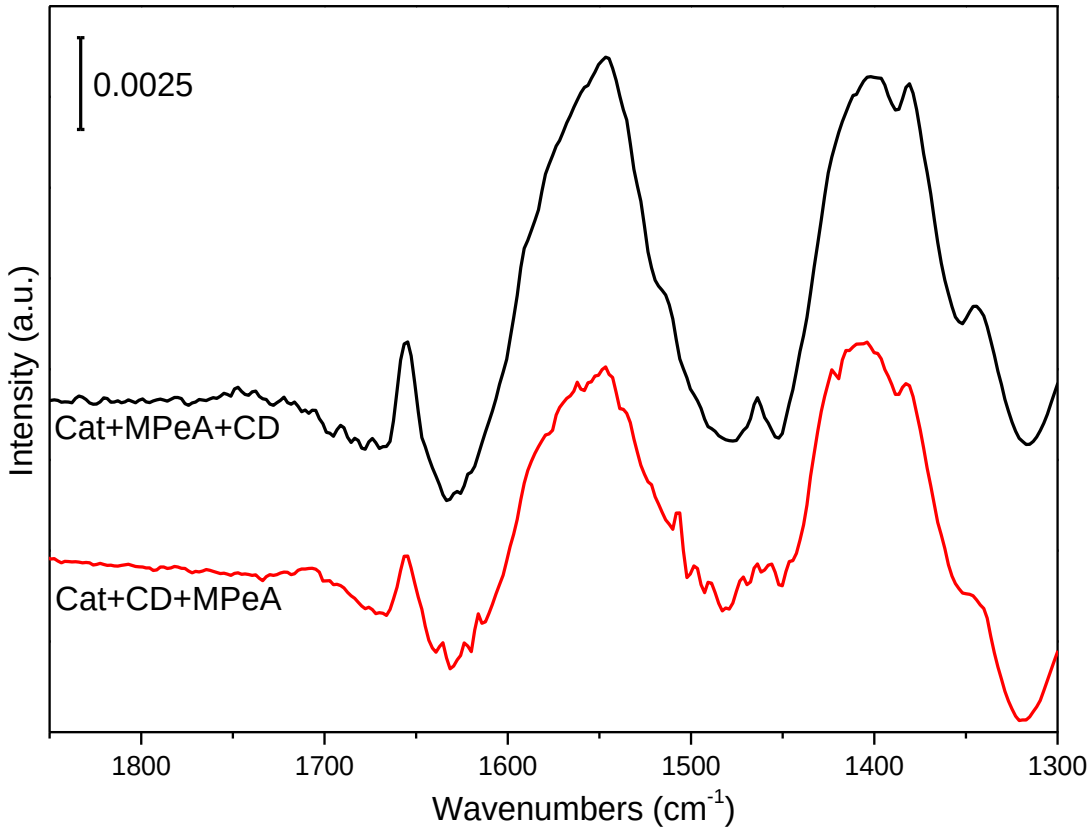

Figure 4.24 Sequential ATR-IR study of CD-MPeA interaction in MeOH solution on Pd/γ-Al_2O_3 surface

Thus, we propose a modifier-acid=1:1 complex model under the current conditions. Previously, Nitta [122], Bartok [145], and Szollosi [144] have assumed this type of intermediate in polar solvent, which is consistent with the current study. In contrast, Baiker, assuming that alkanoic acids prefer to form a dimer in apolar medium, suggested a 1:2 modifier:acid complex in nonpolar solvent. They based this on the observation that no further increase of e.e. value was achieved when CD/acid ratio varied from 0.5 to 1. Since not many studies have been reported regarding the dependence of kinetic behavior on CD/acid ratio, determining the preferred complex structure from a kinetic standpoint requires further investigation. Nevertheless, the

present study provides direct spectroscopic evidence of the active substrate-modifier complex at the metal surface under a liquid phase condition (although in the absence of dissolved hydrogen). Further studies are planned to directly correlate the presence of this species with kinetic behavior observed in batch studies.

In this section, an adsorption study of CD at Al_2O_3 and Pd/Al_2O_3 surfaces in two solvents (MeOH and CH_2Cl_2) with *in-situ* ATR-IR technique was conducted. The different solvents do not appear to affect the adsorption behavior of cinchonidine in terms of adsorption orientation. The fixed band position (1360-1410 cm^{-1} and 1520-1560 cm^{-1}) and peak shape of substrate-modifier complex in the investigation of intermolecular interaction demonstrates that the modifier shows a preferred adsorption on Pd/Al_2O_3 compared to MPeA. Moreover, the complex prefers to form CD-MPeA=1:1 structure either in solution or adsorbed on surface, probably due to H-bonding between "O-H---O" and "N---H-O", respectively. This type of interaction is not affected by the adsorption sequence of two species. Such behavior could possibly explain the fixed raised preferential enantioselectivity in this aliphatic alkenoic acid-cinchonidine system. The current work elucidates the intermolecular interactions of the acid-modifier complex in solution and at the metal oxide surface. Future work will focus on coupling these *in-situ* spectroscopic measurements with kinetic investigations, aiming to understand the reaction mechanism of asymmetric C=C hydrogenation over cinchona-modified Pd.

4.2.4. Monitoring hydrogenation via ATR-IR

Given the behavior of single component, as well as the intermolecular interaction, in both liquid phase and as adsorbate, the next step was to examine the

hydrogenation via *in-situ* ATR-IR spectroscopic technique. Figure 4.25 shows the stacked spectra obtained during the MPeA hydrogenation reaction. After collecting the background baseline in pure MeOH solvent, a 16 mM MPeA solution was flowed through the catalyst-coated IRE for 1 hour. Then, H_2 was bubbled into the mixture and the spectra were continuously collected throughout the entire process. As can be seen, the band at ca. 1650 cm^{-1}, which is assigned as ν(C=C), has slightly decreased its intensity as hydrogenation occurs over time. Meanwhile, a significant peak shift could be observed at ca. 1400-1420 cm^{-1} by comparing the MPeA spectrum and the one after hydrogenation for 1 hour. The new appeared peak remains at same position, while continuing to increase the intensity as the reaction progresses.

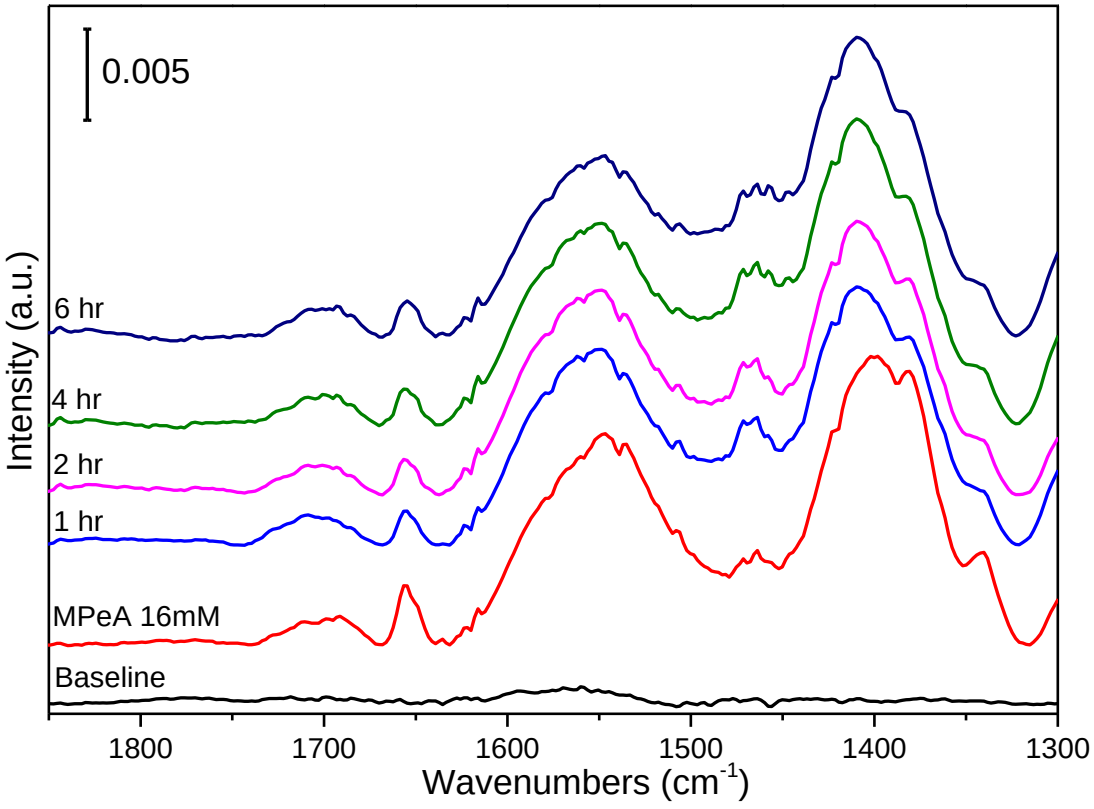

Figure 4.25 ATR-IR spectra obtained during hydrogenation of 16 mM MPeA over 5 wt% Pd/Al_2O_3 in MeOH

To analysis this data in further detail, a series of spectra during the first hour of hydrogenation are stacked in Figure 4.26. It can be clearly seen that during the first 5 min of bubbling H_2 into solution, the ν(C=C) band (ca. 1655 cm^{-1}) decreases its intensity together with a peak shift from 1400 cm^{-1} to 1420 cm^{-1}. Such observation is direct evidence of the reactant (MPeA) being hydrogenated to form product (MPaA).

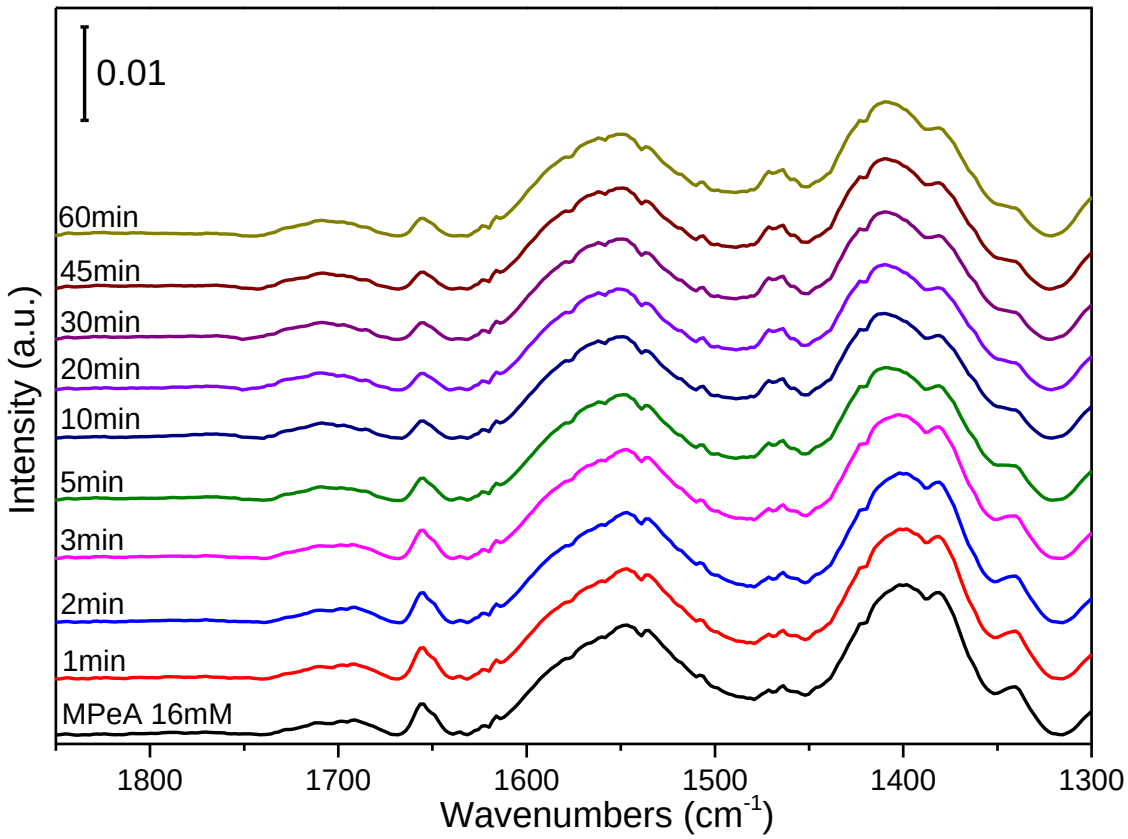

Figure 4.26ATR-IR spectra for first hour of hydrogenation of 16 mM MPeA over 5 wt% Pd/Al_2O_3 in MeOH

Since ν(C=C) is the cleanest feature to distinguish between reactant and product, the change of its intensity with time is plotted in Figure 4.27. As the black dots indicate, the first two points have quite similar intensity. This is possibly due to the delay for H_2 dissolving in MeOH, creating lag time before it can dissociate on the

surface and interact with MPeA adsorbate. However, as the H_2 is bubbled into the liquid mixture, the C=C group was continuously hydrogenated as can be seen by the decrease in ν(C=C) intensity. The intensity decreased to ca. half of its original value at ca. 20 min, and then remained at the same level. The reason for ν(C=C) signal not being completely eliminated is explained by the presence of inactive species containing C=C stretches that are adsorbed on the Al_2O_3 surface rather than Pd particles.

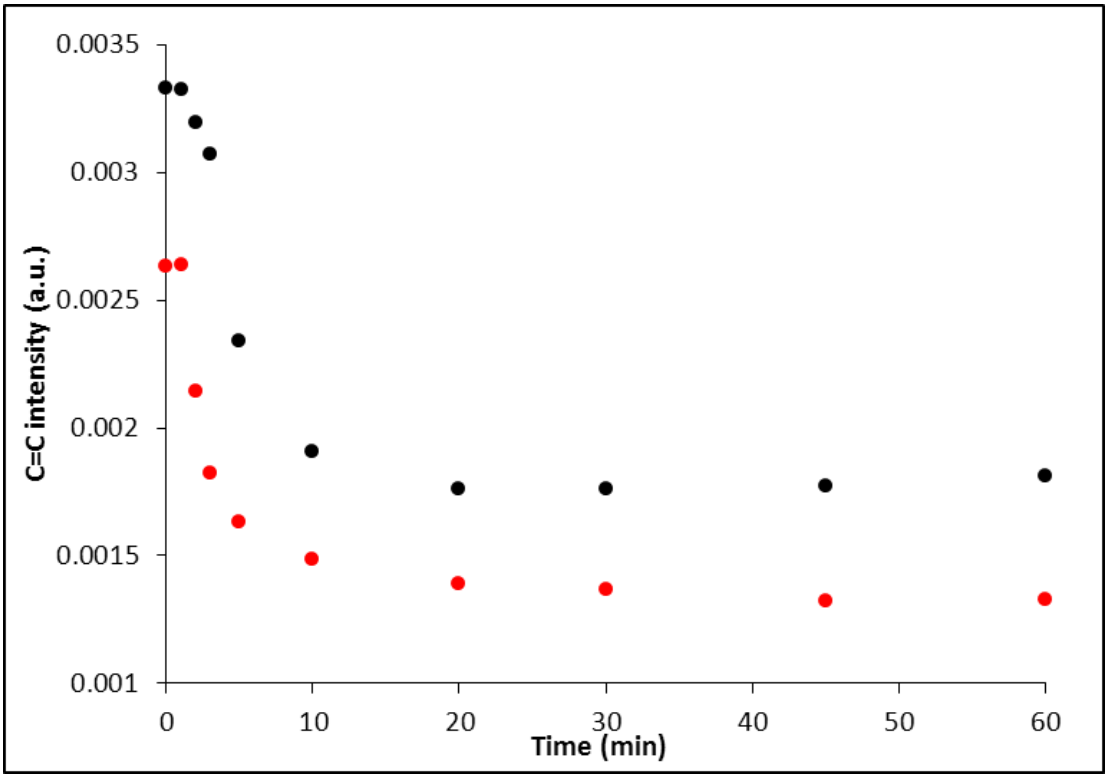

Figure 4.27 Change of ν(C=C) intensities along with hydrogenation time from MPeA as adsorbate (red dots), and in presence of 16 mM MPeA solution (black dots)

Next, we examined the behavior of the adsorbate alone during the hydrogenation. So, after 16 mM MPeA solution flowed through the cell for 1 hour, pure solvent was applied to purge the element surface for 1 hour. This is long enough to leave only adsorbed MPeA on the surface. Then, H_2 was bubbled into system to initiate the

hydrogenation. A similar trend was observed from Figure 4.27, after a short period of time (<3 min) due to H_2 saturation. Once again, the C=C bond was hydrogenated until the ν(C=C) intensity decreased to about half of its original. Again, this result suggests that the adsorbate on Al_2O_3 in inactive and remains on surface.

4.3. Kinetic Evaluation of Asymmetric Hydrogenation

Enantioselective catalytic hydrogenation of unsaturated carboxylic acids has been investigated extensively due to the potential applications in the pharmaceutical, fragrance, and fine chemicals industries [8, 223, 224]. The first report of enantioselective hydrogenation of a C=C bond with cinchona-modified transition metal catalyst was in 1985 [117]. In the research conducted since then, aliphatic and aromatic alkenoic acids are the two main types of probe molecules that have been investigated. Nitta *et al.* chose (E)-α-phenylcinnamic acid as a substrate, and have investigated reaction variables that affect the activity and enantioselectivity [49, 57, 118, 119]. Their best e.e. value reported is ca. 72 % for the S-product with cinchonidine-modified 5 wt% Pd/TiO_2 catalyst in DMF [120]. The sense of enantioselectivity is actually determined by structure of both modifier and substrate. This e.e. value has been slightly improved to 82.6 % by Sugimura and co-workers under more optimal conditions [225]. However, only moderate e.e. values (ca. 40%-50%) have been obtained for hydrogenation of the C=C bond in aliphatic acids (*e.g.*, itaconic acid, tiglic acid) [43, 226, 227].

The adsorption of modifier (cinchona alkaloids) [172, 228] and substrate (α, β-unsaturated carboxylic acids) [208, 218] on metal and oxide surfaces have been investigated. Several substrate-modifier interaction models have been proposed

based on experimental and theoretical studies, aiming at a mechanistic explanation of heterogeneous enantioselective hydrogenation of C=C bonds on cinchonidine-modified Pd [128, 130, 131, 143, 144, 149, 215]. Generally, these models propose that the substrate interacts with modifier through hydrogen-bonding, by a protonated quinuclidine N as well as the hydroxyl group of cinchona and the carboxylic group from the substrate in either monomeric or dimeric formation. However, there is no literature investigating the detailed kinetic features of the heterogeneous catalytic C=C bond hydrogenation of unsaturated carboxylic acid.

In this section, asymmetric hydrogenation of the C=C bond in a model α, β-unsaturated carboxylic acid (2-methyl-2-pentenoic acid) is explored over cinchona-modified 5 wt% Pd/γ-Al_2O_3 catalyst to produce the corresponding (R)- and (S)-2-methylpentanoic acid (see Figure 4.28). The experimental kinetic data obtained during both racemic and enantioselective hydrogenation allowed for increased mechanistic understanding of this important class of reactions.

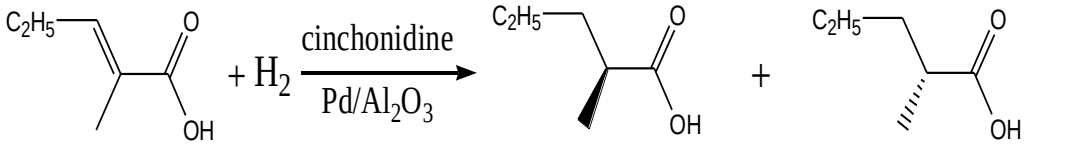

2-methyl-2-pentenoic acid (S)-2-methylpentanoic acid (R)-2-methylpentanoic acid

Figure 4.28 Hydrogenation reaction of *trans*-2-methyl-2-pentenoic acid

4.3.1. Aspects of racemic reaction

Prior to examination of the cinchonidine modified catalyst, the racemic hydrogenation was examined with the aim of establishing and understanding the baseline kinetic behavior of this system. Several parameters were considered for the hydrogenation reaction, including initial substrate concentration, solvent, and H_2

pressure. A summary of these kinetic data are shown in Table 4.3. As the data indicates, this type of hydrogenation reaction is strongly solvent-dependent in terms of the activity. Among the three chosen solvents, methanol exhibits the best activity (see entries 8-14). 1, 4-Dioxane also provides satisfactory values (see entries 3-7), while CH_2Cl_2 exhibits almost no activity (see entries 1-2). The solubility of H_2 in these three solvents under 298.15 K and 0.1 MPa are quite similar (mole fractions = ca. 1.60 - 1.95 x 10^{-4}) [229, 230]. Previous studies have focused on the effect of solvent polarity on enantioselectivity. Generally, the increased polarity of solvent leads to a poorer catalytic performance for aliphatic acids, while in contrast it enhances performance for aromatic acid [56, 143]. However, the effect of solvent polarity on activity has not been extensively examined. Judging from the normalized empirical solvent parameter for polarity, which is E_T^N, methanol gives 0.762, which is greater than dioxane (0.164) or dichloromethane (0.309) [231]. At least in the current study, the highly polar solvent is found to be advantageous for hydrogenation activity. The contrary effects of solvent polarity towards the activity and enantioselectivity of aliphatic acid hydrogenation suggest that the emphasis must be placed on increasing the former by other means than using a high polarity solvent, given the importance of the latter. The data from Table 4.3 also suggest that the H_2 pressure is of importance in terms of conversion and initial reaction rate. Not surprisingly, up to a point, higher pressure leads to higher conversion and faster initial reaction rate.

Table 4.3 Summary of kinetic results of racemic hydrogenation

Hydrogenation of MPeA over Pd/γ-Al_2O_3 catalyst[a]

Entry	Solvent	H_2 Pressure(atm)	Conversion(%)	r_0 (mmol h^{-1} g^{-1}_{cat})
1[b]	CH_2Cl_2	1	0	0.0
2[b]	CH_2Cl_2	5	4	0.1
3	Dioxane	0.5	26	10
4	Dioxane	1.5	64	39
5	Dioxane	2.5	78	61
6	Dioxane	10	97	81
7	Dioxane	20	99	112
8	MeOH	0.5	52	27
9	MeOH	1.5	99	100
10	MeOH	2.5	99	206
11	MeOH	5	99	390
12	MeOH	10	99	513
13	MeOH	20	99	690
14	MeOH	30	99	852

[a] 60 ml solvent, 700 μl substrate, 0.05g 5 wt % Pd/γ-Al_2O_3, 25 ℃, 1000 rpm stirring rate, 8 hr.
[b] carried out with 0.1 g catalyst, 6 hr.

Ensuring the absence of the mass transfer limitation in the system is quite critical in obtaining reliable evaluation for the kinetic aspects. Accordingly, different stirring rates were applied to examine whether the current condition is under external mass transfer control. As Figure 4.29 shows, the initial rates remain similar values at different stirring rate while keeping other reaction condition same. The observation indicates that the hydrogenation reaction under such condition is kinetically controlled.

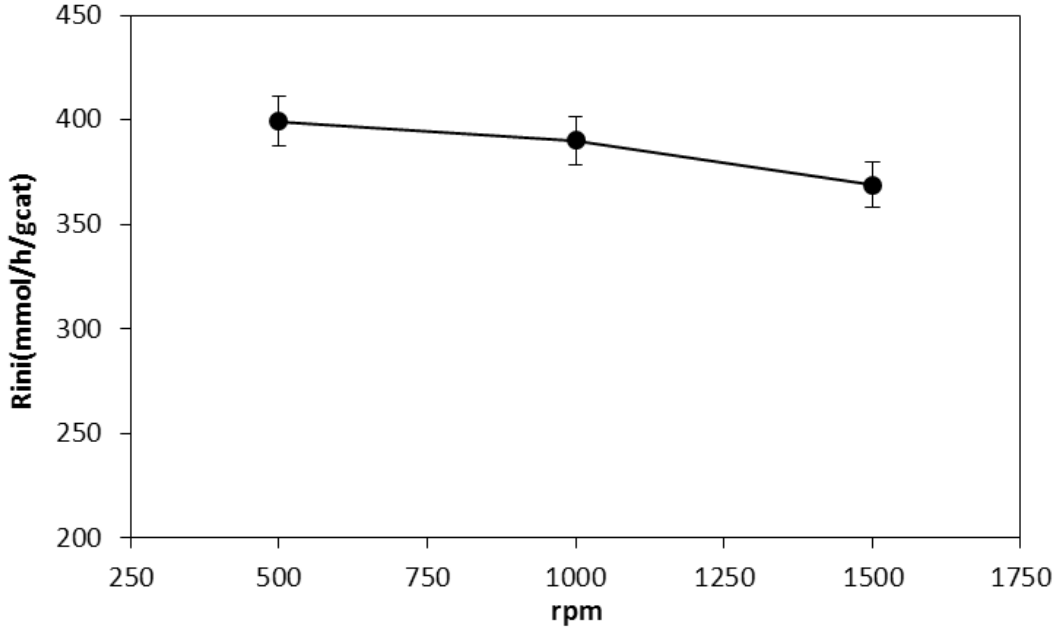

Figure 4.29 External mass transfer limitation on catalytic activity of racemic reaction under 5 atm H_2 pressure

In a typical racemic reaction, the concentrations converted from GC analysis result were plotted as a function of reaction time. Figure 4.30 is an example of a concentration ~ time plot.

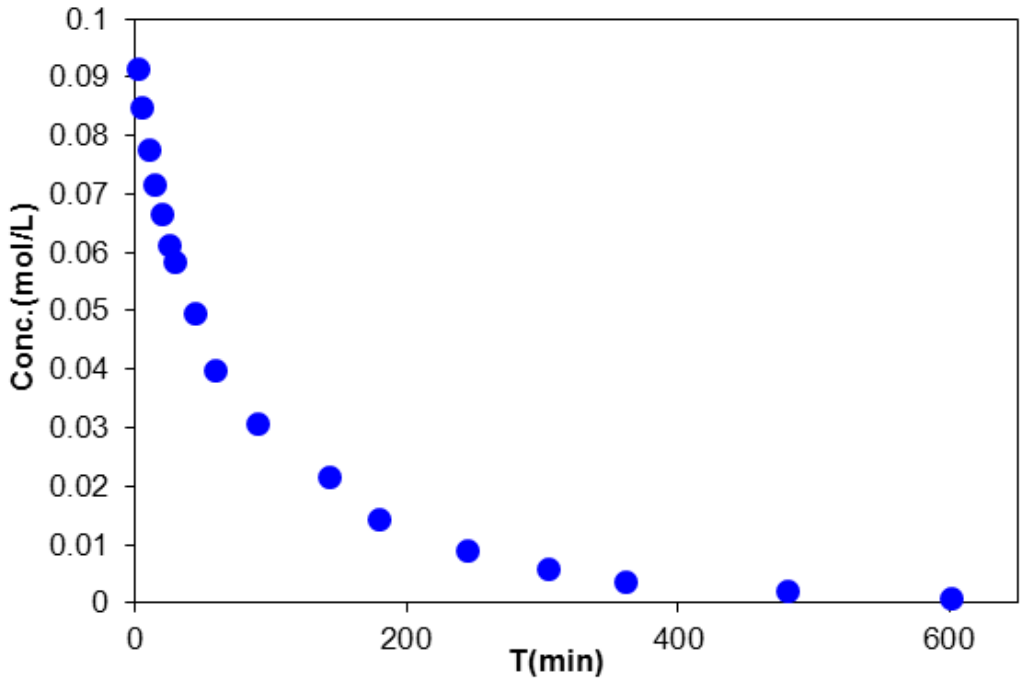

Figure 4.30 An example of typical concentration-time plot of racemic hydrogenation of MPeA under 5 atm H_2 pressure

The experimental data (e.g, concentration from gas chromatography as y-axis, and reaction time as x-axis) was loaded into *CurveExpert* software. Then, the plots fitted in a non-linear regression. More than twenty different equations were applied automatically with the software. The curve fitting procedure was run in a least square regression, and the final results were listed from best to worst (see Figure 4.31). Usually, Complex Exponential Model (Eq. 4.1) and Rational Model (Eq. 4.2) shown as follows were best fits:

$$conc. = ae^{bt} \qquad \text{Equation 4.1}$$

where a and b are the parameters that allowed to vary.

$$conc. = \frac{a + bt}{1 + ct + dt^2} \qquad \text{Equation 4.2}$$

where a, b, c, and d are the parameters that are allowed to vary.

Given the conc. ~ time relationship, the initial reaction rate can be determined by calculating the derivative of the corresponding function at t=0.

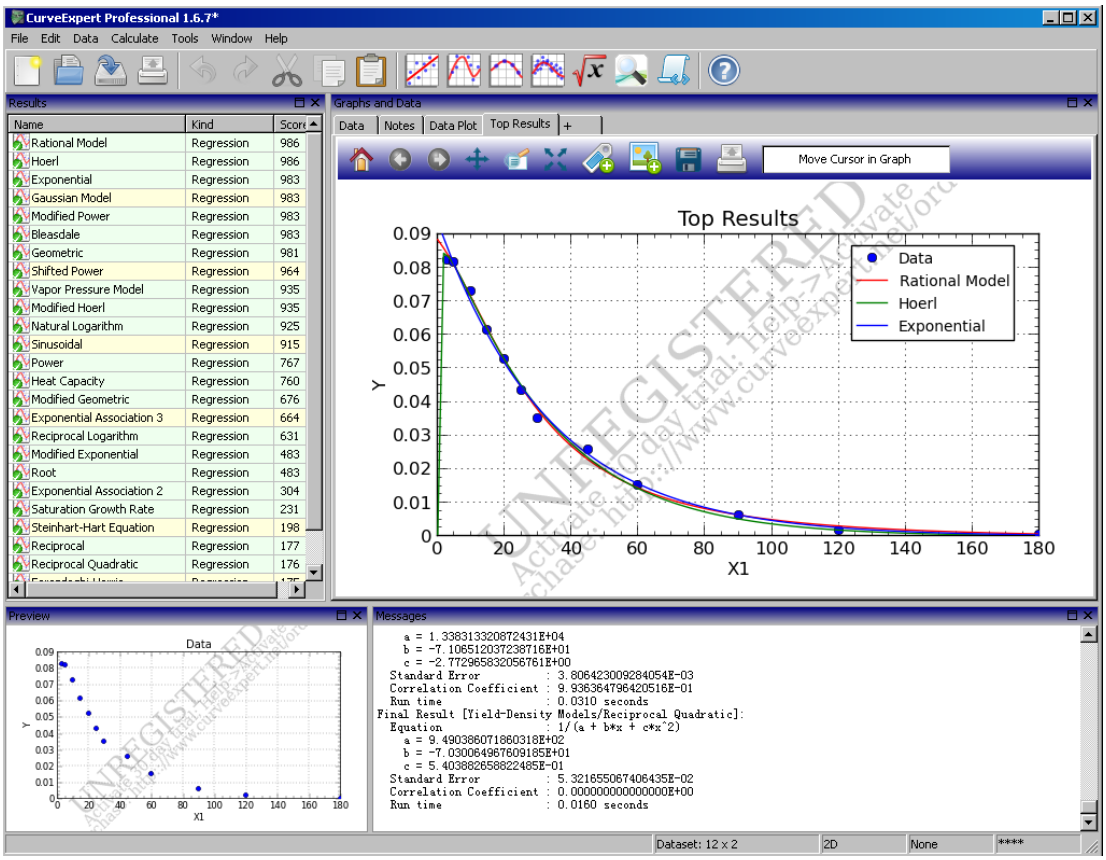

Figure 4.31 Screenshot of an example of curve fitting with *CurveExpert* software

The hydrogenation reaction rate can be expressed in a typical power law form as:

$$r = -\frac{dc}{dt} = kP^{\beta}_{H_2}c^{\alpha} = k_{app}c^{\alpha}. \qquad \text{Equation 4.3}$$

The differential method was applied to calculate the reaction order with respect to the reactant and the H_2 pressure. To be specific, plotting ln(-dc/dt) versus ln(c) yields the reaction order (α) and the apparent reaction constant (k_{app}) with respect to the acid substrate. As shown in Figure 4.32, the MPeA reaction order is ca. 1 up to

around 90 min (corresponding to conversions less than 60%), but increases to about 1.5 to 2 at higher conversions. Figure 4.33 shows further analysis by plotting $\ln k_{app}$ versus $\ln P_{H2}$, which allows for the evaluation of the reaction order with respect to H_2 pressure. Under low to moderate pressure (< 8 atm), the reaction exhibits a 1st order dependence on H_2 pressure. However, the reaction becomes H_2-independent in the higher pressure regime (> 20 atm). The transition regime between 8 and 20 atm is clearly seen. Our observation is contrary to a previous study, in which H_2 exhibits a half-order in Pd enantioselective reaction of methyl pyruvate while first-order in Pt-derived reaction [232, 233]. The linear dependence in the low pressure regime can be explained by the surface coverage of adsorbed H atoms being proportional to dissolved H_2 in liquid phase under low pressure regime. As H_2 pressure increases, the H atoms saturate the surface resulting in the zero-order dependence.

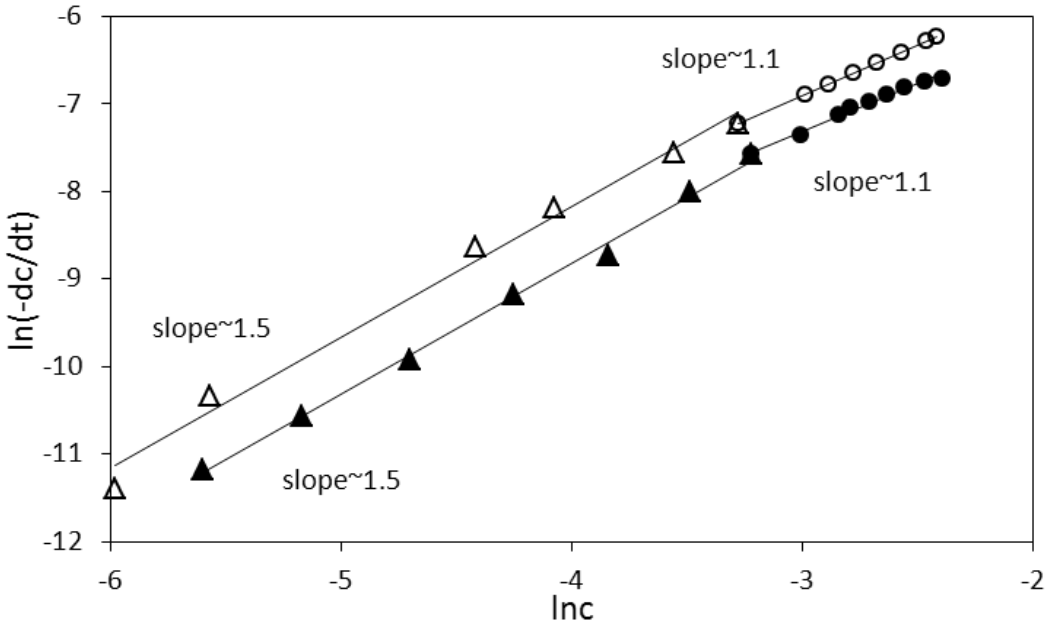

Figure 4.32 Reaction orders with respect to substrate in absence (solid triangles/circles) and presence (open triangles/circles) of modifier

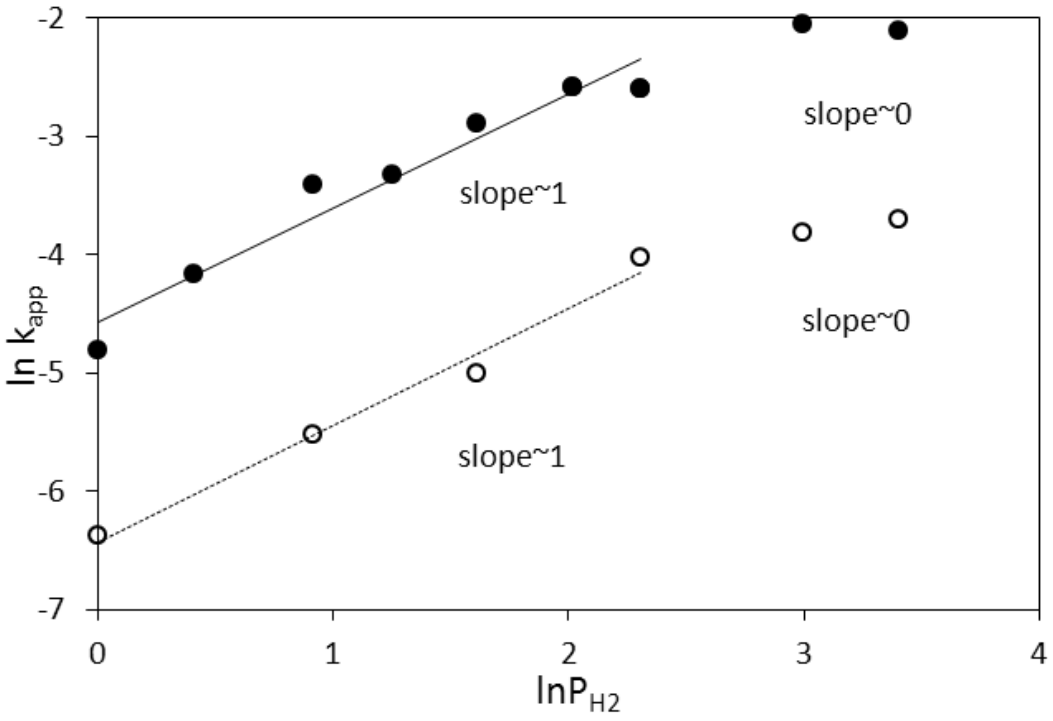

Figure 4.33 Reaction orders with respect to H_2 pressure in absence (solid circles) and presence (open circles) of modifier

4.3.2. Aspects of enantioselective reaction

Having established the baseline kinetic behavior for the racemic hydrogenation of MPeA, cinchonidine modifier was introduced into the system to engender the enantioselectivity. In all enantioselective reactions, the modifier: substrate ratio was chosen as 1/20, which is very typical ratio that has been explored in the literature [127, 234]. Since it is well known that the addition of cinchonidine often retards the rates for this class of reactions [232, 235], MeOH was chosen as the solvent to provide the maximum activity.

The reaction orders with respect to both acid substrate and H_2 were re-examined in the presence of modifier. As demonstrated in Figure 4.32, for the enantioselective hydrogenation, the presence of modifier has no effect on substrate reaction order.

This demonstrates that the mechanism for hydrogen addition to the acid is likely the same even in the presence of adsorbed cinchonidine on metal surface. Also, Figure 4.33 indicates that the H_2 pressure exhibits a similar behavior as the racemic reaction, showing again 1st order dependence below ca. 8 atm and trending to zero order above 20 atm. Again, this indicates that the CD modifier does not affect significantly the population of H atoms on the Pd surface.

Table 4.4 summarizes the kinetic results for the enantioselective hydrogenation. There is a modest increase in enantioselectivity with H_2 pressure. However, unlike the hydrogenation of α-ketoester with cinchona-modified Pt, where the reaction rates are enhanced dramatically with modifier present [153], a significant decrease (by a factor of 4-7) in the initial reaction rate is observed in the presence of modifier (see Table 4.4). Wells and co-workers investigated hydrogenation of some unsaturated acids and esters (e.g., methyl tiglate, and angelic acid) over 1 wt% Pd/SiO_2 catalyst. Similar to our observation, the initial reaction rates diminish by a factor of 3 ~ 6 when cinchonidine is introduced into the system [233]. This has been explained by the blockage of active sites on the Pd surface due to the strong adsorption of cinchonidine modifier.

Table 4.4 Summary of kinetic results of enantioselective hydrogenation

Enantioselective hydrogenation of MPeA over CD-modified Pd/γ-Al_2O_3 catalyst[a]

Entry	H_2 Pressure(atm)	Time(h)	Conversion(%)	r_0 (mmol h^{-1} g^{-1}_{cat})	e.e. (%)	cat.(g)
1	1	12	70	11 (56)	17	0.05
2	2.5	11	95	35 (206)	20	0.05
3	5	9	98	74 (390)	23	0.05
4	10	6	98	133 (513)	26	0.05
5	20	6	99	246 (690)	29	0.05
6	30	6	99	254 (852)	30	0.05

[a] 60 ml solvent (MeOH), 700 μl substrate, 0.088g cinchonidine, 0.05g catalyst, 25 ℃, 1000 rpm stirring rate. As comparison, the initial reaction rate in the absent of modifier under the same reaction condition is shown again in parenthesis.

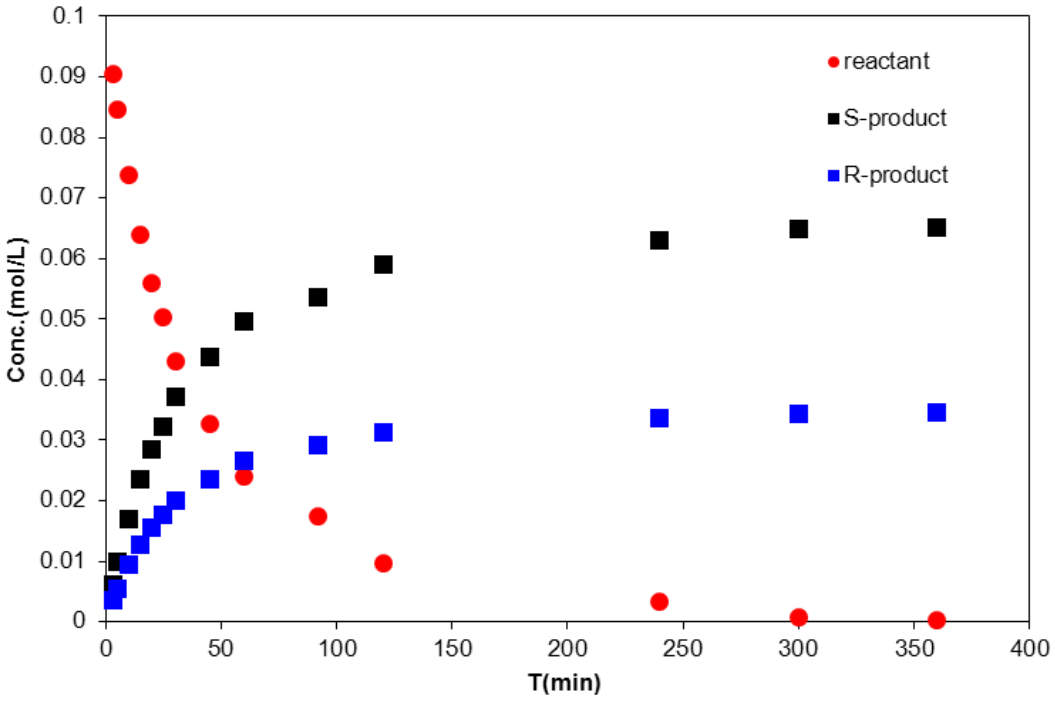

Figure 4.34 An example of typical concentration-time plot of enantioselective hydrogenation of MPeA under 30 atm H_2 pressure

The above Figure 4.34 is a typical concentration ~ time plot of an enantioselective hydrogenation. The reaction rates of reactant, S-product and R-product could be determined by functionalizing the fit with *CurveExpert* software.

To explore these kinetics further, an analysis was performed by making the following assumptions: 1) The total number of sites (S) is constant during the racemic and enantioselective hydrogenation. 2) Unmodified sites (U) exhibit the same activity, whether in the absence or presence of modified sites. 3) Modified sites (M) exhibit a perfect selectivity, directing the hydrogenation 100% towards the S-enantiomer. A series of mathematical manipulations yield the following equations:

$$r_{rac}=S*TOF_U \qquad \text{Equation 4.4}$$

$$r_R=0.5*U*TOF_U \qquad \text{Equation 4.5}$$

$$r_S=0.5*U*TOF_U+(S-U)*TOF_M \qquad \text{Equation 4.6}$$

where r_{rac} is the initial rate of racemic reaction, r_R and r_S are the initial rate of R and S product of enantioselective reaction, respectively.

Using the above equations, Figure 4.35 shows the calculated percentage of modified sites (M) out of the total number of sites (S) as a function of H_2 pressure (see solid dots). The plot indicates that the H_2 pressure has no effect on percentage of modified sites, at least at the substrate: modifier: surface ratio used here (20:1:0.05). Similar conclusions had been drawn in Nitta's previous study of Pd/TiO_2 catalyst for hydrogenation of (E)-2, 3-diphenyl-2-propenoic acid and tiglic acid by estimation of H_2 pressure influence on both reaction rate and e.e. value [121].

To examine the applicability of this conclusion, a less constrained analysis has been made by removing the assumption of perfect enantioselectivity of modified site (M). Thus, the corresponding equations are as follow:

$r_{rac}=S*TOF_U$ Equation 4.7

$r_R=0.5*U*TOF_U+R\%*(S-U)*TOF_M$ Equation 4.8

$r_S=0.5*U*TOF_U+(1-R\%)*(S-U)*TO)_M$ Equation 4.9

Where "R%" refers to the percentage of R-product that formed on modified site.

According the current study, "R%" has a maximum value of 35% to guarantee the physical meaning of the reaction (e.g., all parameters are supposed to be positive number, and percentage of modified site (M) should be less or equal to 1). It can be seen in Figure 4.35 that as increase of R% value from 0 to ca. 0.35, the percentage of modified site also becomes greater (until 100%). The bars above each point indicate the entire possible region of R% value under different H_2 pressure. Again, we could draw the conclusion that the modifier-occupied sites remain very stable regardless of H_2 pressure regime, which indicates that the assumptions have been made are reasonable for this system.

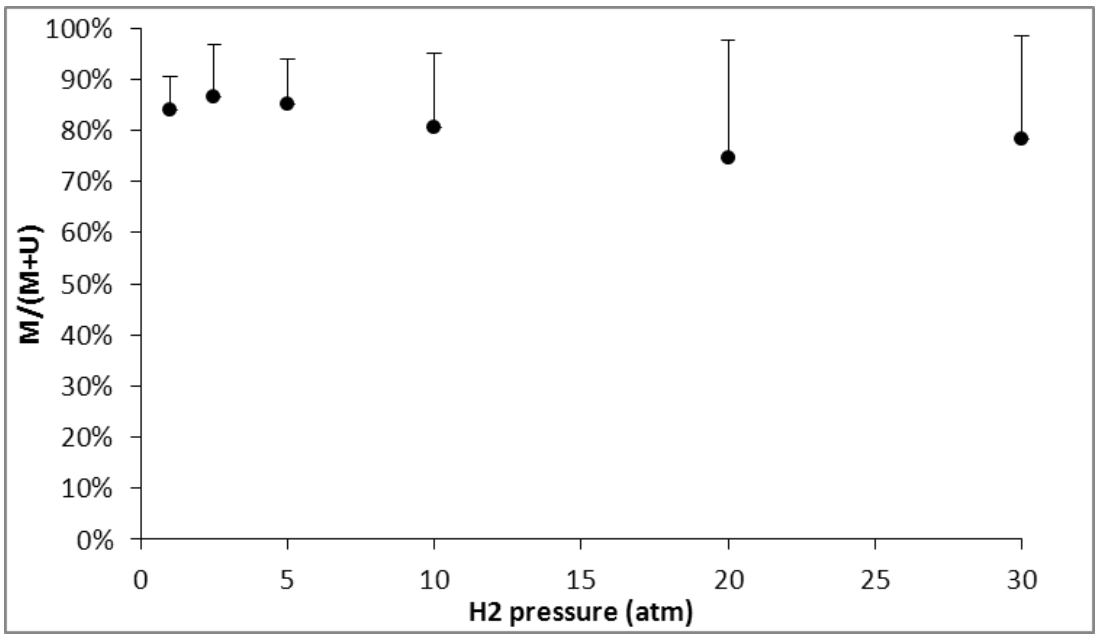

Figure 4.35 Effect of H_2 pressure on percentage of modified site

Moreover, Figure 4.36 shows the corresponding calculated turnover frequency (TOF) of modified and unmodified sites. It suggests that higher H_2 pressure leads to higher TOF on both types of sites. The ratio of unmodified/modified site TOF is in the region of 7 to 28, which is consistent with the previous studies of a similar system [126]. Again, the bar for each point of modified site reflects the TOF region at all possible R% value. Nevertheless, the study suggests that the activity of modified sites due to CD adsorption is quite decreased compared with unmodified sites, and the H_2 pressure effect does not exhibit any priority on one site over another.

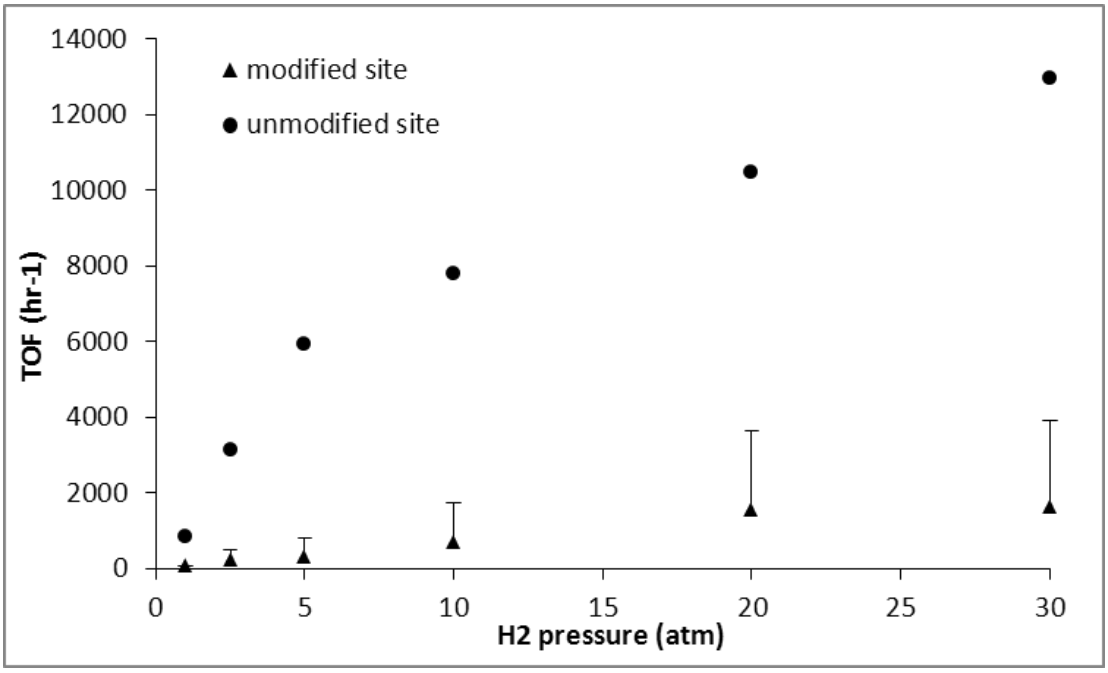

Figure 4.36 Effect of H_2 pressure on TOF (hr^{-1}) of modified and unmodified sites

The effect of CD/MPeA ratio with respect to reaction rate was also examined for enantioselective hydrogenation. The results are summarized in Figure 4.37. The set of experiments were carried out under same condition (e.g., reactant initial concentration, H_2 pressure, mass of catalyst, etc.) except for the amount of cinchonidine-modifier in the mixture solution. The modifier/substrate ratios were chosen from 0 to 1/5. As can be seen, in the case of no modifier added in system, the reaction proceeds at the highest rate. As the modifier/substrate ratio increases, the reaction rate declines. This observation is consistent with the conclusion that the blockage of active site with modifier leads to a decrease of reaction rate.

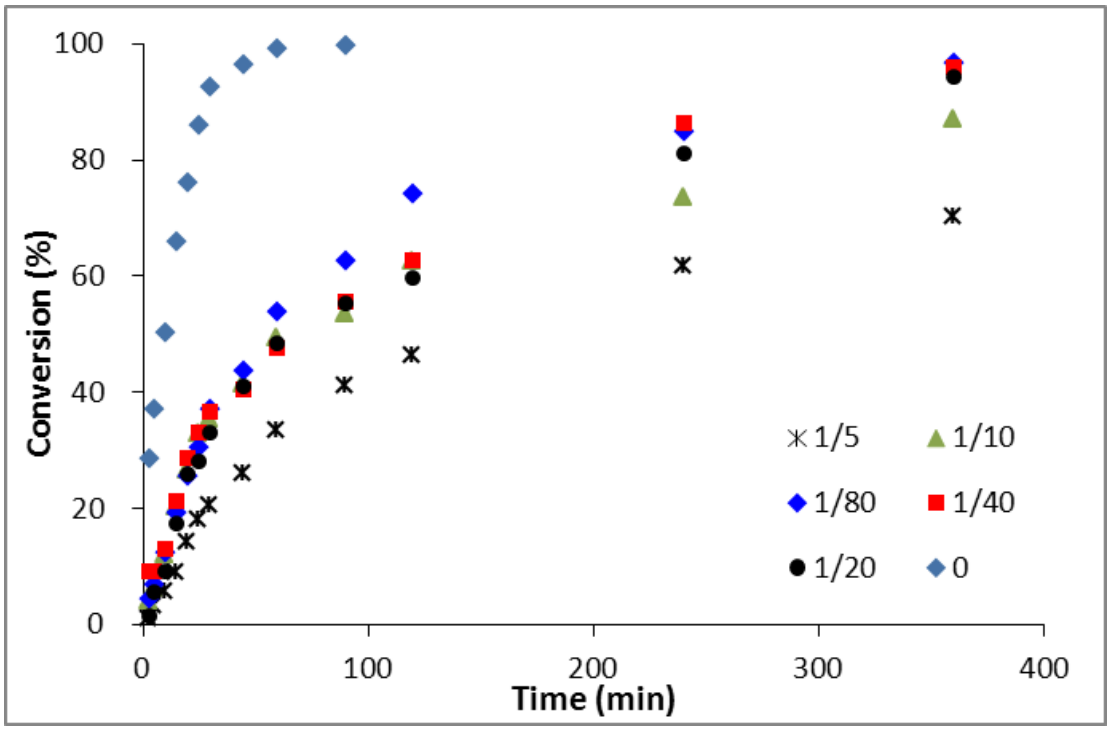

Figure 4.37 CD/MPeA ratio effect on conversion of enantioselective hydrogenation at 10 atm H_2 pressure

The impact of this modifier/substrate ratio on final e.e. value was also examined. As demonstrated in Figure 4.38, addition of trace amount of modifier (as low as 1:80 ratio) into the solution leads to a dramatic increase in enantioselectivity (up to ca. 25%). Further addition of the modifier does not affect the e.e. value significantly. To be specific, the enantioselectivity reaches ca. 30% at modifier: substrate=1/20 ratio, and becomes stable afterward.

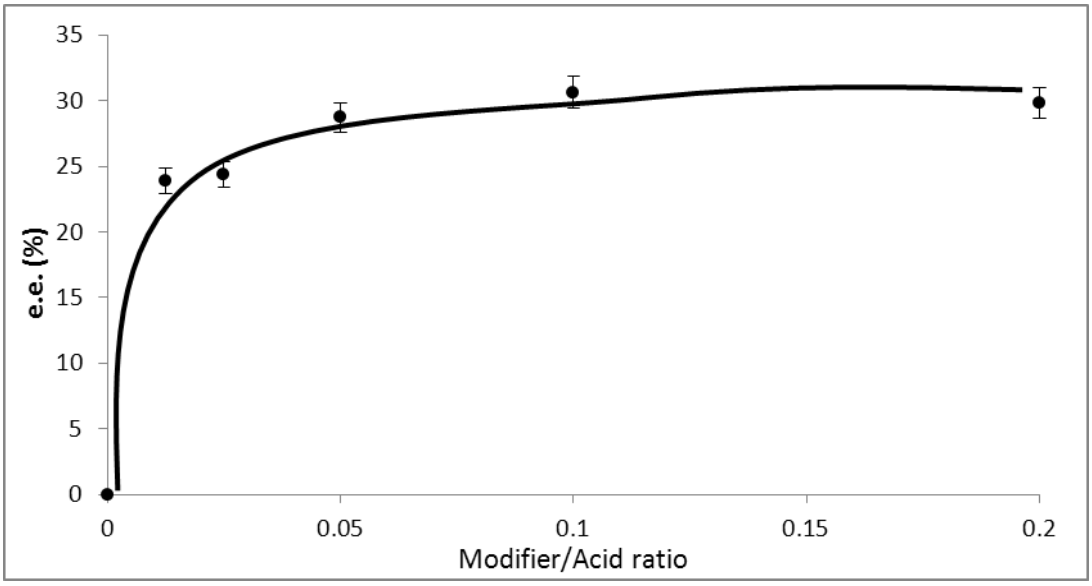

Figure 4.38 Effect of modifier/substrate ratio on e.e. value at 10 atm H_2 pressure

Taking the results of Figure 4.37 and 4.38, it is possible to calculate the final yield with respect to the pair of enantiomer respectively. As the Figure 4.39 shows, when the ratio is lower than 1/20, addition of modifier will slightly increase the yield of S-product. However, after reaching the peak value at ratio=1/20, it begins to decrease continuously with an increase in the amount of modifier. As to the R-product, addition of modifier always leads to a decrease of yield. The blue curve shows the difference between the two products. A conclusion could be drawn that the 1:20 modifier: substrate ratio is the most appropriate for the current catalytic system from the standpoint of balancing the activity and selectivity.

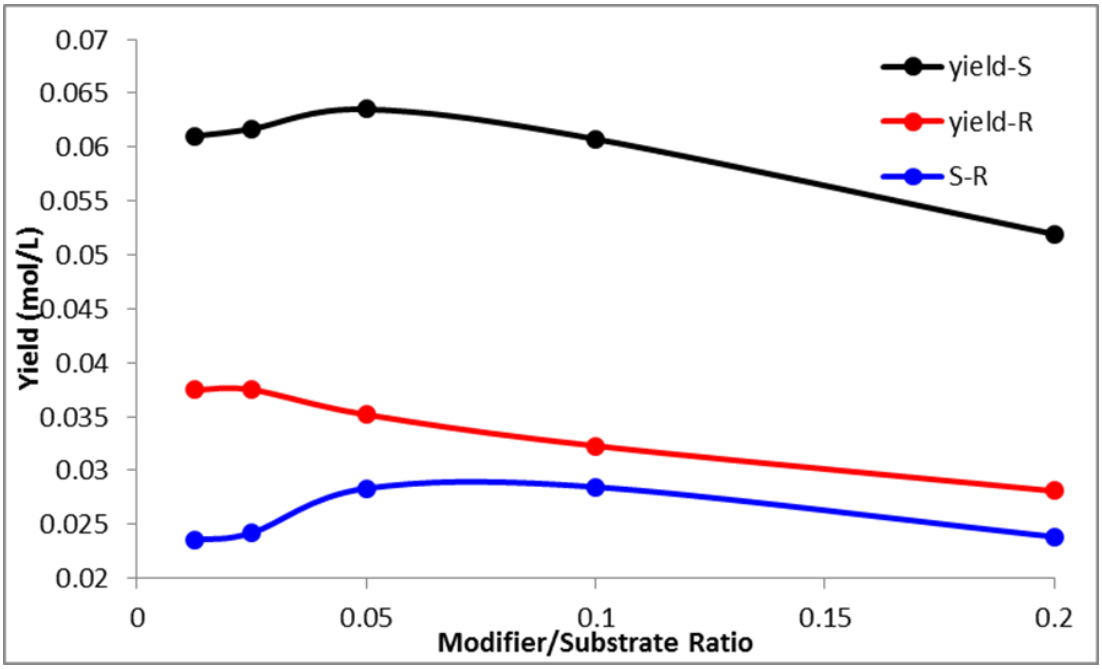

Figure 4.39 The effect of modifier/substrate ratio on the yields to S-enantiomer (black), R-enantiomer (red), and their difference (blue)

The overall implication from this analysis is that from the standpoint of balancing the activity and the selectivity, the catalyst should be carefully modified since the high percentage and rather low TOF of modified sites could decrease the overall reaction rate dramatically.

As mentioned before (also shown in Figure 4.32), the reaction order of substrate increases at high conversion. This phenomenon is possibly due to the accumulation and the consequently competitive adsorption of the product in the liquid mixture. To test this hypothesis, a series of reactions were performed with varying amounts of product injected into liquid mixture prior the hydrogenation, with other reaction conditions kept constant. Figure 4.40 shows clearly that with increased initial product/reactant ratio, the initial reaction rate declines, while the final e.e. value does not change significantly. These experiments, which simulate "product accumulation" in the reaction mixture, suggest that the increased amount of product may be

responsible for the increase in the apparent order of the reaction with respect to the reactant at high conversion. This could be due to the active sites being blocked via the competitive adsorption between product and reactant. The accumulation of product does not affect the e.e. value, which demonstrates that the mechanism of substrate acid adsorption on active sites and the hydrogen addition to acid is likely not affected by product adsorption.

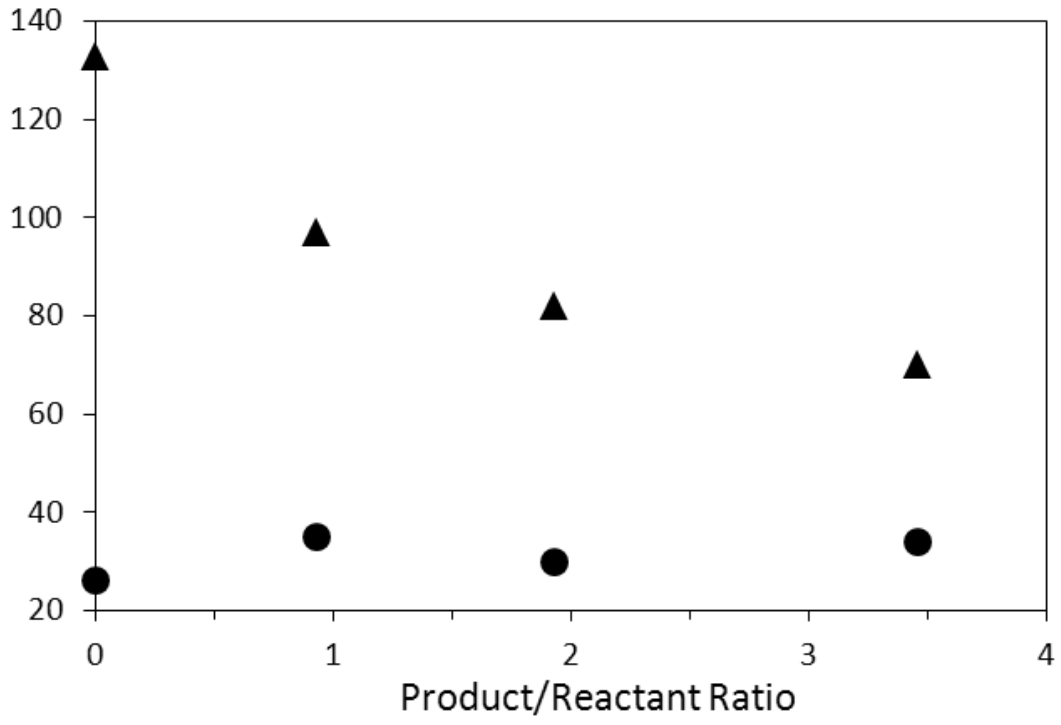

Figure 4.40 Effect of accumulation of product on initial reaction rate (mmol/hr/g_{cat}, triangles) and e.e. value (%, circles)

5. Conclusion

In the current study, the adsorption behaviors of a model acid - MPeA, in bulk phase and on Al_2O_3 and Pd/Al_2O_3 surfaces were examined in two typical solvents - CH_2Cl_2 and MeOH by using ATR-IR spectroscopy for the first time. In the presence of CH_2Cl_2, the MPeA molecules adsorb on both Al_2O_3 and Pd surfaces molecularly and dissociatively under the conditions examined. Both monomeric and dimeric species are observed to be present, with the relative amount of monomer to dimer dependent on the surface and the liquid phase acid concentration. In the case of dissociative adsorption, the acid adsorbs predominantly in a bridged bidentate carboxylate configuration judging from band separation between $\nu_{as}(COO^-)$ and $\nu_s(COO^-)$. For the case of MeOH solvation, the MPeA was found to adsorb on both Al_2O_3 and Pd primarily through bridging bidentate carboxylate instead of molecular species. The vibrations associated with adsorbed carboxylate also exhibit a wavenumber shift. This is explained as the H-bonding interaction between solvent molecule and MPeA.

The adsorption study of the modifier-cinchonidine (CD) on Al_2O_3 and Pd/Al_2O_3 surfaces in these two solvents was conducted with *in-situ* ATR-IR technique as well. However, the different solvents do not appear to affect the adsorption behavior of cinchonidine in terms of adsorption orientation.

For the investigation of the modifier-substrate model complex, it has been found that the bands due to intermolecular interaction appeared at two fixed regions: 1360-

1410 cm^{-1} and 1520-1560 cm^{-1}. The results suggest that the complex prefers to form a CD-MPeA=1:1 structure either in solution or adsorbed on the surface, probably due to H-bonding between "O-H---O" and "N---H-O". This type of interaction is not affected by the adsorption sequence of two species. Such behavior could possibly explain the fixed raised preferential enantioselectivity in this aliphatic alkenoic acid-cinchonidine system. The current work elucidates the intermolecular interactions of the acid-modifier complex in solution and at the metal oxide surface.

More broadly, the present results provide further evidence that ATR-IR is an effective means to monitor the surface phenomena at the solid-liquid interface from a molecular level. Coupled with extensive curve fitting to deconvolute the vibrational data, this approach has value beyond the currently considered catalytic system, especially for application to adsorption and surface reactions of biomass-derived acids and acid esters on solid catalysts.

The kinetic study of C=C bond hydrogenation of MPeA over Pd/Al_2O_3 catalyst with/without cinchonidine modifier was carried out in a batch reactor. The hydrogenation reaction exhibits a strong solvent-dependent behavior, with MeOH showing the best activity performance likely due to its strong polarity, while CH_2Cl_2 is almost inactive. The reaction rate exhibits a linear dependence on H_2 pressure within lower pressure regime up to 8 atm, while becoming H_2-independent when pressure is higher than 20 atm, regardless of the absence or presence of the chiral modifier. The substrate exhibits first order behavior at low conversions (< ca. 60%) while increases to higher order (ca. 1.5-2) at high conversion. The addition of the modifier causes a dramatic decrease of the overall reaction rate. A higher

modifier/substrate ratio leads to lower reaction rate. It has been deduced that the modified site takes up a significant percentage of total metal sites regardless of the H_2 pressure. It is also estimated that the TOF on modified sites is significantly smaller than for unmodified sites, accounting for the overall decrease in hydrogenation rates. The study also reveals that addition of only a tiny amount of modifier (modifier/substrate=1/80) results in a significant enantioselectivity. However, the e.e. value does not change too much after this ratio is higher than 1/20. The accumulation of the product appears to correlate with the increasing reaction order in acid substrate, although this does not affect the final e.e. value.

6. References

[1] R. Noyori, *Science*, 248 (1990) 1194-1199.

[2] F.S. H.U.Blaser, M.Studer, *Applied Catalysis A: General* 221 (2001) 119-143.

[3] H.U. Blaser, *Top. Catal.*, 53 (2010) 997-1001.

[4] H.U. Blaser, *Tetrahedron-Asymmetry*, 2 (1991) 843-866.

[5] H. Nozaki, S. Moriuti, H. Takaya, R. Noyori, *Tetrahedron Lett.*, (1966) 5239-5244.

[6] L. Horner, H. Siegel, H. Buthe, *Angew. Chem. Int. Ed.*, 7 (1968) 942.

[7] W.S. Knowles, M.J. Sabacky, *Chem. Commun.*, (1968) 1445.

[8] H.U. Blaser, C. Malan, B. Pugin, F. Spindler, H. Steiner, M. Studer, *Advanced Synthesis & Catalysis*, 345 (2003) 103-151.

[9] A. Miyashita, A. Yasuda, H. Takaya, K. Toriumi, T. Ito, T. Souchi, R. Noyori, *J. Am. Chem. Soc.*, 108 (1980) 7932-7934.

[10] K. Tani, T. Yamagata, S. Akutagawa, H. Kumobayashi, T. Taketomi, H. Takaya, A. Miyashita, R. Noyori, S. Otsuka, *J. Am. Chem. Soc.*, 106 (1984) 5208-5217.

[11] F. Lagasse, H.B. Kagan, *Chem. Pharm. Bull.*, 48 (2000) 315-324.

[12] I.V. Komarov, A. Borner, *Angew. Chem. Int. Ed.*, 40 (2001) 1197-1200.

[13] K.L. Ding, *Pure Appl. Chem.*, 78 (2006) 293-301.

[14] R.P. Tooze, D.J. Cole-Hamilton, *Catalyst Seperation, Recovery and Recycling*, Springer Netherlands, 2006.

[15] A. Baiker, *J. Mol. Catal. A: Chem.*, 115 (1997) 473-493.

[16] T. Tarnai, A. Tungler, T. Mathe, J. Petro, R.A. Sheldon, G. Toth, *J. Mol. Catal. A: Chem.*, 102 (1995) 41-47.

[17] T. Burgi, A. Baiker, *Acc. Chem. Res.*, 37 (2004) 909-917.

[18] A. Tungler, E. Sipos, V. Hadac, *Arkivoc*, (2004) 223-242.

[19] H.U. Blaser, H.P. Jalett, D.M. Monti, J.F. Reber, J.T. Wehrli, *Stud. Surf. Sci. Catal.*, 41 (1988) 153.

[20] T. Sugimura, J. Watanabe, S. Nakagawa, T. Okuyama, *J. Mol. Catal. A: Chem.*, 248 (2006) 233-236.

[21] T. Mallat, E. Orglmeister, A. Baiker, *Chem. Rev.*, 107 (2007) 4863-4890.

[22] T. Osawa, T. Harada, O. Takayasu, *Curr. Org. Chem.*, 10 (2006) 1513-1531.

[23] S.L. Cai, K. Ma, H.N. Chen, Y.F. Zheng, J. Jiang, R. Li, *Catal. Lett.*, 128 (2009) 227-234.

[24] C.F. Wang, Y.F. Zheng, S.L. Cai, J.T. Ma, R. Li, *React. Kinet. Catal. Lett.*, 95 (2008) 129-134.

[25] H.N. Chen, R. Li, H.L. Wang, L.A. Yin, F.S. Wang, J.T. Ma, *Chem. Lett.*, 35 (2006) 910-911.

[26] T. Osawa, M. Ando, S. Sakai, T. Harada, O. Takayasu, *Catal. Lett.*, 105 (2005) 41-45.

[27] T. Osawa, M. Ando, T. Harada, O. Takayasu, *B. Chem. Soc. Jpn.*, 78 (2005) 1371-1372.

[28] D. Jo, J.S. Lee, K.H. Lee, *J. Mol. Catal. A: Chem.*, 222 (2004) 199-205.

[29] S. Diezi, S. Reimann, N. Bonalumi, T. Mallat, A. Baiker, *J. Catal.*, 239 (2006) 255-262.

[30] M. Bartok, *Curr. Org. Chem.*, 10 (2006) 1533-1567.

[31] A. Vargas, T. Burgi, A. Baiker, *J. Catal.*, 226 (2004) 69-82.

[32] A. Marinas, T. Mallat, A. Baiker, *J. Catal.*, 221 (2004) 666-669.

[33] M. von Arx, T. Mallat, A. Baiker, *Top. Catal.*, 19 (2002) 75-87.

[34] A. Solladie-Cavallo, F. Hoernel, M. Schmitt, F. Garin, *Tetrahedron Lett.*, 43 (2002) 2671-2673.

[35] J.M. Bonello, R.M. Lambert, N. Kunzle, A. Baiker, *J. Am. Chem. Soc.*, 122 (2000) 9864-9865.

[36] K.E. Simons, P.A. Meheux, S.P. Griffiths, I.M. Sutherland, P. Johnston, P.B. Wells, A.F. Carley, M.K. Rajumon, M.W. Roberts, A. Ibbotson, *Recueil Des*

Travaux Chimiques Des Pays-Bas-Journal of the Royal Netherlands Chemical Society, 113 (1994) 465-474.

[37] B. Minder, T. Mallat, P. Skrabal, A. Baiker, *Catal. Lett.*, 29 (1994) 115-124.

[38] P.A. Meheux, A. Ibbotson, P.B. Wells, *J. Catal.*, 128 (1991) 387-396.

[39] H.U. Blaser, H.P. Jalett, J. Wiehl, *J. Mol. Catal.*, 68 (1991) 215-222.

[40] I.M. Sutherland, A. Ibbotson, R.B. Moyes, P.B. Wells, *J. Catal.*, 125 (1990) 77-88.

[41] J.T. Wehrli, A. Baiker, D.M. Monti, H.U. Blaser, *J. Mol. Catal.*, 49 (1989) 195-203.

[42] T. Sugimura, J. Watanabe, T. Okuyama, Y. Nitta, *Tetrahedron-Asymmetry*, 16 (2005) 1573-1575.

[43] G. Szollosi, T. Varga, K. Felfoldi, S. Cserenyi, M. Bartok, *Catal. Commun.*, 9 (2008) 421-424.

[44] J.W. Takashi Sugimura, Takayuki Uchida, Yuriko Nitta, and Tadashi Okuyama, *Catal. Lett.*, 112 (2006) 27-30.

[45] K. Szori, G. Szollosi, M. Bartok, *New J. Chem.*, 32 (2008) 1354-1358.

[46] G. Szollosi, B. Herman, K. Felfoldi, F. Fulop, M. Bartok, *J. Mol. Catal. A: Chem.*, 290 (2008) 54-59.

[47] G. Szollosi, B. Herman, K. Felfoldi, F. Fulop, M. Bartok, *Adv. Synth. Catal.*, 350 (2008) 2804-2814.

[48] T. Sugimura, J. Watanabe, T. Uchida, Y. Nitta, T. Okuyama, *Catal. Lett.*, 112 (2006) 27-30.

[49] Y. Nitta, *J. Synth. Org. Chem. Jpn.*, 64 (2006) 827-835.

[50] Y. Nitta, T. Kubota, Y. Okamoto, *J. Mol. Catal. A: Chem.*, 212 (2004) 155-159.

[51] N. Kunzle, J.W. Soler, T. Mallat, A. Baiker, *J. Catal.*, 210 (2002) 466-470.

[52] Y. Nitta, T. Kubota, Y. Okamoto, *B. Chem. Soc. Jpn.*, 74 (2001) 2161-2165.

[53] Y. Nitta, T. Kubota, Y. Okamoto, *B. Chem. Soc. Jpn.*, 73 (2000) 2635-2641.

[54] Y. Nitta, Y. Okamoto, *Chem. Lett.*, (1998) 1115-1116.

[55] Y. Nitta, K. Kobiro, Y. Okamoto, *Heterogeneous Catalysis and Fine Chemicals Iv*, 108 (1997) 191-198.

[56] Y. Nitta, K. Kobiro, *Chem. Lett.*, (1995) 165-165.

[57] Y. Nitta, Y. Ueda, T. Imanaka, *Chem. Lett.*, (1994) 1095-1098.

[58] T. Satyanarayana, S. Abraham, H.B. Kagan, *Angew. Chem. Int. Ed.*, 48 (2009) 456-494.

[59] I. Ojima, *Catalytic Asymmetric Synthesis*, Third ed., John Wiley & Sons, New York, 2010.

[60] A.P. E. N. Jacobsen, H. Yamamoto, *Comprehensive Asymmetric Catalysis*, Springer- Verlag, Berlin, 1999.

[61] W.S. Knowles, B.D. Vineyard, M.J. Sabacky, *J. Chem. Soc., Chem. Comm.*, (1972) 10-11.

[62] B.D. Vineyard, W.S. Knowles, M.J. Sabacky, G.L. Bachman, D.J. Weinkauff, *J. Am. Chem. Soc.*, 99 (1977) 5946-5952.

[63] T.P. Dang, H.B. Kagan, *J. Chem. Soc., Chem. Comm.*, (1971) 481.

[64] H.B. Kagan, T.P. Dang, *J. Am. Chem. Soc.*, 94 (1972) 6429-6433.

[65] M.D. Fryzuk, B. Bosnich, *J. Am. Chem. Soc.*, 99 (1977) 6262-6267.

[66] M.D. Fryzuk, B. Bosnich, *J. Am. Chem. Soc.*, 101 (1979) 3043-3049.

[67] M. Fiorini, G.M. Giongo, *J. Mol. Catal.*, 5 (1979) 303-310.

[68] M. Fiorini, G.M. Giongo, *J. Mol. Catal.*, 7 (1980) 411-413.

[69] R. Noyori, *Chemtech*, 22 (1992) 360-367.

[70] K. Inoguchi, S. Sakuraba, K. Achiwa, *Synlett*, (1992) 169-178.

[71] M. Devocelle, F. Agbossou, A. Mortreux, *Synlett*, (1997) 1306-1309.

[72] J.F. Carpentier, A. Mortreux, *Tetrahedron-Asymmetry*, 8 (1997) 1083-1099.

[73] K. Mashima, K.H. Kusano, N. Sato, Y. Matsumura, K. Nozaki, H. Kumobayashi, N. Sayo, Y. Hori, T. Ishizaki, S. Akutagawa, H. Takaya, *J. Org. Chem.*, 59 (1994) 3064-3076.

[74] T. Chiba, A. Miyashita, H. Nohira, H. Takaya, *Tetrahedron Lett.*, 34 (1993) 2351-2354.

[75] M. Kitamura, M. Tokunaga, T. Ohkuma, R. Noyori, *Tetrahedron Lett.*, 32 (1991) 4163-4166.

[76] H. Kawano, T. Ikariya, Y. Ishii, M. Saburi, S. Yoshikawa, Y. Uchida, H. Kumobayashi, *J. Chem. Soc., Perkin Trans. 1*, (1989) 1571-1575.

[77] J.B. Hoke, L.S. Hollis, E.W. Stern, *J. Organomet. Chem.*, 455 (1993) 193-196.

[78] M.J. Burk, T.G.P. Harper, C.S. Kalberg, *J. Am. Chem. Soc.*, 117 (1995) 4423-4424.

[79] P.J. Pye, K. Rossen, R.A. Reamer, R.P. Volante, P.J. Reider, *Tetrahedron Lett.*, 39 (1998) 4441-4444.

[80] V. Fehring, R. Selke, *Angew. Chem. Int. Ed.*, 37 (1998) 1827-1830.

[81] R. Noyori, T. Ohkuma, *Angew. Chem. Int. Ed.*, 40 (2001) 40-73.

[82] S. Toros, B. Heil, L. Kollar, L. Marko, *J. Organomet. Chem.*, 197 (1980) 85-86.

[83] J. Bakos, I. Toth, B. Heil, L. Marko, *J. Organomet. Chem.*, 279 (1985) 23-29.

[84] X.Y. Zhang, H. Kumobayashi, H. Takaya, *Tetrahedron-Asymmetry*, 5 (1994) 1179-1182.

[85] T. Ohkuma, M. Koizumi, H. Doucet, T. Pham, M. Kozawa, K. Murata, E. Katayama, T. Yokozawa, T. Ikariya, R. Noyori, *J. Am. Chem. Soc.*, 120 (1998) 13529-13530.

[86] H. Doucet, T. Ohkuma, K. Murata, T. Yokozawa, M. Kozawa, E. Katayama, A.F. England, T. Ikariya, R. Noyori, *Angew. Chem. Int. Ed.*, 37 (1998) 1703-1707.

[87] Q.Z. Jiang, Y.T. Jiang, D.M. Xiao, P. Cao, X.M. Zhang, *Angew. Chem. Int. Ed.*, 37 (1998) 1100-1103.

[88] T. Ohkuma, C.A. Sandoval, R. Srinivasan, Q. Lin, Y. Wei, K. Muniz, R. Noyori, *J. Am. Chem. Soc.*, 127 (2005) 8288-8289.

[89] J. Bakos, A. Orosz, B. Heil, M. Laghmari, P. Lhoste, D. Sinou, *J. Chem. Soc., Chem. Comm.*, (1991) 1684-1685.

[90] D.M. Xiao, X.M. Zhang, *Angew. Chem. Int. Ed.*, 40 (2001) 3425-3428.

[91] S.C. Stinson, *Chem. Eng. News*, 79 (2001) 45-57.

[92] S.C. Stinson, *Chem. Eng. News*, 79 (2001) 79-97.

[93] I.F.J.V. D. E. De Vos, P. A. Jacobs, *Chiral Catalyst Immobilization and Recycling*, Wiley-VCH Verlag GmbH, Weinheim, 2000.

[94] D. Ager, *Handbook of Chiral Chemicals*, 2 ed., CRC Press, Boca Raton, 2005.

[95] A. Tai, K. Ito, T. Harada, *B. Chem. Soc. Jpn.*, 54 (1981) 223-227.

[96] Y. Izumi, M. Imaida, H. Fukawa, S. Akabori, *B. Chem. Soc. Jpn.*, 36 (1963) 155-160.

[97] Y. Izumi, M. Imaida, H. Fukawa, S. Akabori, *B. Chem. Soc. Jpn.*, 36 (1963) 21-25.

[98] T. Harada, M. Imaida, Y. Izumi, *B. Chem. Soc. Jpn.*, 44 (1971) 1419-1420.

[99] Y. Orito, S. Imai, S. Niwa, *Nippon Kagaku Kaishi*, (1979) 1118-1120.

[100] Y. Orito, S. Imai, S. Niwa, *Nippon Kagaku Kaishi*, (1980) 670-672.

[101] A. Baiker, *J. Mol. Catal. A: Chem.*, 163 (2000) 205-220.

[102] P.B. Wells, K.E. Simons, J.A. Slipszenko, S.P. Griffiths, D.F. Ewing, *J. Mol. Catal. A: Chem.*, 146 (1999) 159-166.

[103] H.U. Blaser, H.P. Jalett, M. Muller, M. Studer, *Catal. Today*, 37 (1997) 441-463.

[104] P.B. Wells, A.G. Wilkinson, *Top Catal*, 5 (1998) 39-50.

[105] B. Torok, K. Balazsik, G. Szollosi, K. Felfoldi, M. Bartok, *Chirality*, 11 (1999) 470-474.

[106] M. Schurch, O. Schwalm, T. Mallat, J. Weber, A. Baiker, *J. Catal.*, 169 (1997) 275-286.

[107] G. Bond, K.E. Simons, A. Ibbotson, P.B. Wells, D.A. Whan, *Catal. Today*, 12 (1992) 421-425.

[108] M. Garland, H.U. Blaser, *J. Am. Chem. Soc.*, 112 (1990) 7048-7050.

[109] J.L. Margitfalvi, E. Tfirst, *J. Mol. Catal. A: Chem.*, 139 (1999) 81-95.

[110] J.L. Margitfalvi, M. Hegedus, E. Tfirst, *11th International Congress on Catalysis - 40th Anniversary, Pts a and B*, 101 (1996) 241-250.

[111] O. Schwalm, B. Minder, J. Weber, A. Baiker, *Catal. Lett.*, 23 (1994) 271-279.

[112] O. Schwalm, J. Weber, B. Minder, A. Baiker, *J. Mol. Struc-THEOCHEM*, 330 (1995) 353-357.

[113] O. Schwalm, J. Weber, B. Minder, A. Baiker, *Int. J. Quantum Chem*, 52 (1994) 191-197.

[114] H.U. Blaser, H.P. Jalett, D.M. Monti, A. Baiker, J.T. Wehrli, *Stud. Surf. Sci. Catal.*, 67 (1991) 147.

[115] T. Yoshida, K. Harada, *B. Chem. Soc. Jpn.*, 44 (1971) 1062-1067.

[116] A. Corma, M. Iglesias, C. Delpino, F. Sanchez, *Stud. Surf. Sci. Catal.*, 75 (1993) 2293-2296.

[117] J.R.G. Perez, J. Malthete, J. Jacques, *Cr Acad Sci Ii*, 300 (1985) 169-172.

[118] Y. Nitta, *Top. Catal.*, 13 (2000) 179-185.

[119] T. Kubota, H. Kubota, T. Kubota, E. Moriyasu, T. Uchida, Y. Nitta, T. Sugimura, Y. Okamoto, *Catal. Lett.*, 129 (2009) 387-393.

[120] Y. Nitta, K. Kobiro, *Chem. Lett.*, (1996) 897-898.

[121] Y. Nitta, *B. Chem. Soc. Jpn.*, 74 (2001) 1971-1972.

[122] Y. Nitta, A. Shibata, *Chem. Lett.*, (1998) 161-162.

[123] A. Tungler, Y. Nitta, K. Fodor, G. Farkas, T. Mathe, *J. Mol. Catal. A: Chem.*, 149 (1999) 135-140.

[124] T. Sugimura, T. Uchida, J. Watanabe, T. Kubota, Y. Okamoto, T. Misaki, T. Okuyama, *J. Catal.*, 262 (2009) 57-64.

[125] T. Misaki, H. Otsuka, T. Uchida, T. Kubota, Y. Okamoto, T. Sugimura, *J. Mol. Catal. A: Chem.*, 312 (2009) 48-52.

[126] Y. Nitta, *Chem. Lett.*, (1999) 635.

[127] Y. Nitta, J. Watanabe, T. Okuyama, T. Sugimura, *J. Catal.*, 236 (2005) 164-167.

[128] D. Ferri, T. Burgi, A. Baiker, *J. Chem. Soc., Perkin Trans. 2*, (2002) 437-441.

[129] K. Borszeky, T. Mallat, A. Baiker, *Catal. Lett.*, 59 (1999) 95-97.

[130] K. Borszeky, T. Burgi, Z. Zhaohui, T. Mallat, A. Baiker, *J. Catal.*, 187 (1999) 160-166.

[131] K. Borszeky, T. Mallat, A. Baiker, *Tetrahedron-Asymmetry*, 8 (1997) 3745-3753.

[132] M. Maris, T. Burgi, T. Mallat, A. Baiker, *J. Catal.*, 226 (2004) 393-400.

[133] M. Maris, W.R. Huck, T. Mallat, A. Baiker, *J. Catal.*, 219 (2003) 52-58.

[134] W.R. Huck, T. Burgi, T. Mallat, A. Baiker, *J. Catal.*, 205 (2002) 213-216.

[135] W.R. Huck, T. Burgi, T. Mallat, A. Baiker, *J. Catal.*, 200 (2001) 171-180.

[136] W.R. Huck, T. Mallet, A. Baiker, *J. Catal.*, 193 (2000) 1-4.

[137] W.R. Huck, T. Mallat, A. Baiker, *Catal. Lett.*, 69 (2000) 129-132.

[138] K. Borszeky, T. Mallat, R. Aeschiman, W.B. Schweizer, A. Baiker, *J. Catal.*, 161 (1996) 451-458.

[139] N. Kunzle, J.W. Soler, A. Baiker, *Catal. Today*, 79 (2003) 503-509.

[140] W.R. Huck, T. Mallat, A. Baiker, *Catal. Lett.*, 80 (2002) 87-92.

[141] K. Borszeky, T. Mallat, A. Baiker, *J. Catal.*, 188 (1999) 413-416.

[142] K. Borszeky, T. Mallat, A. Baiker, *Tetrahedron-Asymmetry*, 10 (1999) 4781-4789.

[143] K. Borszeky, T. Mallat, A. Baiker, *Catal. Lett.*, 41 (1996) 199-202.

[144] G. Szollosi, S.I. Niwa, T.A. Hanaoka, F. Mizukami, *J. Mol. Catal. A: Chem.*, 230 (2005) 91-95.

[145] I. Kun, B. Torok, K. Felfoldi, M. Bartok, *Appl. Catal., A-Gen*, 203 (2000) 71-79.

[146] G. Szollosi, T. Hanaoka, S. Niwa, F. Mizukami, M. Bartok, *J. Catal.*, 231 (2005) 480-483.

[147] K. Szori, G. Szollosi, K. Felfoldi, M. Bartok, *React. Kinet. Catal. Lett.*, 84 (2005) 151-156.

[148] A. Casagrande, S. Franceschini, M. Lenarda, O. Piccolo, A. Vaccari, *J. Mol. Catal. A: Chem.*, 246 (2006) 263-267.

[149] R. Bisignani, S. Franceschini, O. Piccolo, A. Vaccari, *J. Mol. Catal. A: Chem.*, 232 (2005) 161-164.

[150] A. Solladie-Cavallo, F. Hoernel, M. Schmitt, F. Garin, *J. Mol. Catal. A: Chem.*, 195 (2003) 181-188.

[151] A. Solladie-Cavallo, C. Marsol, F. Hoernel, F. Garin, *Tetrahedron Lett.*, 42 (2001) 4741-4744.

[152] M. Bartok, G. Wittmann, G. Gondos, G.V. Smith, *J. Org. Chem.*, 52 (1987) 1139-1141.

[153] H.U. Blaser, H.P. Jalett, *Stud. Surf. Sci. Catal.*, 78 (1993) 139.

[154] G.D.H. Dijkstra, R.M. Kellogg, H. Wynberg, *J. Org. Chem.*, 55 (1990) 6121-6131.

[155] M. Aune, A. Gogoll, O. Matsson, *J. Org. Chem.*, 60 (1995) 1356-1364.

[156] G.D.H. Dijkstra, R.M. Kellogg, H. Wynberg, J.S. Svendsen, I. Marko, K.B. Sharpless, *J. Am. Chem. Soc.*, 111 (1989) 8069-8076.

[157] M. Schurch, N. Kunzle, T. Mallat, A. Baiker, *J. Catal.*, 176 (1998) 569-571.

[158] G.D.H. Dijkstra, R.M. Kellogg, H. Wynberg, *Recueil Des Travaux Chimiques Des Pays-Bas-Journal of the Royal Netherlands Chemical Society*, 108 (1989) 195-204.

[159] B.J. Oleksyn, A. Suszkopurzcka, G. Dive, J. Lamottebrasseur, *J. Pharm. Sci.*, 81 (1992) 122-127.

[160] H. Caner, P.U. Biedermann, I. Agranat, *Chirality*, 15 (2003) 637-645.

[161] R.A. Olsen, D. Borchardt, L. Mink, A. Agarwal, L.J. Mueller, F. Zaera, *J. Am. Chem. Soc.*, 128 (2006) 15594-15595.

[162] T. Burgi, A. Baiker, *J. Am. Chem. Soc.*, 120 (1998) 12920-12926.

[163] U. Berg, M. Aune, O. Matsson, *Tetrahedron Lett*, 36 (1995) 2137-2140.

[164] G. Vayner, K.N. Houk, Y.K. Sun, *J Am Chem Soc*, 126 (2004) 199-203.

[165] A. Urakawa, D.M. Meier, H. Rugger, A. Baiker, *J. Phys. Chem. A*, 112 (2008) 7250-7255.

[166] J. Kubota, F. Zaera, *J. Am. Chem. Soc.*, 123 (2001) 11115-11116.

[167] A.F. Carley, M.K. Rajumon, M.W. Roberts, P.B. Wells, *J. Chem. Soc., Faraday Trans.*, 91 (1995) 2167-2172.

[168] G. Bond, P.B. Wells, *J. Catal.*, 150 (1994) 329-334.

[169] T. Evans, A.P. Woodhead, A. Gutierrez-Sosa, G. Thornton, T.J. Hall, A.A. Davis, N.A. Young, P.B. Wells, R.J. Oldman, O. Plashkevych, O. Vahtras, H. Agren, V. Carravetta, *Surf. Sci.*, 436 (1999) L691-L696.

[170] E. Schmidt, D. Ferri, A. Vargas, A. Baiker, *J. Phys. Chem. C*, 112 (2008) 3866-3874.

[171] D. Ferri, T. Burgi, A. Baiker, *Chem. Commun.*, (2001) 1172-1173.

[172] D. Ferri, T. Burgi, *J Am Chem Soc*, 123 (2001) 12074-12084.

[173] W. Chu, R.J. LeBlanc, C.T. Williams, J. Kubota, F. Zaera, *J. Phys. Chem. B*, 107 (2003) 14365-14373.

[174] D. Ferri, T. Burgi, A. Baiker, *J. Phys. Chem. B*, 108 (2004) 14384-14391.

[175] N. Bonalumi, A. Vargas, D. Ferri, A. Baiker, *Chem. Eur. J.*, 13 (2007) 9236-9244.

[176] W. Chu, R.J. LeBlanc, C.T. Williams, *Catal. Commun.*, 3 (2002) 547-552.

[177] Q.M. Xu, D. Wang, L.J. Wan, C.L. Bai, Y. Wang, *J. Am. Chem. Soc.*, 124 (2002) 14300-14301.

[178] C.J. Hirschmugl, *Surf. Sci.*, 500 (2002) 577-604.

[179] A.R. Hind, S.K. Bhargava, A. McKinnon, *Advances in Colloid and Interface Science*, 93 (2001) 91-114.

[180] D.R. Scheuing, *Abstr Pap Am Chem S*, 199 (1990) 35-Coll.

[181] B.W. Johnson, J. Bauhofer, K. Doblhofer, B. Pettinger, *Electrochim. Acta.*, 37 (1992) 2321-2329.

[182] I. Ortiz-Hernandez, C.T. Williams, *Langmuir*, 19 (2003) 2956-2962.

[183] J.R. Anderson, *Structure of Metallic Catalysts*, Academic Press, London, 1975.

[184] H. Cordatos, R.J. Gorte, *J. Catal.*, 159 (1996) 112-118.

[185] H. Cordatos, T. Bunluesin, R.J. Gorte, *Surf. Sci.*, 323 (1995) 219-227.

[186] E.H. Voogt, L. Coulier, O.L.J. Gijzeman, J.W. Geus, *J. Catal.*, 169 (1997) 359-364.

[187] I.V. Yudanov, R. Sahnoun, K.M. Neyman, N. Rosch, J. Hoffmann, S. Schauermann, V. Johanek, H. Unterhalt, G. Rupprechter, J. Libuda, H.J. Freund, *J. Phys. Chem. B*, 107 (2003) 255-264.

[188] M.J. Weaver, *Top. Catal.*, 8 (1999) 65-73.

[189] S.Z. Zou, R. Gomez, M.J. Weaver, *J. Electroanal. Chem.*, 474 (1999) 155-166.

[190] A.M. El-Aziz, L.A. Kibler, *J. Electroanal. Chem.*, 534 (2002) 107-114.

[191] J. Panpranot, U. Toophorm, P. Praserthdam, *J. Porous Mater.*, 12 (2005) 293-299.

[192] Q. Lin, Y. Ji, Z.D. Jiang, W.D. Xiao, *Ind. Eng. Chem. Res.*, 46 (2007) 7950-7954.

[193] M.T. Schaal, A.Y. Metcalf, J.H. Montoya, J.P. Wilkinson, C.C. Stork, C.T. Williams, J.R. Monnier, *Catal. Today*, 123 (2007) 142-150.

[194] J.B. Giorgi, T. Schroeder, M. Baumer, H.J. Freund, *Surf. Sci.*, 498 (2002) L71-L77.

[195] J. Rebelli, M. Detwiler, S.G. Ma, C.T. Williams, J.R. Monnier, *J. Catal.*, 270 (2010) 224-233.

[196] E.M.S. Macoas, P. Myllyperkio, H. Kunttu, M. Pettersson, *J. Phys. Chem. A*, 113 (2009) 7227-7234.

[197] C. Ohe, H. Ando, N. Sato, Y. Urai, M. Yamamoto, K. Itoh, *J. Phys. Chem. B*, 103 (1999) 435-444.

[198] E.M. Aschenbrenner, C.K. Weiss, K. Landfester, *Chem. Eur. J.*, 15 (2009) 2434-2444.

[199] K. Marushkevich, L. Khriachtchev, M. Rasanen, *J. Phys. Chem. A*, 111 (2007) 2040-2042.

[200] E. Spinner, *Aust. J. Chem.*, 38 (1985) 47-68.

[201] P. Waldstein, L.A. Blatz, *J. Phys. Chem.*, 71 (1967) 2271-2276.

[202] M.D. Taylor, J. Bruton, *J Am Chem Soc*, 74 (1952) 4151-4152.

[203] M. Gantenberg, M. Halupka, W. Sander, *Chem. Eur. J.*, 6 (2000) 1865-1869.

[204] X.H. Guan, G.H. Chen, C. Shang, *Journal of Environmental Sciences-China*, 19 (2007) 438-443.

[205] K.T.H.Y.M. Akiyama, *Solvent Extraction and Ion Exchange*, 5 (1987) 29-53.

[206] Y. Nagai, O. Simamura, *B. Chem. Soc. Jpn.*, 35 (1962) 132-134.

[207] K.D. Dobson, A.J. McQuillan, *Spectrochim. Acta., Part A*, 55 (1999) 1395-1405.

[208] D.M. Meier, A. Urakawa, A. Baiker, *Phys. Chem. Chem. Phys.*, 11 (2009) 10132-10139.

[209] T.B.a.A.B. D. Ferri, *Helv Chim Acta*, 85 (2002) 3639.

[210] D. Ferri, T. Bürgi, A. Baiker, *Helv. Chim. Acta.*, 85 (2002) 3639-3656.

[211] M. Nara, H. Torii, M. Tasumi, *J. Phys. Chem.*, 100 (1996) 19812-19817.

[212] G.B. Deacon, R.J. Phillips, *Coord. Chem. Rev.*, 33 (1980) 227-250.

[213] J. van den Brand, O. Blajiev, P.C.J. Beentjes, H. Terryn, J.H.W. de Wit, *Langmuir*, 20 (2004) 6308-6317.

[214] N.W. Alcock, V.M. tracy, T.C. Waddington, *J. Chem. Soc., Dalton Trans*, (1976) 2243-2246.

[215] D.M. Meier, A. Urakawa, N. Turra, H. Ruegger, A. Baiker, *J. Phys. Chem. A*, 112 (2008) 6150-6158.

[216] Z. Li, F. Calaza, F. Gao, W.T. Tysoe, *Surf. Sci.*, 601 (2007) 1351-1357.

[217] G. Socrates, *Infrared and Raman Characteristic Group Frequencies*, John Wiley, New York, 2001.

[218] S. Tan, X.J. Sun, C.T. Williams, *Phys. Chem. Chem. Phys.*, 13 (2011) 19573-19579.

[219] I. Busygin, O.P. Tkachenko, V. Nieminen, R. Sillanpää, E. Toukoniitty, L.M. Kustov, D.Y. Murzin, R. Leino, *J. Phys. Chem. C*, 111 (2007) 9374-9383.

[220] D. Ferri, T. Burgi, A. Baiker, *J. Catal.*, 210 (2002) 160-170.

[221] Z. Liu, X. Li, P. Ying, Z. Feng, C. Li, *J. Phys. Chem. C*, 111 (2006) 823-829.

[222] Z. Ma, F. Zaera, *J. Phys. Chem. B*, 109 (2005) 406-414.

[223] H.U. Blaser, F. Spindler, M. Studer, *Appl. Catal., A-Gen*, 221 (2001) 119-143.

[224] C. Chapuis, D.Jacoby, *Appl. Catal., A-Gen*, 221 (2001) 93-117.

[225] T. Sugimura, H. Ogawa, *Chem. Lett.*, 39 (2010) 232-233.

[226] B. Herman, G. Szollosi, F. Fulop, M. Bartok, *Appl. Catal., A-Gen*, 331 (2007) 39-43.

[227] G. Szollosi, K. Balazsik, M. Bartok, *Appl. Catal., A-Gen*, 319 (2007) 193-201.

[228] R.J. LeBlanc, C.T. Williams, *J. Mol. Catal. A: Chem.*, 220 (2004) 207-214.

[229] K. Shirono, T. Morimatsu, F. Takemura, *J. Chem. Eng. Data*, 53 (2008) 1867-1871.

[230] C.L. Young, *IUPAC Solubility Data Series, Hydrogen and Deuterium*, Pergamon Press, Oxford, England, 1981.

[231] C. Reichardt, T. Welton, *Solvents and Solvent Effects in Organic Chemistry*, Wiley-VCH, Weinheim, 2011.

[232] P. B. Wells, A. G. Wilkinson, *Top. Catal.*, 5 (1998) 39-50.

[233] T.J. Hall, P. Johnston, W.A.H. Vermeer, S.R. Watson, P.B. Wells, *Stud. Surf. Sci. Catal.*, 101 (1996) 221-230.

[234] G.M. Szollosi, Z.; Bartok, M., *React. Kinet. Catal. Lett.*, 96 (2009) 319-325.

[235] A. Tungler, E. Sipos, V. Hada, *Curr. Org. Chem.*, 10 (2006) 1569-1583.

Appendix A: Gas Chromatography Calibration

The GC was calibrated for each organic chemical used in this study by injecting a series of known amount of compound and recording the corresponding peak areas. In the Area (A) ~ mole plot, the slope of straight line region obtained is the response factor (RF). The calibration for chemicals involved in the hydrogenation (i.e., MPeA, MPaA, and MeOH) can be seen in Figure A1.

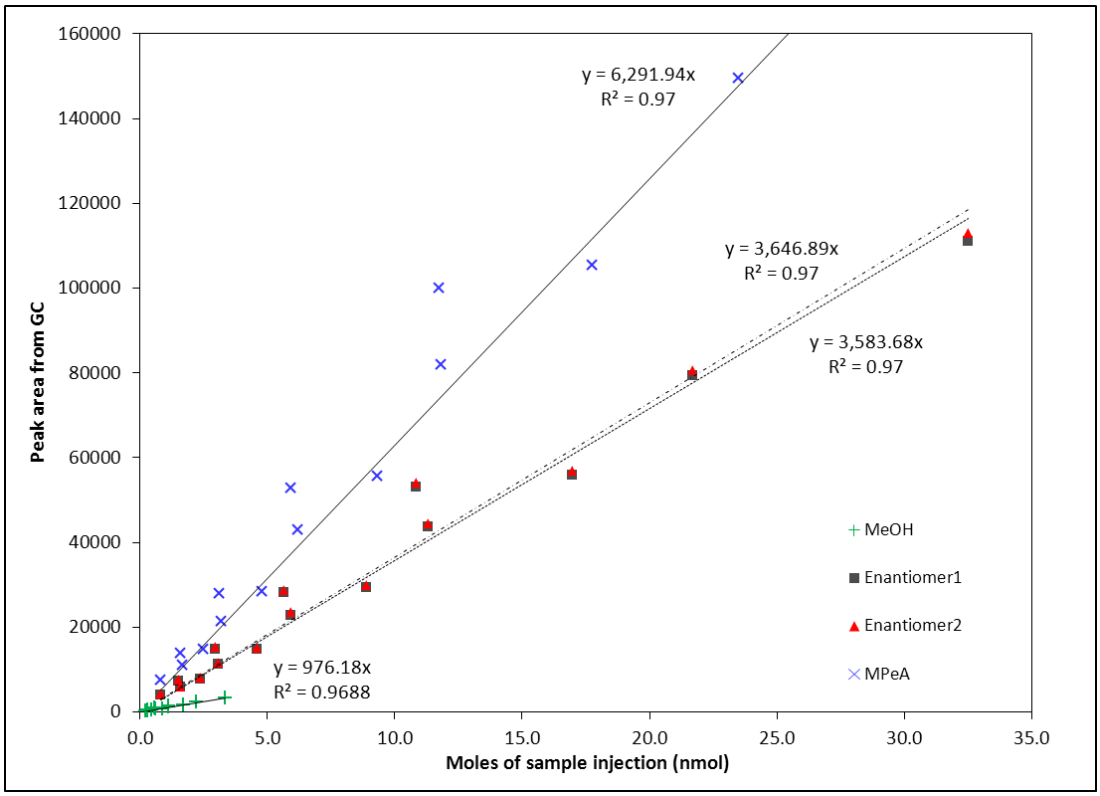

Figure A1. GC calibration for chemicals involve in hydrogenation

During the kinetic experiments carried out with batch reactor, the conversion of reactant (MPeA) was calculated from the obtained peak areas as follows:

$$Conversion = \frac{A_{E1} / RF_{E1} + A_{E2} / RF_{E2}}{A_{E1} / RF_{E1} + A_{E2} / RF_{E2} + A_R / RF_R}$$ Equation A1

Where E_1 and E_2 refer to the pair of enantiomer of product, R is reactant.

Thus, the concentration of MPeA at any time is calculated by

$$C_i = C_0 \times (1 - conversion_i / 100)$$ Equation A2

Appendix B: Calculation of Turnover Frequency

The initial reaction rates of MPeA hydrogenation over 5 wt% Pd/Al_2O_3 in batch autoclave reactor were calculated. The rate is expressed in the following way:

$$r = -\frac{dc}{dt} = kP_{H_2}^{\beta} c^{\alpha} = k_{app} c^{\alpha}$$ Equation B1

Where k is reaction constant, P_{H2} is hydrogenation pressure, c is concentration of MPeA, α and β are reaction order of MPeA and H_2 pressure respectively.

Judging from the Equation B1, the initial reaction rate (r) was in the unit of mol/L/min. Then, this rate was converted its unit by using Equation B2:

$$r(\frac{mmol}{hr \bullet g_{cat}}) = r(\frac{mol}{L \bullet \min}) * \frac{60 \min}{1hr} * \frac{1000mmol}{1mol} * \frac{1L}{1000ml} * V / m_{cat}$$ Equation B2

Where, V is the reaction volume (60ml in the current study), m_{cat} is the mass (in unit of gram) of catalyst used in a set of reaction.

The number of surface Pd atoms per gram (S) was calculated with Equation B3:

$$S(mol / g_{cat}) = \frac{W * PD}{Mw}$$ Equation B3

Where W is metal weight percent of catalyst (5% in the current study), PD is percent dispersion (14% in the current study), Mw is molecular weight of Pd (106.42 g/mol)

The TOF_U for unmodified sites is estimated with Equation B4 by assuming all surface Pd atoms are active sites.

$$TOF_U(hr^{-1}) = \frac{r(\frac{mmol}{hr * g_{cat}})}{S(mol / g_{cat})} * \frac{1mol}{1000mmol}$$ Equation B4

For enantioselective hydrogenation, the rates have been expressed as Equation 4.7-4.9 in section 4.3.2.

$r_{rac}=S*TOF_U$ Equation 4.7

$r_R=0.5*U*TOF_U+R\%*(S-U)*TOF_M$ Equation 4.8

$r_S=0.5*U*TOF_U+(1-R\%)*(S-U)*TO)_M$ Equation 4.9

Mathematical deduction leads to Equation B5, B6 and B7

$$U = \frac{(r_S + r_R) - \frac{r_S - r_R}{1-2R\%}}{TOF_U}$$ Equation B5

Where U is number of unmodified site per gram catalyst in unit of mol/g_{cat}.

$$M = S - U$$ Equation B6

Where M is unmodified site per gram catalyst in unit of mol/g_{cat}.

$$TOF_M = \frac{r_S - r_R}{(1-2R\%) * M}$$ Equation B7

Where TOF_M is turnover frequency of unmodified site in unit of hr^{-1}.

Appendix C: Operation of 6-valve Port for Batch Reactor

The detailed view of the 6-port valve connected with batch reactor is shown in Figure C1.

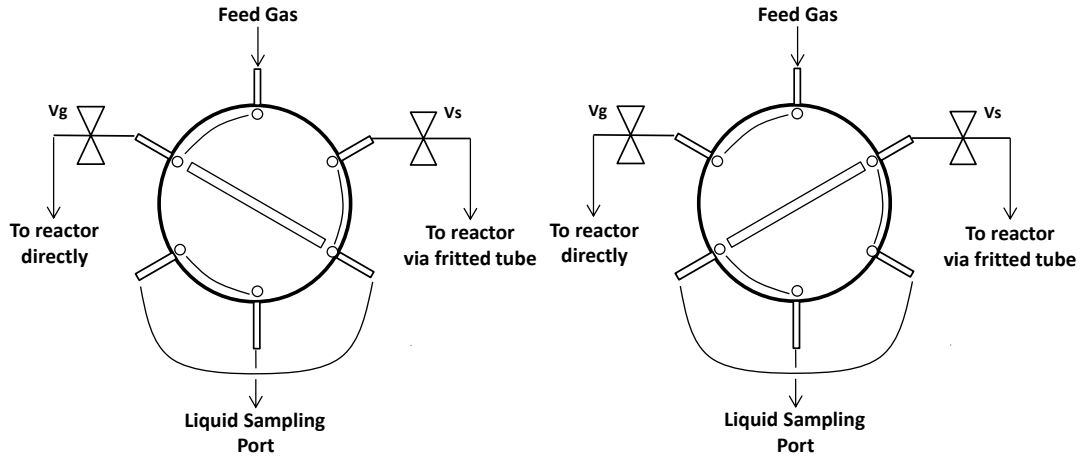

Figure C1. Schematic view of 6-port valve. Left: position-1, Right: position-2

The operations of the valve are listed as follow steps.

Step 1: After sealing the reactor, set the valve at position-1, and keep v_s closed. Use N_2 as feed gas to check leak by only operating v_g.

Step 2: Once ensure the system is airtight, switch feed gas into H_2 to supposed pressure and keep v_g open. This will allow the hydrogenation to initiate.

Step 3: Before collecting each sample, close v_g. Set valve at position-2 and open v_s. By doing this, the liquid mixture stays in the pipeline to sampling port will be purged back to reactor.

Step 4: To collect the liquid sample, set valve back to position-1 while keep v_g closed and v_s open. In this way, the liquid sample will be flushed out of

sampling port under the high pressure inside of the reactor. Since the mixture goes through the fritted tube, the catalyst will be kept within the reactor. It should be mentioned that to increase the accuracy of GC measurement, the first several drops of liquid mixture out of sampling port should be always abnegated, considering the hydrogenation may not occur within the pipeline.

Step 5: After collecting the sample, repeat step 3 to flush the liquid back to reactor. Then, repeat step 2 to allow hydrogenation to be continued.